RESEARCH REPORT

FRACTURE AND FATIGUE-CRACK PROPAGATION CHARACTERISTICS OF 7075-T7351 ALUMINUM ALLOY SHEET AND PLATE

March 15, 1970

by

C. E. Feddersen
W. S. Hyler

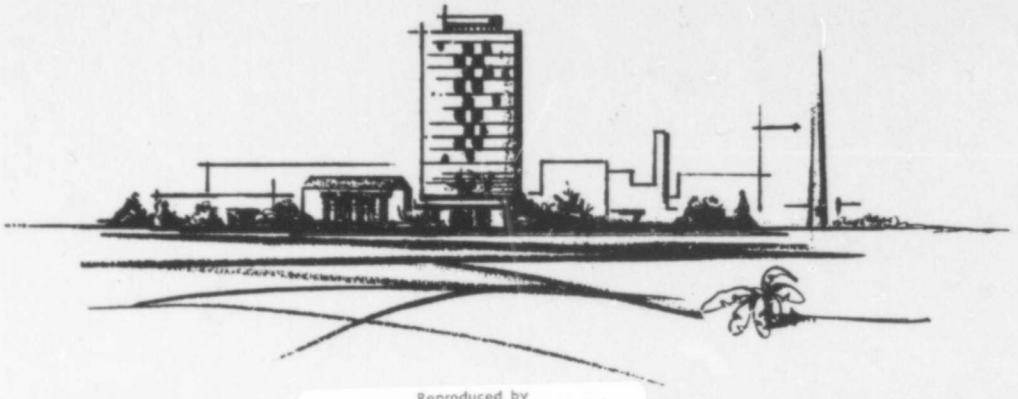

BATTELLE MEMORIAL INSTITUTE

COLUMBUS LABORATORIES

THE COLUMBUS LABORATORIES of Battelle Memorial Institute comprise the original research center of an international organization devoted to research.

The Institute is frequently described as a "bridge" between science and industry – a role it has performed in more than 90 countries. As an independent research institute, it conducts research encompassing virtually all facets of science and its application. It also undertakes programs in fundamental research and education.

Battelle-Columbus – with its staff of 3,000 – serves industry and government through contract research. It pursues:

- research embracing the physical and life sciences, engineering, and selected social sciences
- design and development of materials, products, processes, and systems
- information analysis, socioeconomic and technical economic studies, and management planning research.

505 KING AVENUE • COLUMBUS, OHIO 43201

FINAL REPORT

on

FRACTURE AND FATIGUE-CRACK PROPAGATION CHARACTERISTICS OF 7075-T7351 ALUMINUM ALLOY SHEET AND PLATE

March 15, 1970

by

C. E. Feddersen
W. S. Hyler

Prepared under Contract N00156-68-C-1344
for
Aero Structures Department
Naval Air Development Center
Warminster, Pennsylvania 18974

Report No. G-8902

BATTELLE MEMORIAL INSTITUTE
Columbus Laboratories
505 King Avenue
Columbus, Ohio 43201

FOREWORD

This investigation was conducted by the Department of Mechanical Engineering of the Battelle Memorial Institute, Columbus, Ohio, under Contract No. N00156-68-C-1344. This contract was initiated under Work Unit No. 42, "Fracture Mechanics and Crack Propagation Hypotheses", of basic AIRTASK No. R009-03-01. It was administered under the direction of the Aero Structures Department, Naval Air Development Center, Warminster, Pennsylvania, with E. F. Manolakos and R. E. Vining acting as technical liaison. This report summarizes work performed during the period 25 March 1968 through 31 October 1969. A continuation program of research on the fracture properties and crack-propagation behavior of annealed titanium-6Al-4V alloy is at present being performed by the Battelle Memorial Institute under Contract No. N00156-70-1336.

BLANK PAGE

LIST OF SYMBOLS

$2c, \ell$	Instantaneous crack length or flaw size, inch
$2c_o$	Initial crack or flaw size, inch
$2c_c$	Final crack length, inch
$2c_{fs}$	Measured surface-crack length after fatigue failure, inch
$2c_{fc}$	Measured center section crack length after fatigue failure, inch
C_m	Crack sensitivity
$d\ell/dN$	Rate of crack propagation, in./cycle
E	Modulus of elasticity, psi
E_1	Secant modulus at ultimate strength, psi
K	Stress intensity, stress-intensity factor, psi $inch^{1/2}$
K_c	Plane-stress fracture index, psi $inch^{1/2}$
K_{Ic}	Plane-strain fracture toughness, psi $inch^{1/2}$
K_a	Stress intensity associated with S_a, psi $inch^{1/2}$
$K_r, \Delta K$	Stress intensity associated with $2S_a$, psi $inch^{1/2}$
K_m	Stress intensity associated with S_m, psi $inch^{1/2}$
K_{max}	Stress intensity associated with S_{max}, psi $inch^{1/2}$
$\bar{\Delta}K$	Effective stress intensity associated with $\bar{S}$, psi $inch^{1/2}$
K_t	Theoretical stress-concentration factor
K_u	Effective stress-concentration factor
k_w	Finite-width correction
N	Number of cycles
N_f	Number of cycles to failure
NYS	Net section yield stress, psi
p_{max}	Plastic-zone size associated with S_{max} and K_{max}
p_r	Plastic-zone size associated with $2S_a$ and ΔK
R	Stress ratio, S_{min}/S_{max}
r	Notch-root radius, plastic-zone radius, inch
ρ'	Neuber constant
S, S_g	Gross section stress, psi
S_n, σ_{net}	Net section stress, psi
S_1	Gross section stress at maximum load, psi
S_2	Gross section stress at pop-in load, psi

LIST OF SYMBOLS
(Continued)

S_3	Gross section stress at 5 percent secant offset load, psi
S_a	Alternating stress of stress cycle, psi
ΔS	$2S_a$, psi
S_{min}	Minimum stress of stress cycle, psi
S_m, S_{mean}	Mean stress of stress cycle, psi
S_{max}	Maximum stress of stress cycle, psi
$\bar{S}$	Effective stress, psi
t, T	Sheet or plate thickness, inch
TUS	Ultimate tensile strength, psi
TYS	Tensile yield strength, psi
w, W	Sheet or panel width, inch

TABLE OF CONTENTS

TABLE OF CONTENTS
(Continued)

FRACTURE AND FATIGUE-CRACK PROPAGATION CHARACTERISTICS OF 7075-T7351 ALUMINUM ALLOY SHEET AND PLATE

by

C. E. Feddersen and W. S. Hyler

SUMMARY

This program was directed to provide information relative to damage tolerance of panels of 7075-T7351 sheet and plate. This implied the generation and analysis of information on flat panels containing centrally located flaws and testing either under monotonically increasing load or under cyclic loads. The information obtained provided insight into the two major aspects of damage tolerance – residual strength and fatigue-crack propagation – from tests on panels 1/16 to 1 inch thick and 8 to 36 inches wide.

The program has shown that there are at least two bench marks in crack-growth behavior from the monotonically increasing load test: (1) onset of slow growth at which a flaw initially present begins to grow slowly with increasing load and (2) critical instability at which unstable and rapid crack growth occurs that results in failure. From the data obtained a generalized residual-strength analysis was developed that identifies a fracture-toughness property for thin and transition-thickness materials as well as presents design data and fracture or residual-strength predictions for structural applications. The program has also resulted in the identification of an empirical expression that appears to be quite useful in predicting fatigue-crack propagation and the remaining lifetime of a panel containing a fatigue crack.

INTRODUCTION

One of the most pressing problems in aircraft design and operation is the concept of damage tolerance. It is recognized that real structures may contain flaws initially or that the flaws may develop during service. The growth of these flaws by fatigue and their residual strength at any time during growth are the concerns associated with an accounting of damage tolerance in the design process.

One aspect of flaw tolerance that has received an enormous amount of attention is the brittle fracture of high-strength materials. Out of this effort have evolved the techniques for the analysis of elastic fracture mechanics and the identification of a material constant termed fracture toughness, identified symbolically as K_{Ic}. Fracture toughness in this context is associated with plane-strain stress states that are obtained in thick sections. Failures are brittle with little evidence of plastic deformation or shear-lip formation and can occur at stress levels substantially below the yield strength and sometimes well within the design stress envelope.

Real aircraft structure combines a wide range of thicknesses so that not always do plane-strain stress states obtain. Significant amounts of structure are thin enough so that essentially plane-stress conditions exist. For this stress condition, failure of

flawed components may be at or near the yield strength of the material with evidence of gross plastic deformation. Other structures may be at intermediate thicknesses, and if failure occurs, the fracture surfaces will show evidence of both brittle and ductile failure modes.

The designer has had some unwillingness to employ fracture-toughness values in thin and transition-thickness material since data are available that show that the residual strength of a panel or component under plane stress could be substantially higher than that of a similar panel (but thicker) under plane strain. Accordingly, with the lack of theoretical tools to predict structural strength in the plane-stress and transition conditions, structural verification of damage tolerance has been obtained by means of actual tests of real structure containing artificial flaws of various lengths.

The growing interest in the establishment of more rational procedures to handle this problem is evidenced by the activity of various aerospace companies with their internal programs, and by their external interest in group activities such as those associated with the MIL-HDBK-5 working group and with ASTM Committee E-24.

This program has been focussed toward an examination of the effect of thickness and other geometric factors on fatigue-crack propagation and fracture of a structural aluminum alloy, 7075-T7351. Evaluation of the results of the experimental studies has been accomplished taking into account a number of suggested formulations in the literature.

The test program contained two series of tests. The first of these series was carried out on 8-inch wide panels in thicknesses from 1/16 to 1 inch. Fracture tests and a limited quantity of fatigue-crack-propagation tests were run. These tests were used primarily to select three thicknesses of material for the main body of tests. As a matter of interest, four thicknesses were selected for the main program: 1/16 inch, 1/4 inch, 1/2 inch, and 1 inch. The data and analysis from this initial series of tests are contained in Appendix A.

This report concerns itself primarily with the main program conducted on 7075-T7351 sheet and plate in the above four thicknesses.

PROGRAM DETAILS

Test Plan

It was decided to confine this program to a simulation of through-the-thickness flaws. Therefore, center-cracked panels were selected as the test specimen. In fracture testing particularly, the gross section stress at fracture is influenced by thickness, by crack aspect ratio*, and by panel width. The relationships among these three variables has been difficult to characterize, and, as a matter of fact, was the objective of this program.

* The crack aspect ratio is the ratio of crack length to panel width.

Therefore, the program plan involved compromises and decisions relative to these variables. Figure 1 is a graph of gross stress as a function of material thickness obtained from the initial tests described in Appendix A. This figure suggests that there is a maximum in this curve relating fracture stress and thickness which occurs between 1/8- and 3/8-inch thicknesses. The implications from the data are that fracture stress decreases for $t < 1/8$ inch and $t > 3/8$ inch, and that at about $t = 1$ inch, the fracture stress appears to be leveling out. It was on the basis of these results that test thicknesses of 1/16 inch, 1/4 inch, 1/2 inch, and 1 inch were selected.

The decision regarding panel width was somewhat more arbitrary; however, the decision was influenced by a data review of the wide-panel tests on other aluminum alloys. The aim was to provide at least one panel width where elastic fracture generally would occur. The actual decision was that three panel widths would be employed: 8 inches, 16 inches, and 36 inches. However, for the 1/16-inch sheet, only 8-inch-wide panels were tested.

The third variable evaluated was crack aspect ratio. For 8-inch- and 16-inch-wide panels, many crack aspect ratios were tested between 0.1 and 0.9. However, for 36-inch-wide panels, tests were confined to 2c/w values of 0.2, 0.5, and 0.8.

Fatigue-crack-propagation tests were conducted on 8-inch-wide-panels 1/16, 1/4, 1/2, and 1 inch thick as well as on 16- and 36-inch-wide panels 1/4, 1/2, and 1 inch thick. In all cases, the starter flaw was 0.5 inch long as described subsequently.

The decision in regard to fatigue test stresses was made on the basis that load ratio, R, had a measurable effect on crack propagation. Three mean stress levels and three alternating stress levels were selected for testing the 8-inch-wide panels to provide 9 different load ratios ranging from about 0.1 to 0.5. The maximum test stresses associated with the three mean and alternating stresses represented a range equivalent to about 30 to 50 percent of a nominal limit load stress of 32 ksi that is typical for a naval fighter aircraft.[1]* The actual mean stress levels were 6.8, 8.4, and 10.0 ksi. These stress levels were employed to provide fatigue-crack propagation data for moderately low rates of propagation. The 8-inch-wide panel test stresses were as follows:

(1) 6.8 ± 3.3 ksi
(2) 6.8 ± 4.4 ksi
(3) 6.8 ± 5.5 ksi
(4) 8.4 ± 3.3 ksi
(5) 8.4 ± 4.4 ksi
(6) 8.4 ± 5.5 ksi
(7) 10.0 ± 3.3 ksi
(8) 10.0 ± 4.4 ksi
(9) 10.0 ± 5.5 ksi

In the case of the 16- and 36-inch-wide panels, the stress cycles employed were the three described above, having $S_{mean} = 8.4$ ksi.

* References are listed on page 117.

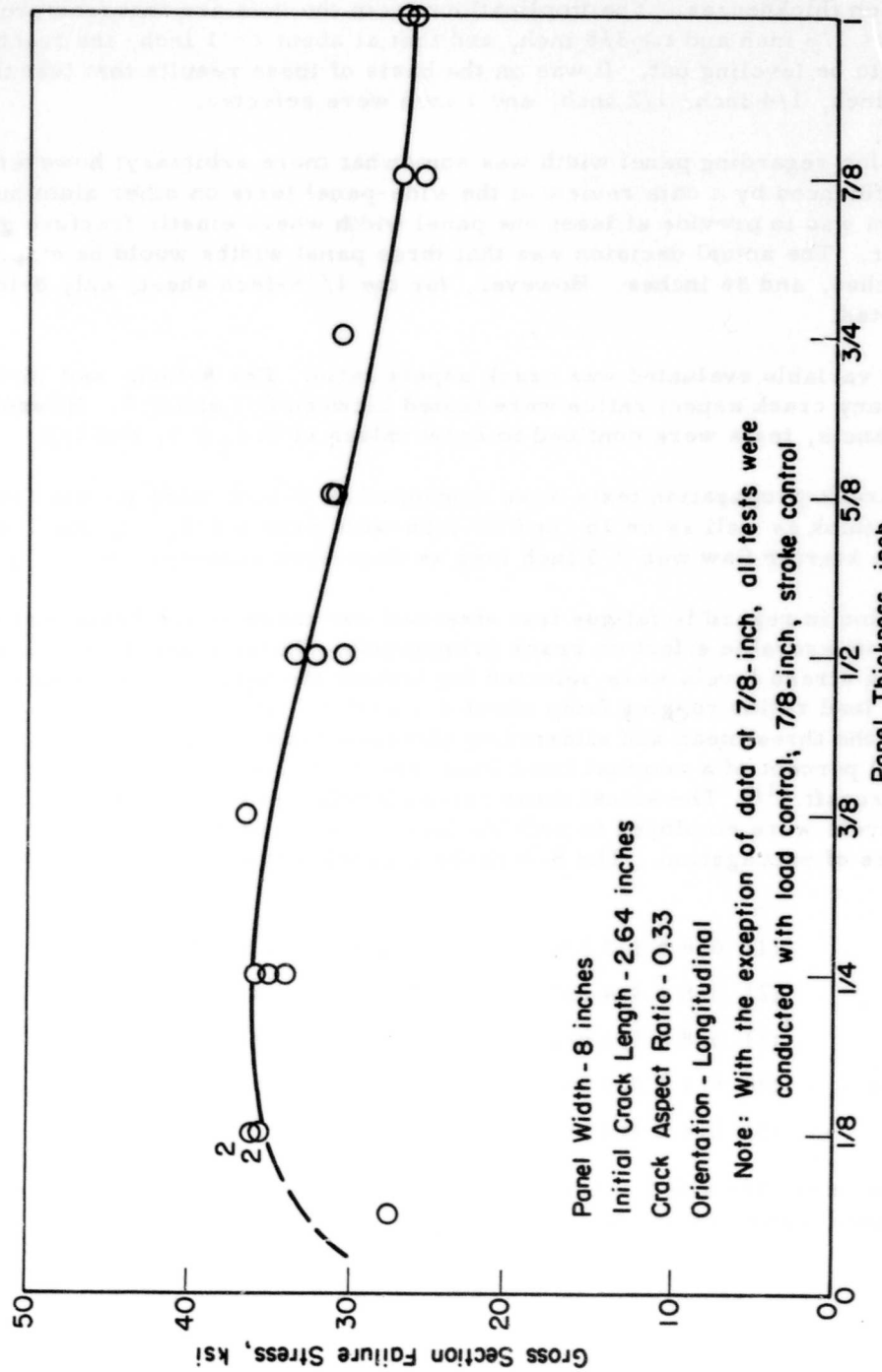

FIGURE 1. GROSS SECTION FRACTURE STRESS AS A FUNCTION OF PANEL THICKNESS

Specimen Preparation

Material

The 7075 aluminum alloy was selected for this program because it has been used considerably in the past in Navy fighter airplanes. The -T7351 heat treatment for 7075 provides somewhat greater toughness and increased stress-corrosion resistance than does the -T6 heat treatment. Purchased material was 7075-T651, and it was sent to the heat-treat source by the vendor as 8 x 32-inch, 16 x 48-inch, and 36 x 96-inch panels. Heat treatment to the 7075-T7351 condition was according to Alcoa Copy No. 78, Alcoa Alloy 7075-T73. This is an Alcoa Green Letter, published in August, 1965. According to the letter, the range of electrical conductivity for this alloy is 38 to 42 percent IACS. A confirmation test showed the conductivity to be actually 40 to 41 percent IACS. Table 1 shows the results of tensile tests performed at Battelle. On the basis of conductivity measurements and tensile tests and the microstructures in Figure 2, it was concluded that the material was 7075-T7351.

Specimen Configuration and Machining

The basic specimen is shown in Figure 3, and the flaw details are given in Figure 4. As noted in Figure 4, the initial flaw is located at the center of the specimen blank. Specimen blanks were sectioned so that the rolling direction was in the direction of loading. Grip and hole patterns for the 8-inch-wide specimens varied somewhat depending on the thickness since several tests machines were used as a consequence of test-load requirements. This was also the case for the 16-inch-wide specimens. For the 8- and 16-inch-wide specimens, the ratio of the test length between grips to the specimen width was 1.5; for the 36-inch-wide specimen, the ratio was 1.75.

Fabrication of specimens at Battelle consisted of drilling grip end holes and machining the starter flaw, since the finished width and length dimensions were established by the supplier. Grip and holes were drilled with the specimens clamped together. Figure 5 shows this operation being carried out for the 1/2-inch-thick, 36-inch-wide specimens. The preparation of the initial flaw, however, was done on each specimen separately. This involved first drilling a hole 0.250 inch in diameter at the center of the specimen. Then the EDM flaw was machined to the dimensions shown in Figure 4. Figure 6 shows this operation in process for a 1-inch-thick, 36-inch-wide specimen.

For the fatigue-crack-propagation specimens, the above operations essentially completed the specimen preparation. However, for the fracture tests, the starter flaw was extended by saw cut to within about 0.8 inch of the required length. As described in a later section, the crack was extended to the test length by fatigue cracking.

Procedures

Apparatus

All testing was accomplished in electrohydraulic servo-controlled machines. Four machines were used, the choice depending upon load requirements and to some extent upon specimen width and thickness. These four machines had dynamic-load

TABLE 1. VERIFICATION TEST DATA FOR TENSILE PROPERTIES OF 7075-T7351 ALUMINUM ALLOY

Specimen	Thickness, in.	0.2 Percent Yield Strength, psi	Ultimate Tensile Strength, psi
1	0.0608	58,300	69,600
2	0.0610	57,900	69,600
3	0.0610	58,800	69,800
4	0.0610	58,400	69,900
5	0.0610	57,800	69,900
Average		58,240	69,700
1	0.2572	60,700	72,000
2	0.2572	60,300	71,900
3	0.2572	60,300	72,000
4	0.2570	60,400	71,900
5	0.2572	60,600	72,000
Average		60,460	71,960
1	0.506	62,700	72,600
2	0.506	61,800	72,500
3	0.5055	62,000	72,600
4	0.5052	62,000	72,600
5	0.506	62,000	73,200
Average		62,100	72,700
1	1.004	61,100	71,600
2	1.0045	61,000	71,400
3	1.004	61,100	71,800
Average		61,066	71,600
1	1.2585	61,700	71,600
2	1.260	61,600	71,400
3	1.258	62,000	71,800
Average		61,766	71,600

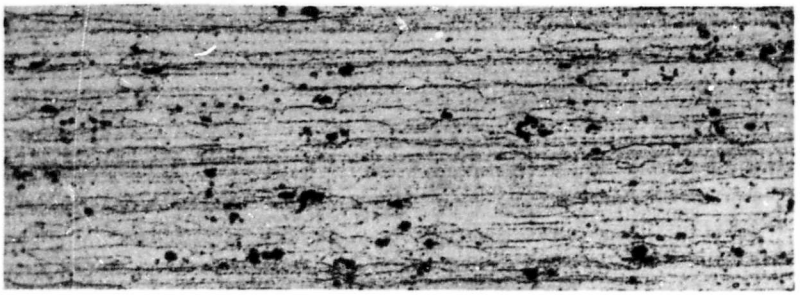

a. 0.0025-Inch Sheet

2E945

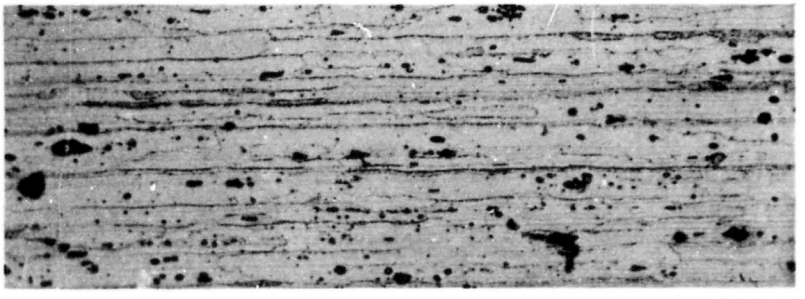

b. 0.250-Inch Plate

2E944

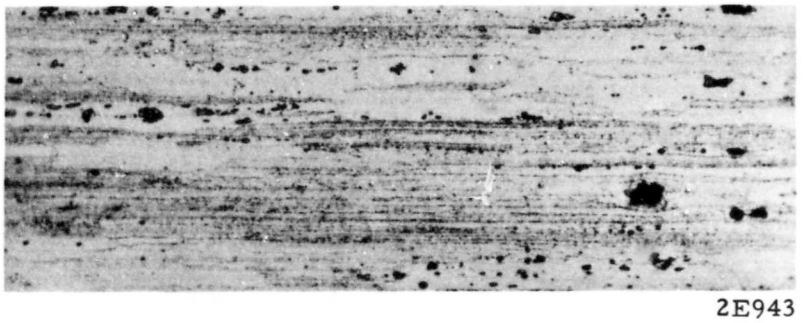

c. 0.500-Inch Plate

2E943

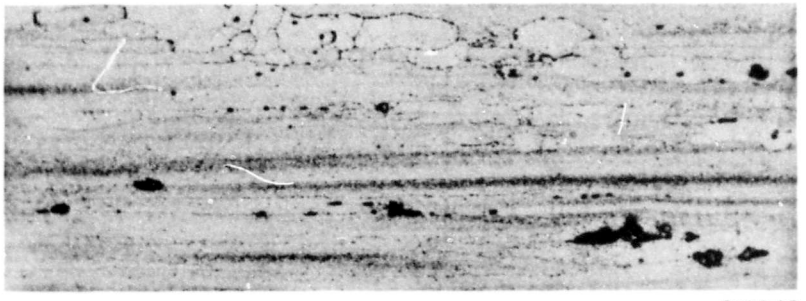

d. 1.0-Inch Plate

2E942

FIGURE 2. TYPICAL MICROSTRUCTURE OF 7075-T7351 ALUMINUM ALLOY
Magnification: 250X.

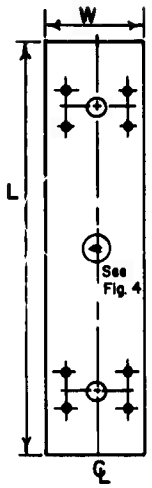

W	L
8	32
16	48
36	96

FIGURE 3. SPECIMEN CONFIGURATION

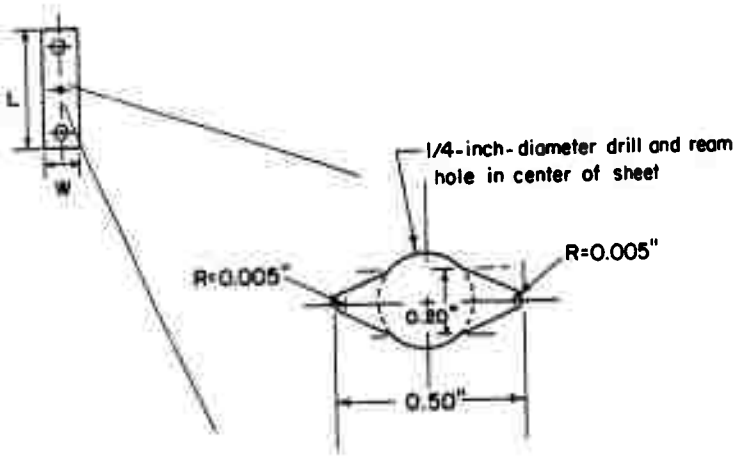

FIGURE 4. DETAILS OF INITIAL EDM FLAW

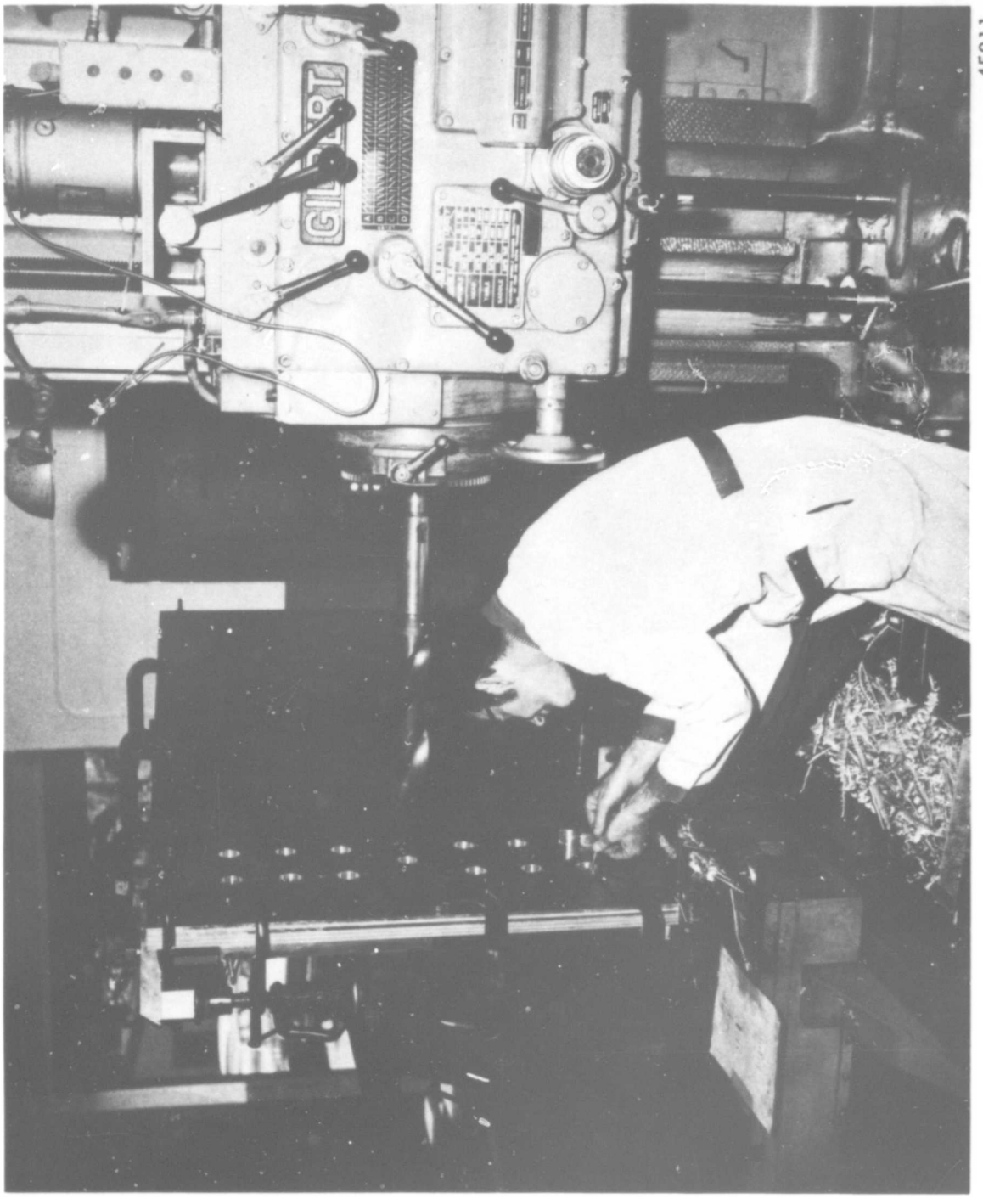

45911

FIGURE 5. MACHINING OF GRIP END HOLES IN 36-INCH-WIDE SPECIMENS

45435

FIGURE 6. EDM OPERATION ON 1-INCH-THICK, 36-INCH-WIDE SPECIMEN

capacities ranging from 25 kip to 500 kip. All tests were conducted in a controlled laboratory environment of 70 F and a relative humidity of 50 ± 10 percent. Cycling rates for the fatigue-crack-propagation tests varied between 10 and 25 cps after a few tests showed that in this limited range there did not appear to be a frequency effect.

Crack-Propagation Procedures

Fatigue-crack propagation measurements were performed optically. A plastic film prepared photographically was centered on the EDM flaw. The film had an embossed grid with 0.05-inch spacing in the central 2 inches and 0.10-inch spacing for the remainder of the width. Various short-distance viewing telescopes were used, and a remote counter was employed to provide a cycle reading when the crack had propagated to a given length.

A strobo-slave light was integrated into the electronic circuit of each test machine which was triggered at the peak load of each cycle. Thus, it was not necessary to stop the test to get an accurate measurement of crack length. By triggering at peak load, the crack movement was frozen at the time of maximum crack opening. Figures 7 and 8 show one setup in the 500-kip machine where guide plates were not used. However, to prevent out-of-plane buckling, strip-type guide plates were positioned on either side of the flaw for all crack-propagation tests and fracture tests on the 1/16- and 1/4-inch-thick specimens and on the 1/2-inch-thick, 36-inch-wide specimens.

Crack-propagation measurements were taken on 8-inch-wide panels to about 6 inches' length; on 16-inch-wide panels to about 8 to 10 inches; and on 36-inch-wide panels to about 10 to 12 inches. Upon completion of each test, the fracture surface was examined for significant facets.

Fracture Test Procedures

For the fracture tests, the EDM slot shown in Figure 7 was extended by saw cut to within 0.8 inch of the desired crack length. The last 0.8 inch of crack length was introduced by fatigue cycling at stress levels that would result in a stress intensity about half that expected in the test. About 50,000 fatigue cycles were required.

After the fatigue crack was completed, a plastic grid was taped below the plane of the crack and a compliance gage was inserted into the crack opening as shown in Figure 9. This gage is a double-cantilever clip gage to measure crack-opening displacement (COD) during the fracture tests. The gage was constructed from 17-7PH stainless steel and had a bridge of four active electrical-resistance strain gages.

The compliance gage output was the X-axis input to an X-Y recorder, with the Y-axis recording load. Thus, from the load-COD trace, the significant events could be determined. In addition, movies were taken during slow growth and fracture at about 128 frames per second. These two records comprise the information used in the fracture-data analysis.

As with the fatigue-crack-propagation specimens, fracture surfaces were examined to observe salient features.

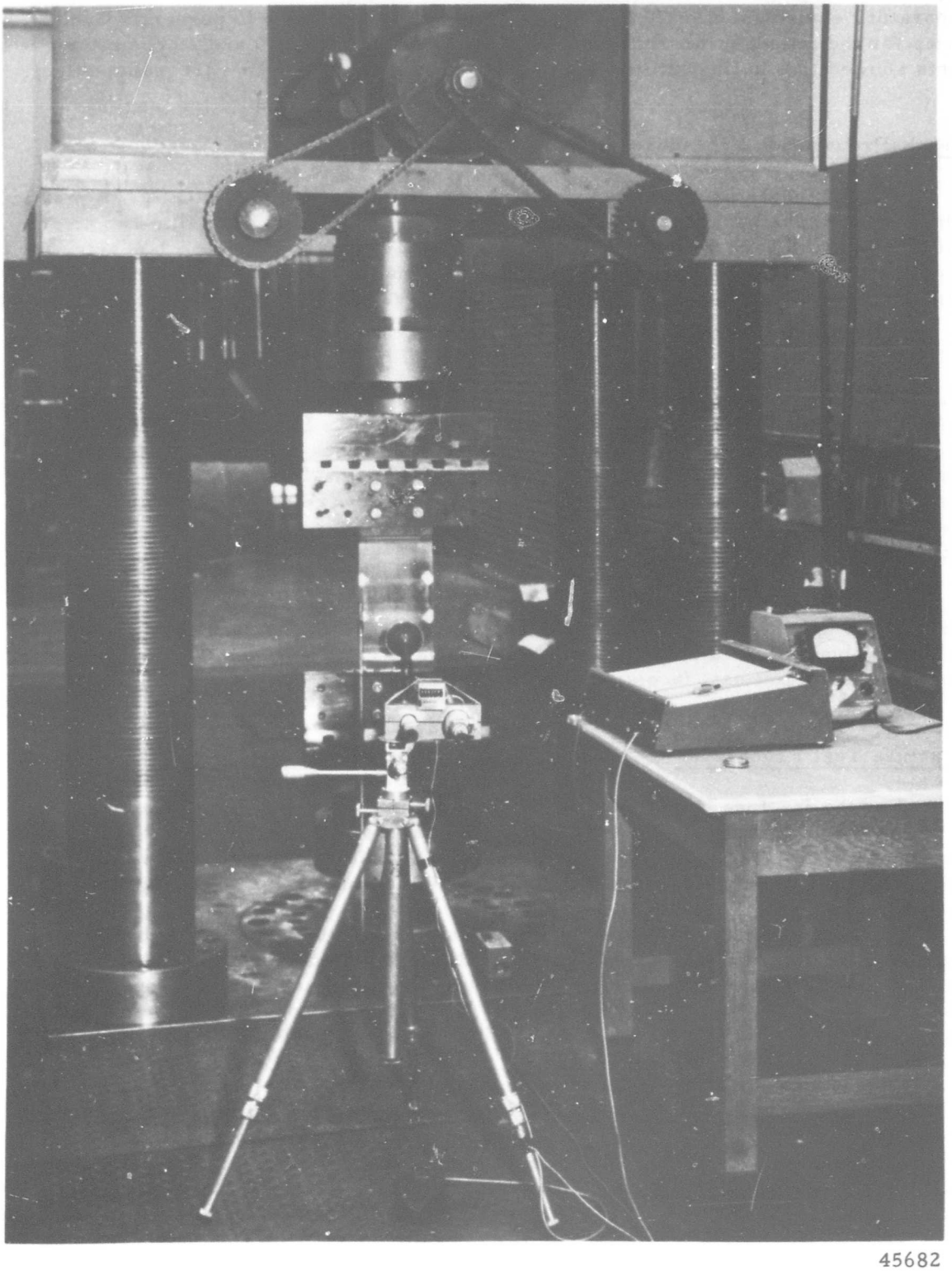

45682

FIGURE 7. EXPERIMENTAL SETUP FOR FATIGUE-CRACK-PROPAGATION STUDIES

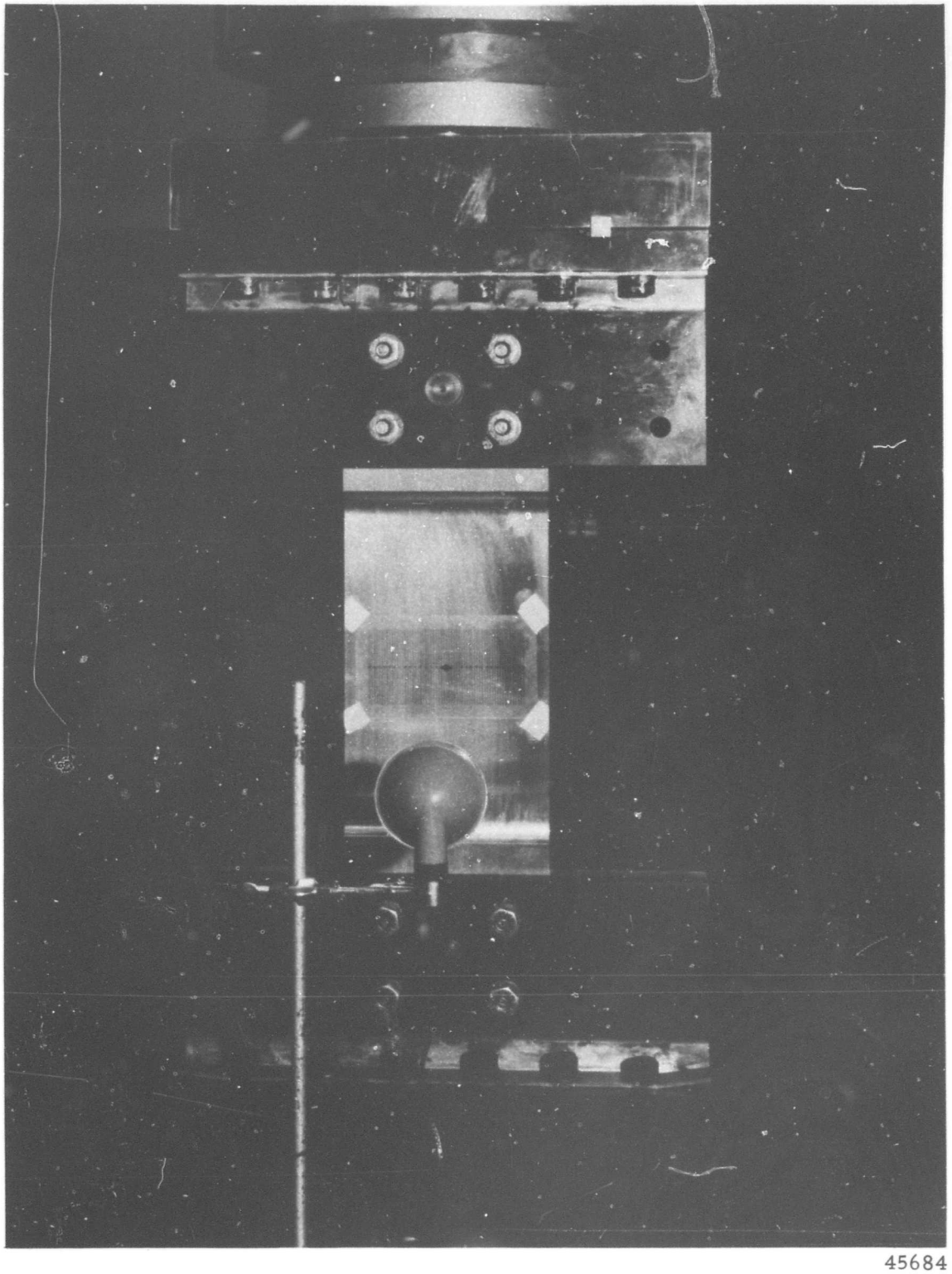

45684

FIGURE 8. CENTER-NOTCHED SPECIMEN WITH PLASTIC GRID AND STROBO-SLAVE SETUP FOR FATIGUE-CRACK-PROPAGATION STUDY

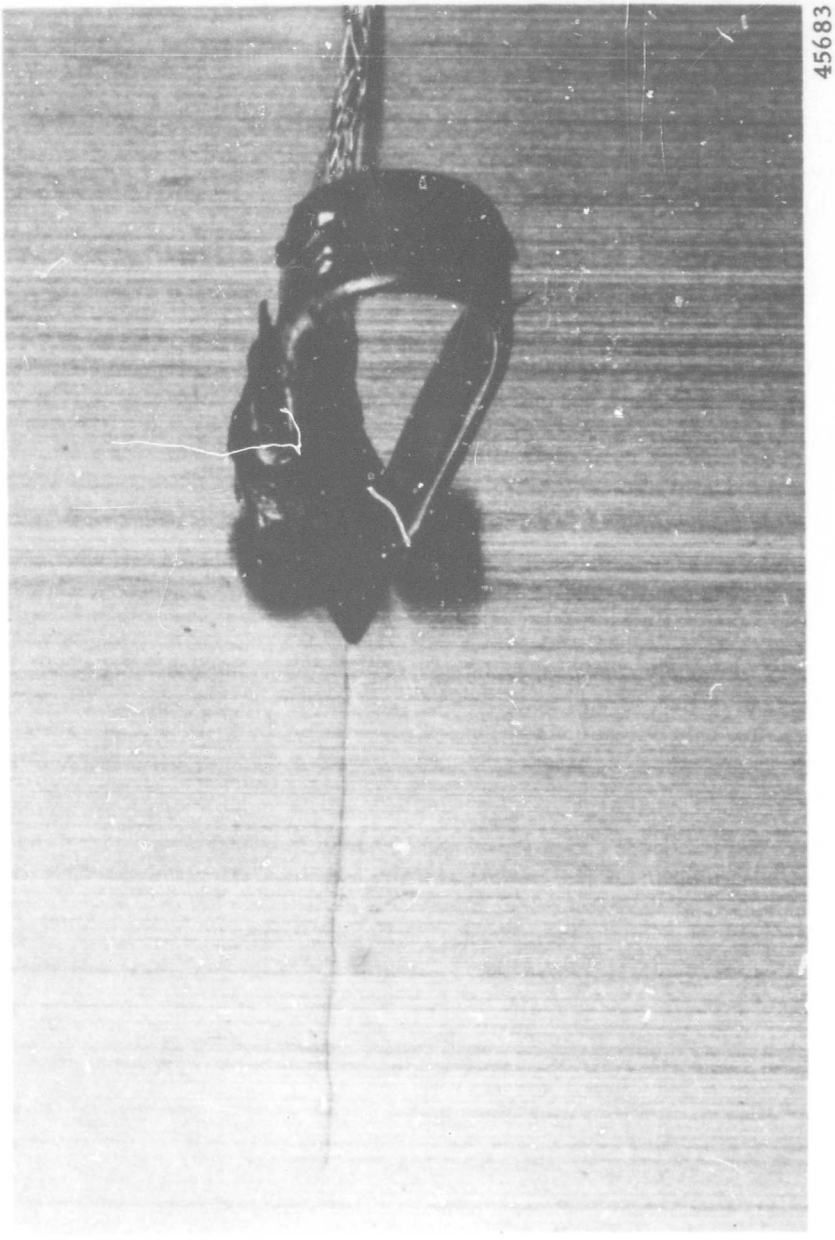

45683

FIGURE 9. COMPLIANCE GAGE IN POSITION TO RECORD CRACK-OPENING DISPLACEMENT DURING FRACTURE TEST

EXPERIMENTAL RESULTS

Fracture Data

Data Presentation

The basic fracture data derived in this program are presented in Tables 2 through 5. The data format is based on the typical load-compliance record illustrated in Figure 10.

Following the specimen-identification column are the thickness, T, and width, W, columns denoting the measured gross dimensions of the critical section of the respective specimens. Next is the initial crack length, $2c_o$, denoting the initial fatigue-crack length existing prior to the rising-load fracture test. The two following columns list alternative measures of the threshold stress associated with the onset of slow crack growth. First is the pop-in stress, S_2, which is identified by a distinct horizontal offset on the load compliance and an audible "pop". This characteristic stress or load behavior is frequently elusive to identify or is even nonexistent in the thin sheet materials. It is identified here only when it was positively recognized. The second measure of threshold stress for slow crack growth is the 5 percent secant offset stress, S_3, which is a graphical approximation[2] to the crack-growth threshold. Because the mechanical determination of the latter stress (S_3) is more reproducible, it is the threshold stress that is used with the initial crack length to define initiation of crack growth. The pop-in value, S_2, is presented only for comparative purposes and is noted to be sparsely distributed among test specimens.

The last two columns identify the maximum load conditions. The final crack length, $2c_c$, is the last measurable crack length prior to fracture as determined from the photographic record. The maximum load stress, S_1, is the stress at maximum load associated with fracture or "rapid" crack propagation.

Graphical Displays

From the above data, the basic stress-flaw size relationship is graphically illustrated in Figure 11. There are two sets of points on these figures corresponding to two events in the fracture test that have some significance. The first of these is onset of slow crack growth associated with the 5 percent offset stress, S_3, in the tables (identified on the graph by triangular symbols). The second event is identified with onset of rapid crack propagation (fracture at maximum stress, S_1) and is shown by the open circles. The coordinates on each figure are gross stress, S, as the ordinate, with crack aspect ratio 2c/w as the abscissa. The initial crack length, $2c_o$, is paired with the 5 percent offset stress, S_3, and the critical crack length, $2c_c$, is paired with the maximum stress, S_1.

Initial Observations

Although the subsequent data analysis in another section of this report will refine and mold the conclusions of this task, it is important to recognize certain indicators immediately apparent within the data compiled.

TABLE 2. FRACTURE DATA FOR 1/16-INCH-THICK 7075-T73 ALUMINUM ALLOY SHEET

Specimen	Thickness, T, in.	Width, W, in.	Initial Crack, $2c_o$, in.	Pop-In Stress, S_2, ksi	5% Secant Offset Stress, S_3, ksi	Final Crack, $2c_c$, in.	Maximum Stress, S_1, ksi
57	0.062	8.00	0.78	--	30.2	1.40	45.9
58	0.062	8.00	1.60	35.7	24.2	1.95	38.7
59	0.061	8.00	2.35	16.0	20.5	3.55	33.8
60	0.060	8.00	3.17	--	16.5	4.20	27.7
61	0.061	8.00	3.97	--	16.4	5.00	23.8
62	0.061	8.00	4.76	--	10.3	5.62	18.4
63	0.061	8.00	5.55	7.9	11.3	6.08	13.3
64	0.060	8.00	6.40	--	6.0	6.60	9.1
65	0.061	8.01	7.28	--	3.0	7.38	4.0

TABLE 3. FRACTURE DATA FOR 1/4-INCH-THICK 7075-T7351 ALUMINUM ALLOY PLATE

Specimen	Thickness, T, in.	Width, W, in.	Initial Crack, $2c_o$, in.	Pop-In Stress, S_2, ksi	5% Secant Offset Stress, S_3, ksi	Final Crack, $2c_c$, in.	Maximum Stress, S_1, ksi
28	0.254	8.04	0.77	--	27.7	1.80	46.8
29	0.258	8.04	1.22		27.7	--	43.4
30	0.257	8.04	1.66		31.3	2.90	39.3
31	0.258	8.04	2.00		27.2	3.00	36.3
32	0.258	8.04	2.47		20.0	3.40	33.7
33	0.253	8.00	2.86		19.3	3.80	30.6
34	0.255	8.03	3.23		18.5	4.45	28.2
35	0.257	8.03	3.65		16.7	4.90	25.2
36	0.259	8.04	4.01		17.5	5.05	23.0
37	0.256	8.04	4.35		12.9	5.10	20.8
38	0.256	8.03	4.87		11.4	5.60	17.8
39	0.255	8.05	5.23		10.2	5.85	15.5
41	0.255	8.03	5.65		9.2	6.00	13.6
43	0.260	8.02	6.00		8.2	--	11.5
44	0.253	8.02	6.42		6.8	6.60	8.5
45	0.257	8.03	6.69		7.0	7.00	7.4
46	0.260	8.03	7.27		4.0	7.30	4.7
47	0.255	8.04	7.66		1.8	--	1.9
48	0.252	15.90	1.58		23.5	2.30	45.3
49	0.252	15.95	3.16		19.9	--	35.8
50	0.252	15.91	4.84		19.3	7.00	31.3
51	0.252	16.02	6.47		23.0	8.60	24.8
52	0.251	15.90	8.15		14.6	10.20	19.7
53	0.253	15.91	9.56		12.0	10.85	16.3
54	0.248	15.92	11.45		8.9	13.50	11.4
55	0.252	15.91	12.93		6.2	--	8.0
56	0.252	15.88	14.50		3.0	14.70	3.7
89	0.259	36.12	7.35		17.4	9.25	25.9
90	0.259	36.12	18.00		10.2	24.88	15.0
91	0.253	36.12	28.83	--	4.5	33.10	7.8

TABLE 4. FRACTURE DATA FOR 1/2-INCH-THICK 7075-T7351 ALUMINUM ALLOY PLATE

Specimen	Thickness, T, in.	Width, W, in.	Initial Crack, $2c_o$, in.	Pop-In Stress, S_2, ksi	5% Secant Offset Stress, S_3, ksi	Final Crack, $2c_c$, in.	Maximum Stress, S_1, ksi
1	0.504	8.01	1.63	--	20.3	1.85	35.5
2	0.507	8.02	0.82	--	30.6	--	46.1
3	0.505	8.11	2.40	18.9	16.7	3.45	32.2
4	0.506	8.02	3.17	20.0	15.0	3.85	27.2
5	0.507	8.10	4.07	--	16.1	5.08	21.2
6	0.506	8.11	4.84	--	9.8	5.50	17.7
7	0.502	8.00	5.63	--	8.1	5.90	12.1
8	0.508	8.12	6.45	--	5.8	6.50	8.0
9	0.508	8.12	6.07	--	6.9	--	10.4
10	0.503	8.00	5.25	--	8.7	5.42	14.3
11	0.502	8.01	4.47	--	11.7	4.60	19.0
12	0.508	8.11	3.61	--	13.4	4.20	23.4
13	0.501	8.01	2.86	--	15.0	3.42	27.2
14	0.507	8.13	2.03	--	24.8	--	35.0
15	0.506	8.11	1.22	21.9	33.1	--	43.4
16	0.501	8.00	6.90	--	5.1	6.95	6.2
17	0.507	8.02	7.34	--	2.6	--	3.9
18	0.506	8.11	1.65	--	21.3	2.20	39.2
19	0.508	8.10	3.15	16.9	16.8	5.00	27.2
20	0.507	8.13	4.75	9.9	10.8	4.95	16.9
21	0.508	8.14	1.61	--	26.0	2.45	38.9
23	0.502	8.01	3.14	--	16.5	4.15	27.3
24	0.508	8.09	3.98	--	15.6	4.50	23.4
25	0.501	7.96	2.43	16.8	18.6	3.25	30.2
27	0.507	8.11	3.27	--	15.4	3.90	25.2
66	0.505	16.10	1.58	--	22.8	5.73	41.0
67	0.498	16.10	3.10	13.2	18.7	6.34	35.5
68	0.504	16.10	4.80	15.7	--	9.84	27.4
69	0.504	16.09	6.35	--	15.4	11.09	21.5
70	0.503	16.10	8.25	--	11.0	10.16	19.9
71	0.508	16.12	11.20	--	7.95	13.10	12.5
72	0.500	16.09	12.90	--	5.6	13.16	8.3
73	0.506	16.09	14.20	--	3.44	15.57	5.2
86	0.497	36.07	7.31	--	--	--	15.1
87	0.479	36.05	18.14	2.8	7.2	26.35	8.5
88	0.486	36.01	28.80	--	3.1	--	3.7

TABLE 5. FRACTURE DATA FOR 1-INCH-THICK 7075-T7351 ALUMINUM ALLOY PLATE

Specimen	Thickness, T, in.	Width, W, in.	Initial Crack, $2c_o$, in.	Pop-In Stress, S_2, ksi	5% Secant Offset Stress, S_3, ksi	Final Crack, $2c_c$, in.	Maximum Stress, S_1, ksi
92	1.006	8.07	1.50	21.1	--	1.70	24.9
93	1.010	8.03	4.01	14.7	--	4.27	16.4
94	1.009	8.06	6.31	7.1	--	6.47	7.6
74	1.008	16.03	1.80	--	19.2	2.20	25.9
75	1.007	16.03	3.30	--	14.6	4.50	21.4
76	1.007	16.03	4.73	--	12.7	5.20	17.3
77	1.017	16.03	6.43	7.4	10.7	6.60	15.3
78	0.995	16.05	8.04	--	9.9	8.09	14.0
79	1.012	16.09	9.60	8.9	9.1	9.60	10.5
80	1.004	16.05	11.07	--	6.8	11.07	7.1
81	1.014	16.05	12.75	--	4.2	13.15	5.3
82	1.016	16.05	14.42	--	2.1	--	2.5
83	1.026	36.12	7.11	--	--	9.48	17.0
84	1.017	36.13	17.00	--	7.9	19.16	10.2
85	1.011	36.19	28.90	--	3.7	31.16	4.2

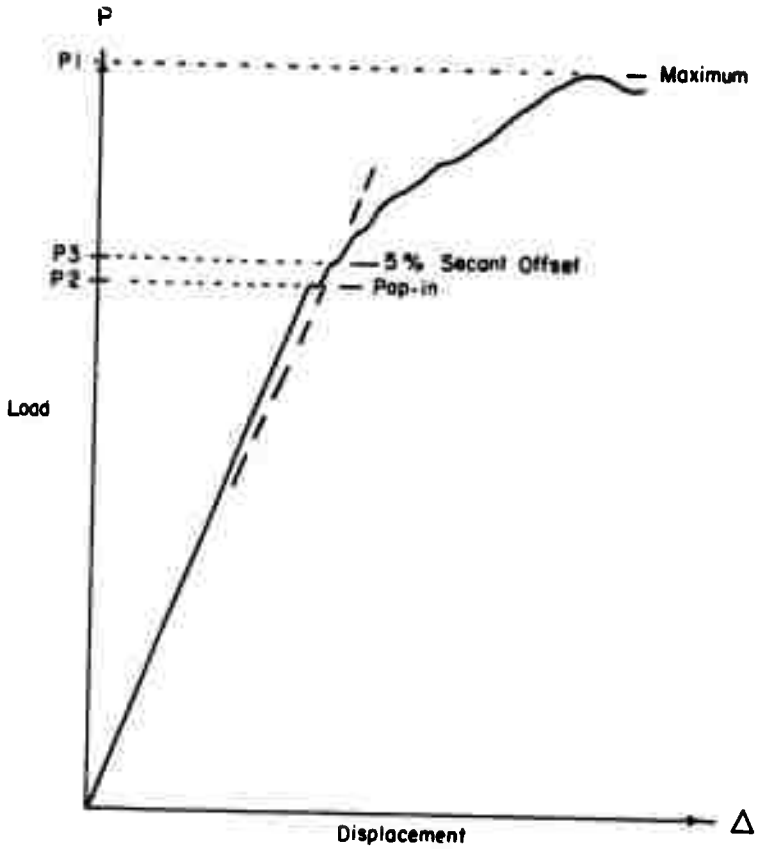

FIGURE 10. LOAD LEVELS OF INTEREST SHOWN ON A TYPICAL LOAD-COMPLIANCE RECORD

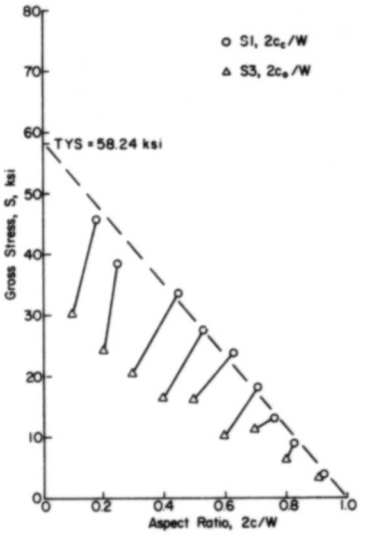

a. t = 1/16 Inch, w = 8 Inches

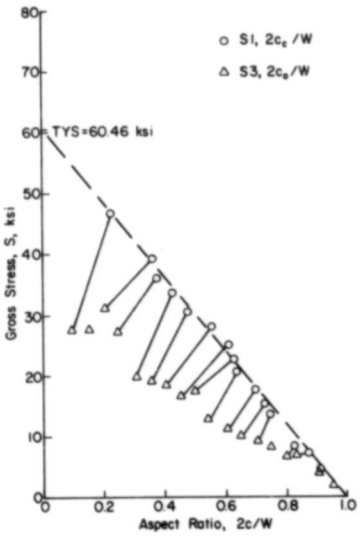

b. t = 1/4 Inch, w = 8 Inches

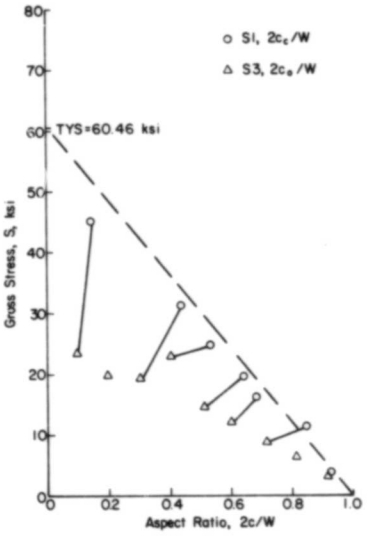

c. t = 1/4 Inch, w = 16 Inches

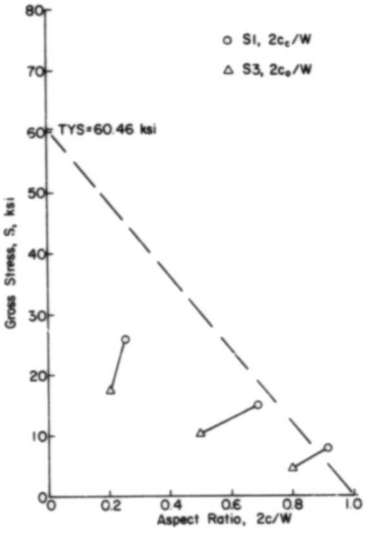

d. t = 1/4 Inch, w = 36 Inches

FIGURE 11. FRACTURE DATA FOR 7075-T7351 ALUMINUM ALLOY

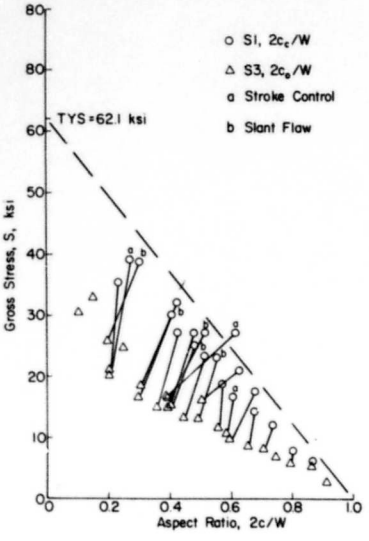

e. t = 1/2 Inch, w = 8 Inches

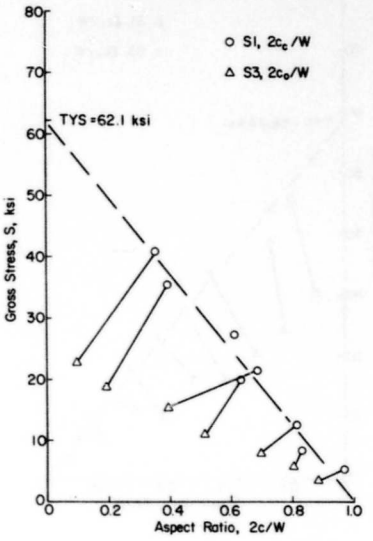

f. t = 1/2 Inch, w = 16 Inches

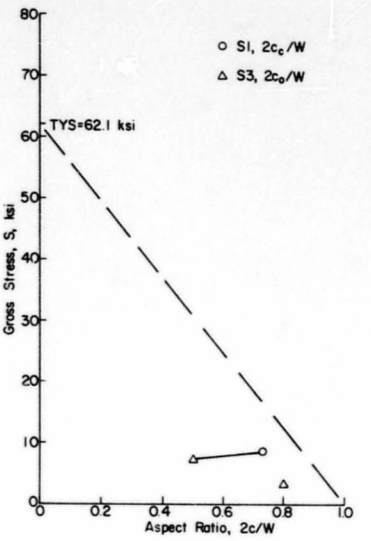

g. t = 1/2 Inch, w = 36 Inches

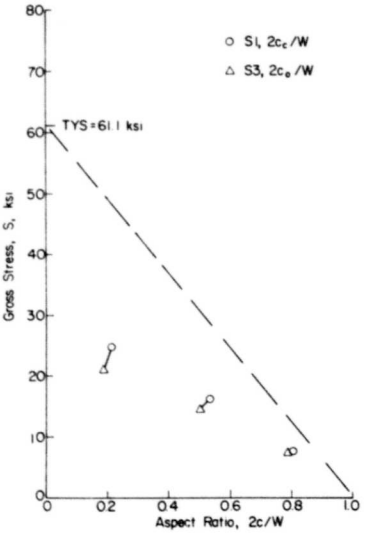

h. t = 1.0 Inch, w = 8 Inches

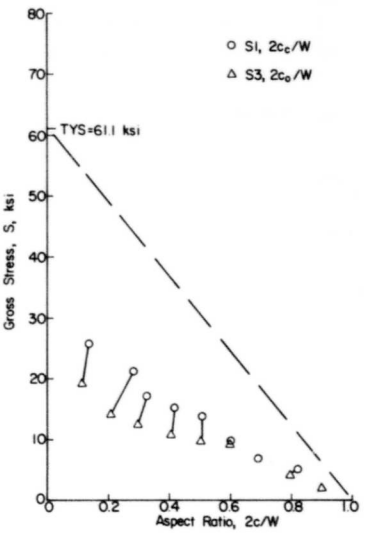

i. t = 1.0 Inch, w = 16 Inches

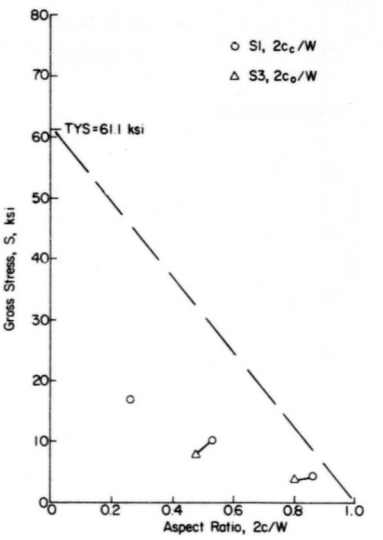

j. t = 1.0 Inch, w = 36 Inches

FIGURE 11. (CONTINUED)

First note an important graphical detail on the stress/aspect-ratio plots of Figure 11. A negatively sloping straight line passing through the coordinate point (2c/w = 1.0, S = 0), i.e., the right-hand graphical limit, and intersecting the ordinate (S-axis) line is a line of constant net section stress. That is, it is the locus of points whose product

$$S(1 - 2c/w) = S_n$$

is constant. The magnitude of the net section stress is the value of the ordinate intercept. Thus, the limiting dashed line passing through TYS on each figure is the net section yield (NSY) line.

In this fashion, one can readily observe in each of the figures that the threshold condition of flaw growth appears to occur at a net section stress of one-half of TYS or less. Furthermore, the threshold appears to decrease with increasing thickness, which is consistent with thickness or stress-state transition effect. Specifically, it is noted that for the 1/16- and 1/4-inch-thick material, the threshold occurs at a net section stress of one-half of TYS. For the 1/2- and 1-inch-thick material, it appears to be about one-third of TYS.

The next important observations are the conditions of fracture or critical flaw propagation. For the 1/16-, 1/4-, and 1/2-inch-thick material, critical-fracture conditions appear to fit a net section yield criterion (the tensile instability condition) for widths up to 16 inches. In contrast, the 36-inch-wide specimens appear to exhibit something significantly less than this. The implication is that the increased width serves to influence the basic stress state as well as to alter boundary effects. The 1-inch-thick material in all widths tested appears to exhibit an energy instability, i.e., elastic net section stresses.

Failure Surfaces of Fracture-Test Specimens

The surface appearance of the failed sections of the fracture-test specimens can be categorized very simply. The 1/16-, 1/4-, and 1/2-inch-thick specimens failed in a full-shear mode (with either a 45-degree slant or vee profile); the 1-inch-thick specimens failed in a flat mode. In both cases, four distinct zones can be recognized. This is more fully detailed in the following paragraph.

Consider Figure 12(a) which illustrates schematically the typical full-shear fracture surface observed on this program. Zone I is the starter flaw surface, either an EDM or a sawed-notch surface. Zone A is the fatigue-cracked surface generated as the initial flaw for the fracture test. This surface exhibited a variation in texturing visible to the naked eye. A very smooth and satiny surface was noted for apparent maximum stress-intensity factors (SIF) less than 20 ksi-inch $^{1/2}$. Increased graininess was noted with an increase in the maximum fatiguing SIF. This also increased the tendency for slanting of the initial flaw plane. Zones B and C are the surfaces developed during slow growth and final rapid fracture. Zone B is that transitional zone between the nearly flat initial flaw and the full-shear surface. No particular preference for 45-degree shear or vee shear was noted. The singular difference was that the tongue length for 45-degree shear was about 3t, whereas that for vee shear extended to about 5t.

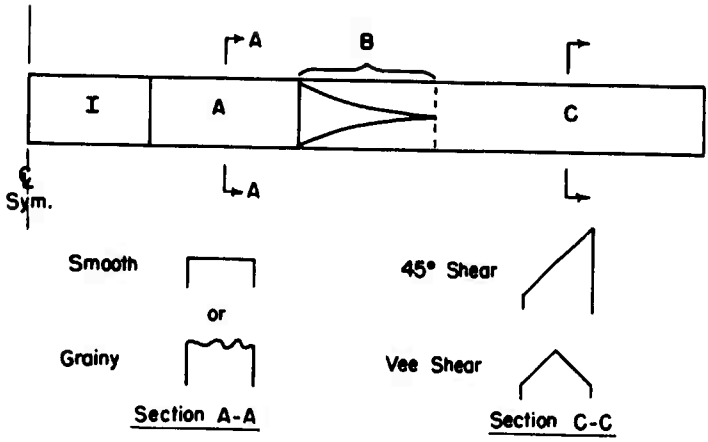

a. Typical Fracture Surface Zones on 1/16, 1/4, and 1/2-inch-Thick Specimens

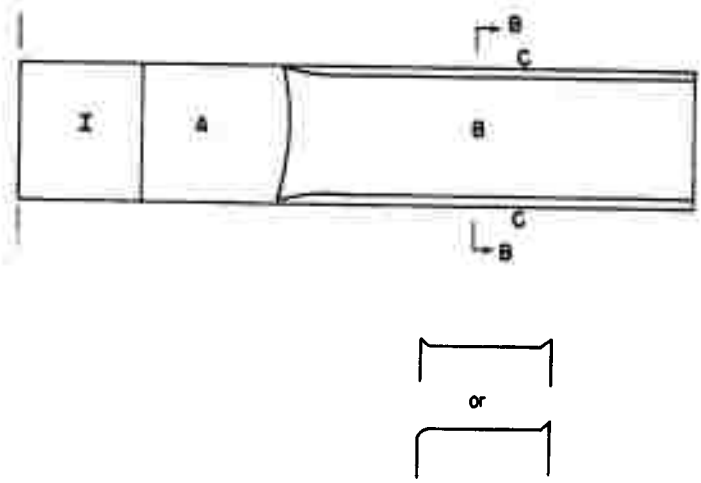

b. Typical Fracture Surface Zones on 1-inch-Thick Specimens

FIGURE 12. SCHEMATIC DIAGRAM OF FRACTURE SURFACES

The flat fracture characteristic of the 1-inch-thick plate is illustrated in Figure 12(b). Zones I and A are quite similar to those noted for the thinner plate and sheet. However, Zone B was very flat with a slight chevron pattern extending over the width. A small 45-degree, shear lip, Zone C, occurred along each surface for about 5 percent of the thickness.

Fatigue-Crack-Propagation Data

Data Presentation

Because the test machines are hydraulic in nature, their maximum operating frequency is a function of the specimen deflection under load. Since different loads are required for the thickness range tested, different machine response was anticipated. For these reasons, it was concluded that a constant test frequency could not practically be employed. Thus, four tests were conducted to determine whether there was a significant frequency effect over the frequency range of interest. Figure 13 shows the basic data plotted as crack length versus kilocycles. Two different test conditions were studied at the frequencies noted on the figure. For two of the specimens, the frequency was changed during the test, as noted on Figure 13. No consistent trend relating to frequency is observed in the data.

The fatigue-crack-propagation measurements are summarized in Tables 6 through 15. In each of these tables are listed in a vertical array instantaneous crack length, 2c, and lifetime, N, for each specimen tested. Immediately under the specimen number are given numerical values in ksi of the test stress cycle. At the bottom of each vertical array of data are listed three quantities for each specimen. N_f is the total number of cycles to cause failure of the specimen. The quantities $2c_{fs}$ and $2c_{fc}$ are crack lengths measured on the fracture surface after failure. Since the crack front indicated more rapid crack propagation in the center of the cross section in comparison with the surface, both measurements were made. $2c_{fc}$ is the crack length taken along the center of the cross section. $2c_{fs}$ is the average of two measurements taken, one on each side of the specimen, and represents the length of the crack at the surface. This latter length always was smaller than the value of $2c_{fc}$, except for the 1/16-inch-thick specimens. For 1/16-inch specimens, the crack front was essentially straight.

Tables 6, 7, 8, and 9 list data on 8-inch wide specimens of 1/16-, 1/4-, 1/2-, and 1-inch thickness, respectively.

Tables 10, 11, and 12 list data on 16-inch-wide specimens of 1/4-, 1/2-, and 1-inch thickness, respectively.

Tables 13, 14, and 15 list data on 36-inch-wide specimens of 1/4-, 1/2-, and 1-inch thickness, respectively.

The data from Tables 6 through 15 also are plotted in Figures 14 through 23. On each of these figures, fatigue crack length is the ordinate and number of cycles is the abscissa. Each figure page contains data for three specimens of one sheet thickness, panel width, and mean stress. The variable among the three specimens is alternating stress. The open symbols represent the test data. The solid symbols will be described in detail in a subsequent section. Through the data points for each specimen is drawn

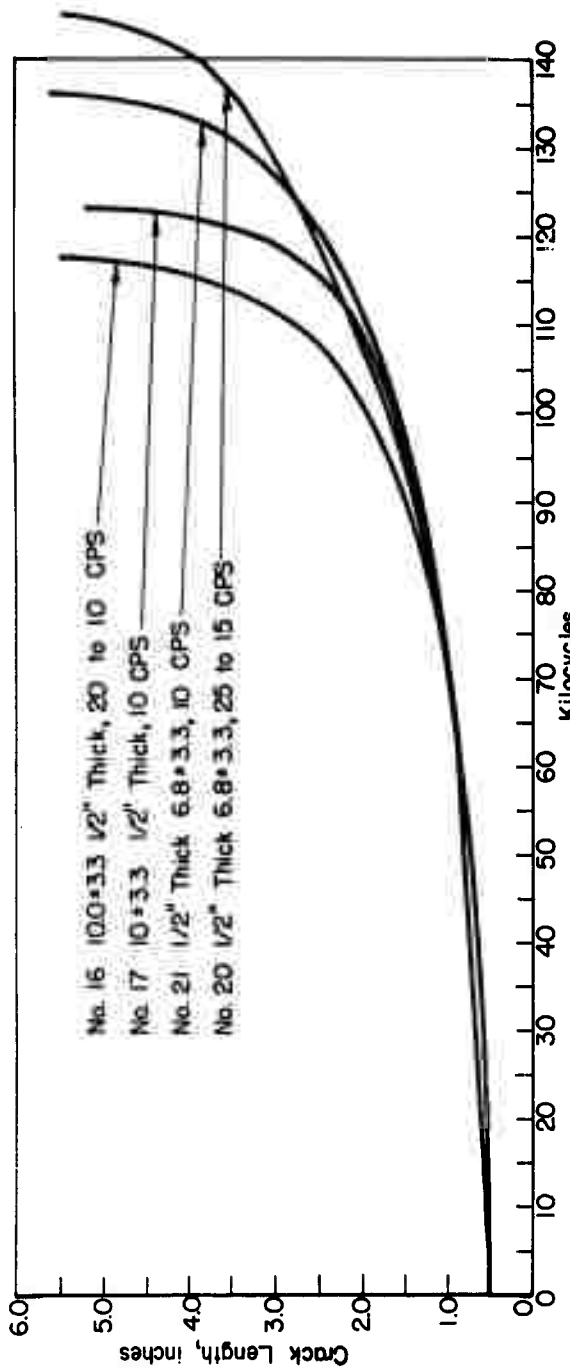

FIGURE 13. DATA SHOWING THE INFLUENCE OF FREQUENCY FOR 1/2-INCH-THICK 7075-T7351 TESTED AT TWO DIFFERENT STRESS LEVELS

TABLE 6. FCP MEASUREMENTS FOR 1/16-INCH THICK, 8-INCH-WIDE PANELS

Specimen 46 6.8 ± 3.3 ksi		Specimen 42 6.8 ± 4.4 ksi		Specimen 43 6.8 ± 5.5 ksi		Specimen 53 8.4 ± 3.3 ksi		Specimen 41 8.4 ± 4.4 ksi		Specimen 55 8.4 ± 5.5 ksi		Specimen 44 8.4 ± 5.5 ksi		Specimen 39 10.0 ± 3.3 ksi		Specimen 52 10.0 ± 3.3 ksi		Specimen 54 10.0 ± 4.4 ksi		Specimen 56 10.0 ± 5.5 ksi	
$2c_i$, in.	N_f, kc	$2c_i$, in.	N_f, kc	$2c_i$, in.	N_f, kc	$2c_i$, in.	N_f, kc	$2c_i$, in.	N_f, kc	$2c_i$, in.	N_f, kc	$2c_i$, in.	N_f, kc	$2c_i$, in.	N_f, kc	$2c_i$ in.	N_f, kc	$2c_i$ in.	N_f, kc	$2c_i$ in.	N_f, kc
0.50	--	0.50	--	0.50	--	0.50	--	0.50	--	0.50	--	0.50	--	0.50	--	0.50	--	0.50	--	0.50	--
0.60	37.30	0.80	32.04	0.60	40.40	0.60	19.21	0.70	23.00	0.60	6.40	0.60	8.5	0.60	31.3	0.60	21.40	0.60	10.65	0.60	9.40
0.80	63.07	0.80	52.27	0.80	52.21	0.70	33.95	0.80	28.60	0.70	10.65	0.80	16.4	0.80	56.0	0.70	34.70	0.70	15.65	0.70	11.54
1.00	90.35	1.00	61.55	1.00	59.36	0.80	44.62	1.00	37.80	0.80	13.50	1.00	22.2	1.00	70.5	0.80	48.10	0.80	21.00	0.80	13.10
1.20	112.63	1.20	71.73	1.20	64.70	0.90	56.50	1.20	43.42	0.90	16.85	1.20	26.9	1.20	81.4	0.90	60.00	0.90	25.95	0.90	15.90
1.40	125.98	1.40	78.43	1.40	70.77	1.00	65.20	1.40	47.24	1.00	20.10	1.40	29.8	1.40	90.2	1.00	67.00	1.00	30.65	1.00	18.50
1.60	137.68	1.60	84.60	1.60	75.55	1.20	77.60	1.60	52.18	1.20	24.75	1.60	32.6	1.60	97.9	1.20	80.00	1.20	37.25	1.20	22.95
1.80	148.22	1.80	89.80	1.80	78.90	1.40	86.75	1.80	56.28	1.40	28.65	1.80	35.3	1.80	103.7	1.40	90.25	1.40	41.85	1.40	26.40
2.00	156.50	2.00	95.03	2.00	82.22	1.60	96.24	2.00	60.13	1.60	32.25	2.00	37.1	2.00	109.5	1.60	94.65	1.60	46.80	1.60	30.00
2.20	163.00	2.20	99.85	2.20	84.87	1.80	103.10	2.20	62.40	1.80	35.45	2.20	38.7	2.20	114.0	1.80	103.80	1.80	50.50	1.80	32.85
2.40	168.62	2.40	104.18	2.40	87.95	2.00	109.40	2.40	64.83	2.00	38.50	2.40	39.9	2.40	118.2	2.00	111.58	2.00	53.75	2.00	35.00
2.60	174.13	2.60	107.01	2.60	90.53	2.20	113.40	2.60	66.81	2.20	40.55	2.60	41.1	2.69	122.5	2.20	116.30	2.20	56.95	2.20	37.05
2.80	179.57	2.80	111.11	2.80	92.85	2.40	117.75	2.80	68.15	2.40	41.95	2.80	42.0	2.80	125.3	2.40	120.55	2.40	59.20	2.40	38.65
3.00	184.07	3.00	114.26	3.00	94.11	2.60	122.48	3.00	69.66	2.60	43.25	3.00	42.8	3.00	128.1	2.60	124.60	2.60	61.90	2.60	40.00
3.20	188.29	3.20	117.38	3.20	95.57	2.80	126.50	3.20	70.61	2.80	44.35	3.20	43.4	3.20	130.5	2.80	128.35	2.80	63.15	2.80	41.20
3.40	192.30	3.40	119.43	3.40	97.06	3.00	129.38	3.40	71.48	3.00	45.10	3.40	44.0	3.40	133.2	3.00	130.80	3.00	64.70	3.00	41.95
3.60	195.77	3.60	122.16	3.60	98.30	3.20	131.95	3.20	72.38	3.20	45.75	3.60	44.4	3.60	135.5	3.20	133.60	3.20	65.95	3.20	42.50
3.80	198.88	3.80	123.67	3.80	99.49	3.40	134.40	3.80	--	3.40	46.45	3.80	44.8	3.80	137.6	3.40	135.85	3.40	67.12	3.40	43.00
4.00	201.55	4.00	125.75	4.00	100.00	3.60	136.60	4.00	73.81	3.60	46.85	4.0	45.1	4.00	138.5	3.60	137.95	3.60	67.80	3.60	43.45
4.20	204.75	4.20	127.39	4.20	100.49	3.80	138.80	4.20	74.31	3.80	47.25	4.20	--	4.20	139.4	3.80	139.75	3.80	68.50	3.80	43.75
4.40	207.22	4.40	128.73	4.40	100.98	4.00	140.85	4.40	74.81	4.00	47.85	4.40	45.6	4.40	140.1	4.00	140.90	4.00	69.05	4.00	44.05
4.60	209.77	4.60	129.99	4.60	101.44	4.20	141.70	4.60	75.25	4.20	48.15	4.60	--	4.60	140.8	4.20	142.05	4.20	69.40	4.20	44.25
4.80	211.89	4.80	131.94	4.80	101.79	4.60	142.72	4.80	75.54	4.40	48.25	4.80	45.9	4.80	141.3	4.60	143.25	4.40	69.75	4.40	44.45
5.0	213.75	5.00	131.94	5.00	102.06	4.60	143.65	5.00	75.87					5.00	141.8	4.60	144.10	4.60	70.10	4.60	44.55
5.2	215.39	5.20	132.69	5.20	102.31	4.80	144.50	5.20	76.06					5.20	142.2	4.80	144.65	4.80	70.30	4.80	44.67
5.4	216.72	5.40	133.20	5.40	102.47	5.00	144.85	5.40	76.25					5.40	142.6	5.00	145.15	5.00	70.50	5.00	44.72
5.6	218.20	5.60	133.81	5.60	102.68	5.20	145.20	5.60	76.37					5.80	143..	5.20	145.50	5.20	70.64		
5.8	218.88	5.80	134.23	5.80	102.84	5.40	145.60	5.80	76.46							5.40	145.85	5.40	70.74		
6.0	219.59	6.00	134.75	6.00	102.94	5.60	145.90	6.00	76.57							5.60	146.10				
6.2	220.18	6.20	135.12	6.20	103.04	5.80	146.16	6.20	76.63							5.80	146.25				
6.4	220.77	6.40	135.39																		
6.6	221.31	6.60	135.63																		
6.8	221.62																				
N_f = 221,690		N_f = 135,810		N_f = 103,160		N_f = 146,230		N_f = 76,650		N_f = 48,690		N_f = 46,290		N_f = 143,290		N_f = 146,360		N_f = 70,870		N_f = 44,880	
$2c_{fs}$ = 7.2		$2c_{fs}$ = 7.0		$2c_{fs}$ = 6.8		$2c_{fs}$ = 6.32		$2c_{fs}$ = 6.76		$2c_{fs}$ = 6.04		$2c_{fs}$ = --		$2c_{fs}$ = 6.12		$2c_{fs}$ = --		$2c_{fs}$ = 5.97		$2c_{fs}$ = 5.82	

TABLE 7. FATIGUE-CRACK-PROPAGATION MEASUREMENTS FOR 1/4-INCH-THICK, 8-INCH-WIDE PANELS

Specimen 2 6.8 ± 3.3 ksi		Specimen 11 6.8 ± 4.4 ksi		Specimen 12 6.8 ± 5.5 ksi		Specimen 7 8.4 ± 3.3 ksi		Specimen 10 8.4 ± 4.4 ksi		Specimen 13 8.4 ± 5.5 ksi		Specimen 8 10.0 ± 3.3 ksi		Specimen 9 10.0 ± 4.4 ksi		Specimen 14 10.0 ± 5.5 ksi	
2c, in.	N, kc	2c, in.	N, kc	2c, in.	N, kc	2c, in.	N, kc	2c, in.	N, kc	2c, in.	N, kc	2c, in.	N, kc	2c, in.	N, kc	2c, in.	N, kc
0.50	--	0.50	--	0.50	--	0.50	--	0.50	--	0.50	--	0.50	--	0.50	--	0.50	--
0.60	28.50	0.60	13.10	0.60	7.72	0.65	39.36	0.60	11.85	0.60	6.94	0.55	30.75	0.60	12.30	0.60	6.14
0.80	56.50	0.80	28.50	0.80	16.02	0.75	49.66	0.80	28.04	0.80	10.13	0.70	40.90	0.70	16.60	0.80	12.23
1.00	66.50	1.00	38.65	1.00	23.08	0.85	61.88	1.00	37.20	1.00	15.70	0.75	47.03	0.80	22.82	1.00	15.87
1.20	78.00	1.20	46.67	1.20	29.48	0.95	70.70	1.20	44.60	1.20	19.93	0.85	52.65	1.00	27.59	1.20	19.25
1.40	89.00	1.40	53.22	1.40	34.08	1.00	76.55	1.40	49.71	1.40	22.93	0.95	66.53	1.10	32.66	1.40	22.00
1.60	95.00	1.60	53.62	1.60	38.57	1.20	85.00	1.60	54.27	1.60	25.95	1.05	73.55	1.30	39.57	1.60	23.75
1.80	102.95	1.80	63.54	1.80	42.63	1.35	93.95	1.80	58.60	1.80	28.35	1.15	80.00	1.60	43.75	1.80	25.98
2.00	108.00	2.00	67.69	2.00	44.65	1.45	97.08	2.00	61.79	2.00	29.70	1.25	84.60	1.80	46.80	2.00	27.51
2.20	112.84	2.20	69.90	2.20	46.84	1.55	101.85	2.20	65.00	2.20	30.76	1.35	88.30	2.00	49.30	2.20	28.06
2.40	118.17	2.50	72.51	2.40	49.13	1.65	105.00	2.40	66.71	2.40	31.94	1.45	91.72	2.20	51.20	2.40	29.03
2.60	122.00	2.70	75.00	2.60	50.79	1.75	107.60	2.60	69.08	2.60	32.78	1.55	97.20	2.40	52.60	2.60	29.90
2.80	125.56	2.90	78.92	2.80	52.25	1.85	109.85	2.80	70.70	2.80	33.56	1.65	99.23	2.60	53.80	2.80	30.60
3.00	128.80	3.10	79.95	3.00	53.24	1.95	112.16	3.00	71.59	3.00	34.04	1.75	101.87	2.80	54.72	3.00	31.27
3.20	131.50	3.30	81.25	3.20	53.95	2.10	115.84	3.20	72.62	3.20	34.57	1.85	104.29	3.00	55.43	3.20	31.70
3.40	134.50	3.40	82.05	3.40	54.70	2.20	117.69	3.40	73.30	3.40	34.99	1.95	106.26	3.20	56.10	3.40	32.05
3.60	137.22	3.50	83.19	3.60	55.29	2.30	119.33	3.60	73.72	3.60	35.45	2.00	107.22	3.40	56.74	3.60	32.60
3.90	139.80	3.70	83.74	3.80	55.80	2.40	120.54	3.80	74.52	3.80	35.65	2.20	110.58	3.60	57.03	3.80	32.77
4.10	141.20	3.90	84.41	4.00	56.24	2.50	121.68	4.00	74.70	4.00	35.82	2.40	113.64	3.80	57.50	4.00	32.99
4.20	142.00	4.10	84.95	4.20	56.68	2.60	123.50	4.20	74.86	4.20	36.14	2.65	116.92	4.00	57.88	4.20	33.14
4.40	143.00	4.30	85.30	4.40	56.82	2.70	125.00	4.40	75.15	4.40	36.24	2.80	118.20	4.20	58.33	4.40	33.30
4.60	144.13	4.50	85.57	4.60	57.07	2.80	125.89	4.60	75.37	4.60	36.39	3.00	120.00	4.40	58.50	4.60	33.43
		4.70	85.99	4.80	57.24	2.90	127.10	4.80	75.50	4.80	36.48	3.20	121.30	4.60	58.62	4.80	33.55
		4.90	86.13	5.00	57.39	3.00	127.89	5.00	75.55	5.00	36.60	3.40	122.30	4.80	58.74		
		5.10	86.24	5.20	57.65	3.10	128.70					3.60	123.20	5.00	58.82		
				5.40	57.76	3.20	129.40					3.80	124.00	5.20	58.88		
						3.30	130.20					4.00	124.50	6.00	59.15		
						3.40	130.85					4.20	124.90				
						3.50	131.25					4.40	125.20				
						3.70	132.30										
						3.90	133.18										
						4.10	133.80										
						4.20	134.20										
						4.40	134.60										
						4.60	135.07										
						4.80	135.45										
						5.00	135.65										
N_f = 145,540		N_f = 86,580		N_f = 57,940		N_f = 136,360		N_f = 75,680		N_f = 36,850		N_f = 126,430		N_f = 59,170		N_f = 33,760	
$2c_{fs}$ = 6.7		$2c_{fs}$ = 6.15		$2c_{fs}$ = 6.535		$2c_{fs}$ = 6.21		$2c_{fs}$ = 6.05		$2c_{fs}$ = 5.7		$2c_{fs}$ = 6.105		$2c_{fs}$ = 6.065		$2c_{fs}$ = 5.89	
		$2c_{fc}$ = 6.25		$2c_{fc}$ = 6.75		$2c_{fc}$ = 6.4		$2c_{fc}$ = 6.15		$2c_{fc}$ = 5.75		$2c_{fc}$ = 6.25		$2c_{fc}$ = 6.25		$2c_{fc}$ = 6.00	

TABLE 8. FCP MEASUREMENTS FOR 1/2-INCH-THICK, 8-INCH-WIDE PANELS

Specimen 4 6.8 ± 3.3 ksi		Specimen 21 6.8 ± 3.3 ksi		Specimen 20 6.8 ± 4.4 ksi		Specimen 22 6.8 ± 5.5 ksi		Specimen 15 8.4 ± 3.3 ksi		Specimen 19 8.4 ± 4.4 ksi		Specimen 23 8.4 ± 5.5 ksi		Specimen 16 10.0 ± 3.3 ksi		Specimen 18 10.0 ± 4.4 ksi		Specimen 24 10.0 ± 5.5 ksi	
2c, in.	N, kc	2c, in.	N, kc	2c, in.	N, kc	2c, in.	N, kc	2c, in.	N, kc	2c, in.	N, kc	2c, in.	N, kc	2c, in.	N, kc	2c in.	N, kc	2, in.	N, kc
0.50	--	0.50	--	0.50	--	0.50	--	0.50	--	0.50	--	0.50	--	0.50	--	0.50	--	0.50	--
0.60	48.86	0.60	29.59	0.60	14.73	0.60	9.01	0.60	35.42	0.60	11.60	0.60	9.04	0.60	25.66	0.60	15.50	0.60	7.98
0.80	75.80	0.70	37.12	0.70	21.32	0.70	13.68	0.80	50.32	0.70	19.37	0.80	15.70	0.80	49.92	0.70	22.54	0.80	14.02
1.00	101.50	0.80	51.08	0.80	29.18	0.80	18.07	1.00	67.90	0.80	23.67	1.00	21.07	1.00	68.22	0.80	29.46	1.00	19.14
1.20	124.90	0.90	66.30	0.90	36.45	0.90	22.27	1.20	80.42	0.90	27.96	1.20	25.78	1.20	79.19	0.90	33.33	1.20	22.84
1.40	140.00	1.00	75.00	1.00	38.24	1.00	25.43	1.40	90.48	1.00	32.55	1.40	29.22	1.40	87.87	1.00	36.84	1.40	24.78
1.60	150.10	1.20	83.62	1.10	40.99	1.20	29.62	1.60	96.43	1.10	33.96	1.60	31.52	1.60	92.69	1.00	40.76	1.80	29.18
1.80	160.10	1.40	93.69	1.20	44.20	1.40	33.43	1.80	102.96	1.20	37.66	1.80	33.69	1.80	97.11	1.30	43.34	2.00	30.60
2.00	167.20	1.60	100.17	1.30	47.73	1.60	36.84	2.00	106.85	1.30	39.62	2.00	35.67	2.00	101.28	1.40	45.03	2.20	31.69
2.20	173.00	1.80	107.69	1.40	49.50	1.80	39.70	2.20	110.33	1.40	40.78	2.20	37.42	2.20	104.35	1.50	47.23	2.40	32.29
2.40	179.66	2.00	114.28	1.50	52.02	2.00	41.88	2.40	114.03	1.50	43.26	2.40	38.66	2.40	106.85	1.60	48.63	2.60	32.97
2.60	183.20	2.20	116.31	1.60	54.02	2.20	43.90	2.60	116.72	1.60	44.79	2.60	39.61	2.60	109.31	1.70	49.94	2.80	33.48
2.80	187.40	2.40	119.15	1.70	56.10	2.40	45.11	2.80	118.55	1.70	46.50	2.80	40.50	2.80	111.15	1.80	51.19	3.00	33.80
3.00	190.60	2.60	122.26	1.80	58.30	2.60	46.65	3.00	120.38	1.80	47.82	3.00	41.10	3.00	112.32	1.90	52.52	3.20	34.12
3.20	194.60	2.80	125.64	1.90	60.12	2.80	47.47	3.20	121.61	1.90	49.29	3.20	41.50	3.20	113.43	2.00	53.63	3.40	34.31
3.40	197.00	3.00	127.00	2.00	63.50	3.00	48.36	3.40	122.80	2.00	50.00	3.40	41.96	3.40	114.17	2.20	55.19	3.60	34.92
3.60	199.80	3.20	128.89	2.20	64.60	3.20	48.99	3.60	123.64	2.20	52.31	3.60	42.14	3.60	114.87	2.40	56.37	3.80	--
3.80	202.40	3.40	130.52	2.40	66.65	3.40	49.53	3.80	124.24	2.40	54.35	3.80	42.39	3.80	115.58	2.60	57.78	4.00	34.69
4.00	203.70	3.60	131.69	2.60	68.90	3.60	49.88	4.00	124.57	2.60	55.50	4.00	42.58	4.00	116.08	2.80	58.63	4.20	34.77
4.20	205.70	3.80	132.54	2.80	71.40	3.80	50.17	4.20	124.86	2.80	56.96	4.20	42.75	4.20	116.37	3.00	59.51	4.40	34.85
--	--	4.00	133.41	3.00	72.20	4.00	50.39	4.40	125.32	3.00	57.87	4.40	42.83	4.40	116.62	3.20	59.80	4.60	34.89
5.00	208.00	4.20	134.14	3.20	73.32	4.20	50.48	4.60	125.48	3.20	58.54	4.60	--	4.60	116.84	3.40	60.21		
5.40	209.00	4.40	134.70	3.40	73.86	4.40	50.62	4.80	125.72	3.40	59.14	4.80	42.95	4.80	116.98	3.60	60.51		
5.80	210.00	4.60	135.06	3.60	74.65	4.80	50.84			3.60	59.70	5.00	43.03	5.00	117.09	3.80	--		
5.90	210.40	4.80	135.37	3.80	75.27					3.80	60.03			5.20	117.19	4.00	60.87		
		5.00	135.62	4.00	75.73					4.00	60.32					4.20	60.99		
		5.20	135.78	4.20	76.08					4.20	--					4.40	61.13		
		5.40	135.93	4.40	76.37					4.40	60.86					4.70	61.22		
		5.60	136.01	4.60	76.59					4.60	--					5.00	61.33		
		5.80	136.19	4.80	76.75					4.80	61.03								
		6.00	136.26	5.00	76.88					5.00	61.13								
		6.20	136.31	5.20	76.97					5.20	61.23								
				5.60	77.10					5.40	61.29								
				6.00	77.18														
N_f = 210,740		N_f = 136,340		N_f = 77,210		N_f = 50,940		N_f = 125,720		N_f = 61,330		N_f = 43,160		N_f = 117,270		N_f = 61,440		N_f = 35,020	
$2\bar{\epsilon}_{fs}$ = 6.52				$2\bar{\epsilon}_{fs}$ = 6.34		$2\bar{\epsilon}_{fs}$ = 6.06		$2\bar{\epsilon}_{fs}$ = 5.83		$2\bar{\epsilon}_{fs}$ = 6.15		$2\bar{\epsilon}_{fs}$ = 6.0		$2\bar{\epsilon}_{fs}$ = 5.82		$2\bar{\epsilon}_{fs}$ = 5.75		$2\bar{\epsilon}_{fs}$ = 5.66	
$2c_{fc}$ = 6.70				$2c_{fc}$ = 6.53		$2c_{fc}$ = 6.20		$2c_{fc}$ = 6.15		$2c_{fc}$ = 6.55				$2c_{fs}$ = 6.20		$2c_{fs}$ = 6.20		$2c_{fc}$ = 5.90	

TABLE 9. FATIGUE-CRACK-PROPAGATION MEASUREMENTS FOR 1-INCH-THICK, 8-INCH-WIDE PANELS

Specimen 25 6.8 ± 3.3 ksi		Specimen 36 6.8 ± 4.4 ksi		Specimen 31 6.8 ± 5.5 ksi		Specimen 26 8.4 ± 3.3 ksi		Specimen 29 8.4 ± 4.4 ksi		Specimen 34 8.4 ± 5.5 ksi		Specimen 27 10.0 ± 3.3 ksi		Specimen 28 10.0 ± 4.4 ksi		Specimen 33 10.0 ± 5.5 ksi	
2c, in.	N, kc	2c, in.	N, kc	2c, in.	N, kc	2c, in.	N, kc	2c, in.	N, kc	2c, in.	N, kc	2c, in.	N, kc	2c, in.	N, kc	2c, in.	N, kc
0.50	--	0.50	--	0.50	--	0.50	--	0.50	--	0.50	--	0.50	--	0.50	--	0.50	--
0.60	--	0.60	12.46	0.60	12.43	0.60	25.53	0.60	31.60	0.60	6.66	0.60	26.63	0.60	14.58	0.60	5.42
0.90	55.95	0.80	22.91	0.80	18.69	0.90	67.19	0.80	38.91	0.80	9.69	0.80	45.15	0.80	22.86	0.80	10.76
1.00	64.97	1.00	39.90	1.00	22.63	1.00	71.95	1.00	44.45	1.00	15.59	1.00	55.90	1.00	29.63	1.00	15.12
1.20	79.68	1.20	44.16	1.20	26.19	1.20	76.80	1.20	48.84	1.20	17.30	1.20	70.62	1.20	34.54	1.20	17.21
1.40	86.98	1.40	48.41	1.40	29.38	1.50	84.70	1.40	52.49	1.40	19.88	1.40	80.02	1.40	37.95	1.40	19.23
1.60	93.76	1.60	52.27	1.60	32.34	1.60	89.90	1.60	56.31	1.60	22.36	1.60	86.94	1.60	41.20	1.60	21.06
1.80	100.40	1.80	56.01	1.80	34.58	1.80	95.82	1.80	60.00	1.80	24.10	1.80	92.11	1.80	43.41	1.80	22.74
2.00	106.40	2.00	58.50	2.00	37.08	2.00	99.70	2.00	61.29	2.00	25.48	2.00	95.78	2.00	45.24	2.00	23.98
2.20	109.71	2.20	61.00	2.20	38.41	2.20	103.50	2.20	63.14	2.20	27.27	2.20	99.87	2.20	46.88	2.20	24.95
2.40	112.24	2.40	62.48	2.40	40.41	2.40	105.74	2.40	65.51	2.40	27.94	2.40	101.37	2.40	48.25	2.40	25.57
2.60	115.47	2.60	64.32	2.60	41.90	2.60	108.08	2.60	67.03	2.60	29.09	2.60	103.64	2.60	49.45	2.60	26.25
2.80	117.31	2.80	66.40	2.80	43.14	2.80	110.10	2.80	68.78	2.80	29.64	2.80	105.15	2.80	50.17	2.80	26.64
3.00	120.26	3.00	69.12	3.00	44.00	3.00	111.77	3.00	69.35	3.00	30.19	3.00	106.50	3.00	50.83	3.00	26.97
3.20	122.59	3.20	70.74	3.20	44.70	3.20	112.85	3.20	70.50	3.20	30.75	3.20	107.30	3.20	51.27	3.20	27.28
3.40	124.10	3.40	71.60	3.40	45.22	3.40	114.14	3.40	71.11	3.40	30.90	3.40	107.95	3.40	51.63	3.40	27.40
3.60	125.31	3.60	72.50	3.60	45.79	3.60	115.04	3.60	71.75	3.60	31.07	3.60	108.30	3.60	52.04	3.60	27.49
3.80	126.47	3.80	73.30	3.80	46.28	3.80	115.73	3.80	72.29	3.80	31.30	3.80	108.74	3.80	52.22	3.80	27.53
4.00	127.69	4.00	73.82	4.00	46.54	4.00	116.28	4.00	72.71	4.00	31.36	4.00	109.02	4.00	52.35	4.00	27.57
4.20	128.14	4.20	74.22	4.20	46.81	4.20	116.61	4.20	73.08	4.20	31.43	4.20	109.24	4.20	52.47	4.20	27.59
4.40	128.72	4.40	74.48	4.40	46.96	4.40	116.84	4.40	73.28	4.40	31.50	4.40	109.40	4.40	52.55	4.40	27.62
4.60	128.95	4.60	74.83	4.60	47.14	4.60	117.00	4.60	73.43	4.60	31.55	4.60	109.51				
4.80	129.36	4.80	74.98	4.80	--	4.80	117.14	4.80	73.63			4.80	109.61				
5.00	129.54	5.00	75.11	5.00	--	5.00	117.30	5.00	73.74			5.00	109.69				
5.20	129.61	5.20	75.21	5.20	47.40			5.20	73.80								
5.40	129.68	5.40	75.28					5.40	73.84								
5.60	--	5.60	75.32														
5.80	129.74																
N_f = 129,770		N_f = 75,350		N_f = 47,510		N_f = 117,430		N_f = 73,890		N_f = 31,630		N_f = 109,740		N_f = 52,640		N_f = 27,640	
$2c_{fs}$ = 5.62		$2c_{fs}$ = 5.77				$2c_{fs}$ = 5.30		$2c_{fs}$ = 5.41		$2c_{fs}$ = 4.82		$2c_{fs}$ = 4.97		$2c_{fs}$ = 4.93		$2c_{fs}$ = 4.34	
$2c_{fc}$ = 6.50		$2c_{fc}$ = 6.40				$2c_{fc}$ = 6.47		$2c_{fc}$ = 6.15		$2c_{fc}$ = 5.70		$2c_{fc}$ = 5.68		$2c_{fc}$ = 5.70		$2c_{fc}$ = 5.33	

TABLE 10. FCP MEASUREMENTS FOR 1/4-INCH-THICK, 16-INCH-WIDE PANELS

Specimen 57 8.4 ± 3.3 ksi		Specimen 58 8.4 ± 4.4 ksi		Specimen 59 8.4 ± 5.5 ksi	
2c, in.	N, kc	2c, in.	N, kc	2c, in.	N, kc
0.50	--	0.50	--	0.50	--
0.60	24.80	0.60	11.37	0.60	5.32
0.70	37.56	0.70	14.39	0.70	8.11
0.80	46.60	0.80	16.17	0.80	10.00
0.90	56.73	0.90	20.66	0.90	13.13
1.00	64.85	1.00	25.20	1.00	15.39
1.20	76.50	1.20	32.25	1.20	18.33
1.40	83.63	1.40	34.90	1.40	--
1.60	90.55	1.60	39.02	1.60	23.69
1.80	97.05	1.80	42.00	1.80	25.42
2.00	101.63	2.00	44.11	2.00	26.33
2.20	106.57	2.20	46.00	2.20	27.90
2.40	109.35	2.40	47.96	2.40	28.77
2.60	113.27	2.60	49.96	2.60	29.79
2.80	116.20	2.80	51.44	2.80	30.36
3.00	119.80	3.00	53.21	3.00	30.91
3.20	121.39	3.20	54.75	3.20	31.45
3.40	123.47	4.00	55.75	3.40	31.89
3.60	124.77	4.20	56.30	3.60	32.39
3.80	126.19	4.40	56.60	3.80	32.74
4.00	127.30	4.60	57.00	4.00	32.95
4.20	128.50	4.80	57.35	4.20	33.30
4.40	129.52	5.00	57.77	4.40	33.59
4.60	130.17	5.20	57.98	4.60	33.84
4.80	130.85	5.40	58.18	4.80	33.98
5.00	131.44	5.60	58.38	5.00	34.16
5.20	132.10	5.80	58.57	5.20	34.32
5.40	132.64	6.00	58.75	5.40	34.42
5.60	133.15	6.20	--	5.60	34.57
5.80	133.58	6.40	59.13	5.80	34.65
6.00	134.09	6.60	--	6.00	34.74
6.20	134.46	6.80	59.23	6.20	34.86
6.40	134.80	7.00	59.33	6.40	34.93
6.60	135.17	7.20	--	6.60	35.03
6.80	135.40	7.40	59.61	6.80	35.11
7.00	135.59	7.60	59.76	7.00	35.17
7.20	135.81	7.80	59.84	7.20	35.23
7.40	135.98	8.00	59.89	7.40	35.28
7.60	136.05	8.20	59.95	7.60	35.33
7.80	136.33			7.80	35.40
8.00	136.55			8.00	35.43
8.20	136.74				
8.40	136.85				
8.60	137.02				
8.80	137.16				
9.00	137.32				
9.20	137.45				
9.40	--				
9.60	137.57				
9.80	--				
10.00	137.80				
N_f = 138,330		N_f = 60,360		N_f = 35,590	
$2c_{f_a}$ = 12.18		$2c_{f_a}$ = 11.9		$2c_{f_a}$ = 12.1	
$2c_{f_c}$ = 12.18		$2c_{f_c}$ = 11.9		$2c_{f_c}$ = 12.27	

TABLE 11. FCP MEASUREMENTS FOR 1/2-INCH-THICK, 16-INCH-WIDE PANELS

Specimen 63 8.4 ± 3.3 ksi		Specimen 64 8.4 ± 4.4 ksi		Specimen 65 8.4 ± 5.5 ksi	
2c, in.	N, kc	2c, in.	N, kc	2c in.	N, kc
0.50	--	0.50	--	0.50	--
0.60	27.90	0.60	14.82	0.60	6.45
0.80	46.54	0.80	26.14	0.80	13.43
1.00	61.35	1.00	30.62	1.00	18.41
1.20	71.19	1.20	34.37	1.20	23.22
1.40	79.57	1.40	38.80	1.40	26.06
1.60	87.00	1.60	45.26	1.60	29.84
1.80	91.61	1.80	48.38	1.80	31.57
2.00	96.32	2.00	52.12	2.00	33.56
2.20	100.00	2.20	54.79	2.20	34.99
2.40	103.73	2.40	--	2.40	35.97
2.60	107.57	2.60	58.00	2.60	36.93
2.80	110.58	2.80	59.65	2.80	37.68
3.00	112.80	3.00	60.57	3.00	38.35
3.20	114.87	3.20	61.39	3.20	38.80
3.40	116.21	3.40	62.16	3.40	39.25
3.60	118.39	3.60	62.88	3.60	39.55
3.80	119.68	3.80	63.40	3.80	39.98
4.00	120.78	4.00	63.80	4.00	40.29
4.20	121.20	4.20	64.08	4.20	40.50
4.40	121.95	4.40	64.37	4.40	40.65
4.60	122.23	4.60	64.64	4.60	40.89
4.80	123.12	4.80	64.82	4.80	41.03
5.00	123.36	5.00	65.03	5.00	41.18
5.20	123.69	5.20	65.20	5.20	41.28
5.40	123.92	5.40	65.33	5.50	41.45
5.60	124.40	5.60	65.66	6.00	41.69
5.80	124.59	5.80	--	7.00	42.05
6.00	124.74	6.00	65.73	8.00	42.28
6.20	125.06	6.50	65.96		
6.60	125.45	7.00	66.16		
6.90	125.70	7.50	66.36		
7.50	125.90	8.00	66.48		
7.90	126.00				
N_f = 126,890		N_f = 66,820		N_f = 42,560	
$2c_{f_a}$ = 12.5		$2c_{f_a}$ = 11.7		$2c_{f_a}$ = 13.0	
$2c_{f_c}$ = 12.78		$2c_{f_c}$ = 12.0		$2c_{f_c}$ = 13.3	

TABLE 12. FCP MEASUREMENTS FOR 1-INCH-THICK, 16-INCH-WIDE PANELS

Specimen 66 8.4 ± 3.3 ksi		Specimen 67 8.4 ± 4.4 ksi		Specimen 68 8.4 ± 5.5 ksi	
2c, in.	N, kc	2c, in.	N, kc	2c, in.	N kc
0.50	--	0.50	--	0.50	--
0.50	36.43	0.60	14.86	0.60	8.40
0.80	59.14	0.80	27.22	0.80	11.93
1.00	70.66	1.00	29.26	1.00	14.96
1.20	82.43	1.20	34.52	1.20	17.64
1.40	85.92	1.40	37.33	1.40	20.26
1.60	88.55	1.60	40.23	1.60	22.82
1.80	92.61	1.80	43.02	1.80	24.27
2.00	98.35	2.00	45.23	2.00	26.13
2.20	100.60	2.20	48.00	2.20	27.23
2.40	103.79	2.40	49.45	2.40	--
2.60	105.88	2.60	51.15	2.60	28.88
2.80	107.77	2.80	52.07	2.80	--
3.00	110.03	3.00	53.16	3.00	--
3.20	113.57	3.20	54.06	3.20	30.28
3.40	115.70	3.40	54.91	3.40	30.31
3.60	116.70	3.60	--	3.60	31.00
3.80	117.67	3.80	55.71	3.80	31.21
4.00	118.76	4.00	56.05	4.00	31.30
4.20	119.88	4.20	56.60	4.20	31.46
4.40	120.59	4.40	56.78	4.40	31.57
4.60	121.34	4.60	57.12	4.60	31.72
4.80	121.88	4.80	57.25	4.80	31.72
5.00	122.20	5.00	57.37	5.00	31.78
5.20	122.71	5.20	57.52	5.20	31.83
5.40	123.03	5.40	57.56	6.00	31.93
5.60	123.35	5.60	57.62		
5.80	123.83	5.80	57.68		
6.00	123.95	6.00	57.77		
6.50	124.30	7.00	57.99		
7.00	124.55				
8.00	124.95				
N_f = 125,180		N_f = 58,060		N_f = 31,990	
$2c_{f_a}$ = 9.375		$2c_{f_a}$ = 8.65		$2c_{f_a}$ = 7.23	
$2c_{f_c}$ = 10.50		$2c_{f_c}$ = 11.00		$2c_{f_c}$ = 9.2	

TABLE 13. PCP MEASUREMENTS FOR 1/4-INCH-THICK, 36-INCH-WIDE PANELS

Specimen 75 8.4 ± 3.3 ksi		Specimen 76 8.4 ± 4.4 ksi		Specimen 77 8.4 ± 5.5 ksi	
$2c_f$, in.	N_f, kc	$2c_f$, in.	N_f, kc	$2c_f$, in.	N_f, kc
0.50	--	0.50	--	0.50	--
0.60	24.13	0.60	10.18	0.60	7.69
0.80	47.39	0.80	21.84	0.80	14.30
1.00	64.11	1.00	30.00	1.00	18.73
1.20	77.12	1.20	34.89	1.20	22.07
1.40	87.25	1.40	--	1.40	25.38
1.60	95.35	1.60	42.94	1.60	28.16
1.80	104.72	1.80	46.02	1.80	30.02
2.00	108.68	2.00	48.60	2.00	31.71
2.20	111.83	2.20	50.35	2.20	33.39
2.40	117.03	2.40	52.11	2.40	33.89
2.60	120.60	2.60	54.06	2.60	34.37
2.80	123.80	2.80	--	2.80	35.56
3.00	126.96	3.00	56.75	3.00	36.59
3.20	128.87	3.20	57.24	3.20	37.13
3.40	130.66	3.40	59.09	3.40	37.66
3.60	131.94	3.60	--	3.60	38.13
3.80	134.90	3.80	59.78	3.80	38.65
4.00	136.03	4.00	60.10	4.00	39.33
4.20	137.38	4.20	60.75	4.20	--
4.40	138.41	4.40	61.27	4.40	39.65
4.60	139.80	4.60	61.76	4.60	39.97
4.80	140.76	4.80	62.01	4.80	40.25
5.00	141.84	5.00	62.48	5.00	40.42
6.00	145.41	6.00	63.98	6.00	41.24
7.00	147.95	7.00	65.05	7.00	41.93
8.00	149.73	8.00	65.87	8.00	42.41
9.00	150.50	9.00	66.50	9.00	42.70
10.00	151.40	10.00	67.00	10.00	42.95
11.00	152.00	11.00	67.35	11.00	43.15
12.0	152.65	12.00	67.60		
N_f = 156,420		N_f = 68,530		N_f = 43,650	
$2c_{f_s}$ = 26.68		$2c_{f_s}$ = 23.09		$2c_{f_s}$ = 19.62	
$2c_{f_c}$ = 26.82		$2c_{f_c}$ = 24.34		$2c_{f_c}$ = 19.74	

TABLE 14. PCP MEASUREMENTS FOR 1/2-INCH-THICK, 36-INCH-WIDE PANELS

Specimen 72 8.4 ± 3.3 ksi		Specimen 73 8.4 ± 4.4 ksi		Specimen 74 8.4 ± 5.5 ksi	
$2c_f$, in.	N_f, kc	$2c_f$, in.	N_f, kc	$2c_f$, in.	N_f, kc
0.50	--	0.50	--	0.50	--
0.60	24.65	0.60	10.52	0.60	8.37
0.80	50.53	0.80	20.67	0.80	16.00
1.00	55.75	1.00	29.83	1.00	19.73
1.20	69.34	1.20	35.96	1.20	22.14
1.40	79.70	1.40	40.00	1.40	26.47
1.60	90.00	1.60	43.81	1.60	28.86
1.80	96.43	1.80	46.89	1.80	30.77
2.00	98.98	2.00	48.72	2.00	32.19
2.20	104.24	2.20	51.00	2.20	33.66
2.40	108.01	2.40	52.94	2.40	34.61
2.60	111.33	2.60	54.43	2.60	35.85
2.80	114.96	2.80	55.30	2.80	37.20
3.00	116.96	3.00	56.60	3.00	37.85
3.20	119.45	3.20	57.53	3.20	38.36
3.40	121.45	3.40	58.77	3.40	38.75
3.60	123.15	3.60	59.70	3.60	39.14
3.80	125.62	3.80	60.41	3.80	39.84
4.00	126.22	4.00	61.04	4.00	40.15
4.20	127.58	4.20	61.74	4.20	40.38
4.40	129.50	4.40	62.15	4.40	40.62
4.60	--	4.60	62.69	4.60	40.95
4.80	131.06	4.80	62.94	4.80	41.22
5.0	132.13	5.0	63.37	5.0	41.39
6.0	135.13	6.0	64.60	6.0	42.07
7.0	137.48	7.0	65.45	7.0	42.60
8.0	138.72	8.0	66.16	8.0	42.94
9.0	139.50			9.0	43.20
10.0	140.10			10.0	43.40
11.0	140.55			11.0	43.50
12.0	141.00				
N_f = 143,470		N_f = 68,230		N_f = 44,200	
$2c_{f_s}$ = 28.85		$2c_{f_s}$ = 28.2		$2c_{f_s}$ = 28.07	
$2c_{f_c}$ = 29.05		$2c_{f_c}$ = 28.63		$2c_{f_c}$ = 28.38	

TABLE 15. PCP MEASUREMENTS FOR 1-INCH-THICK, 36-INCH-WIDE PANELS

Specimen 69 8.4 ± 3.3 ksi		Specimen 70 8.4 ± 4.4 ksi		Specimen 71 8.4 ± 5.5 ksi	
$2c_f$, in.	N_f, kc	$2c_f$, in.	N_f, kc	$2c_f$, in.	N_f, kc
0.50	--	0.50	--	0.50	--
9.60	--	0.60	21.74	0.60	12.55
0.80	56.30	0.80	25.37	0.80	15.33
1.00	68.20	1.00	33.20	1.00	20.52
1.20	82.11	1.20	40.10	1.20	25.95
1.40	92.68	1.40	43.93	1.40	28.99
1.60	94.30	1.60	48.50	1.60	31.50
1.80	96.62	1.80	50.75	1.80	32.70
2.00	104.10	2.00	52.66	2.00	34.77
2.20	106.72	2.20	54.76	2.20	36.11
2.40	110.39	2.40	55.92	2.40	37.21
2.60	113.28	2.60	57.53	2.60	38.28
2.80	115.15	2.80	58.85	2.80	39.21
3.00	117.63	3.00	60.25	3.00	40.15
3.20	119.28	3.20	61.35	3.20	40.63
3.40	121.12	3.40	62.07	3.40	41.13
3.60	122.37	3.60	63.36	3.60	41.40
3.80	123.48	3.80	63.79	3.80	41.87
4.00	124.16	4.00	64.27	4.00	42.43
4.20	125.14	4.20	64.57	4.20	42.70
4.40	126.31	4.40	65.04	4.40	43.02
4.60	126.75	4.60	65.23	4.60	43.27
4.80	127.07	4.80	65.35	6.80	43.36
5.00	127.45	5.0	65.61	5.0	43.60
5.20	127.65	5.4	65.91	6.0	44.19
5.40	127.95	6.0	66.30	7.0	44.53
5.60	128.22	7.0	66.64	8.0	44.81
5.80	128.40	8.0	67.03	9.0	44.90
6.00	128.68	9.0	67.13	10.0	45.00
6.20	128.90	10.0	67.20	11.0	45.07
6.40	129.03	11.0	67.26	12.0	45.12
6.60	129.21	12.0	67.30		
6.80	129.32				
7.0	129.49				
7.2	129.59				
7.4	129.71				
7.6	129.82				
7.8	129.97				
8.0	130.04				
9.0	130.30				
10.0	130.55				
N_f = 130,930		N_f = 67,340		N_f = 45,230	
$2c_{f_s}$ = 14.2		$2c_{f_s}$ = 13.4		$2c_{f_s}$ = 15.16	
$2c_{f_c}$ = --		$2c_{f_c}$ = --		$2c_{f_c}$ = 18.01	

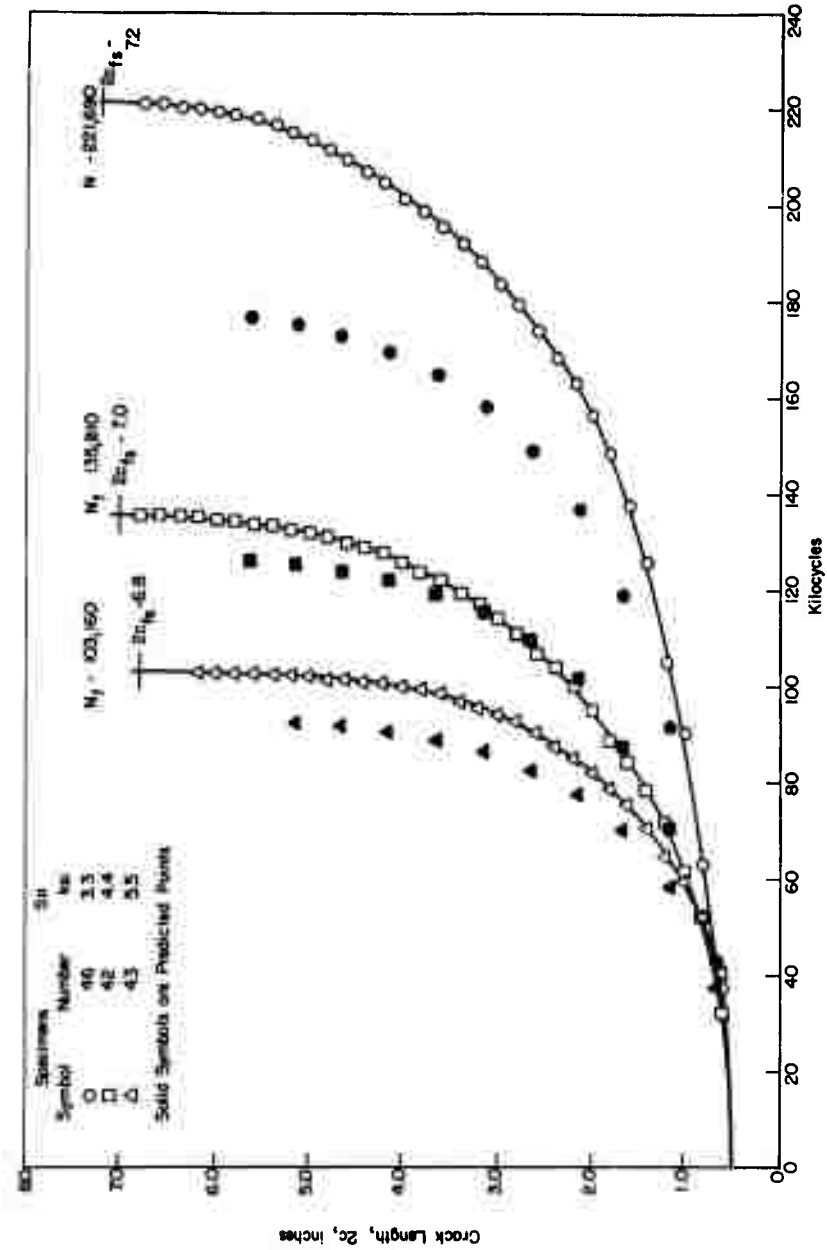

a. Mean Stress S_m = 6.8 KSI

FIGURE 14. FATIGUE-CRACK-PROPAGATION DATA FOR 8-INCH-WIDE PANELS, 1/16 INCH THICK

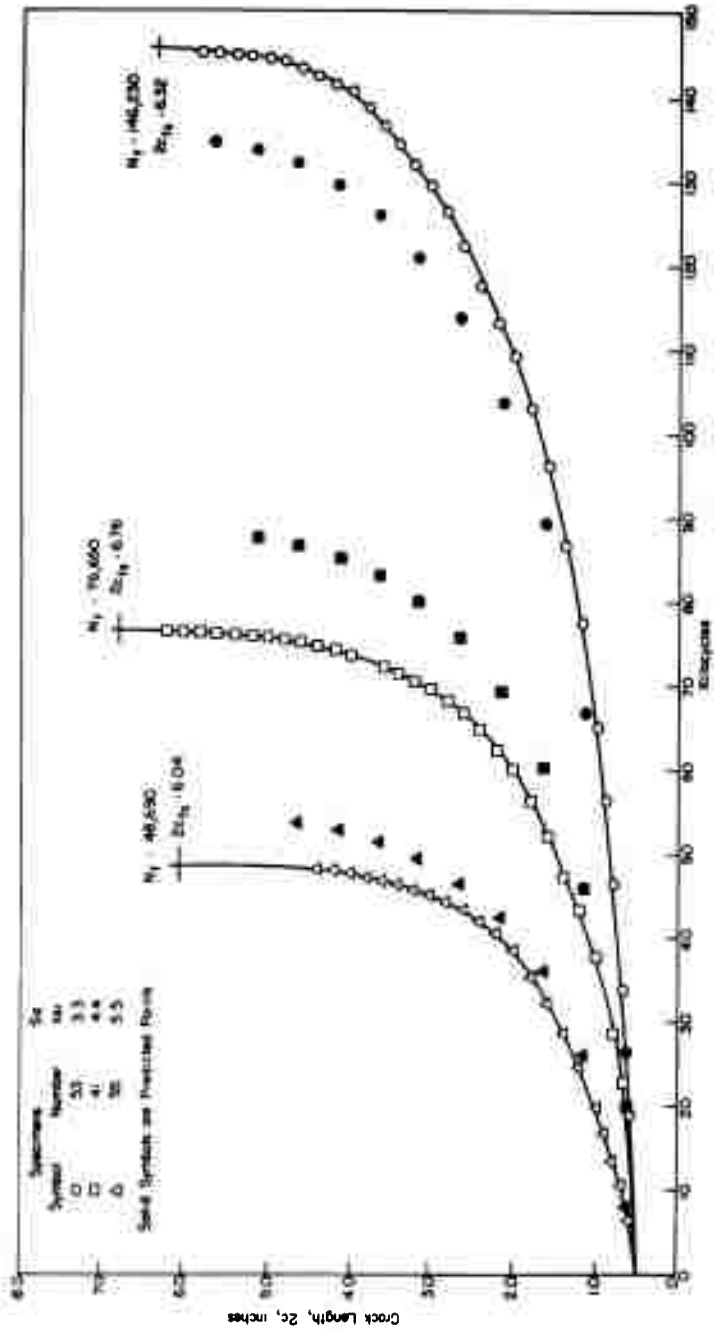

b. Mean Stress S_m = 8.4 KSI

FIGURE 14. (CONTINUED)

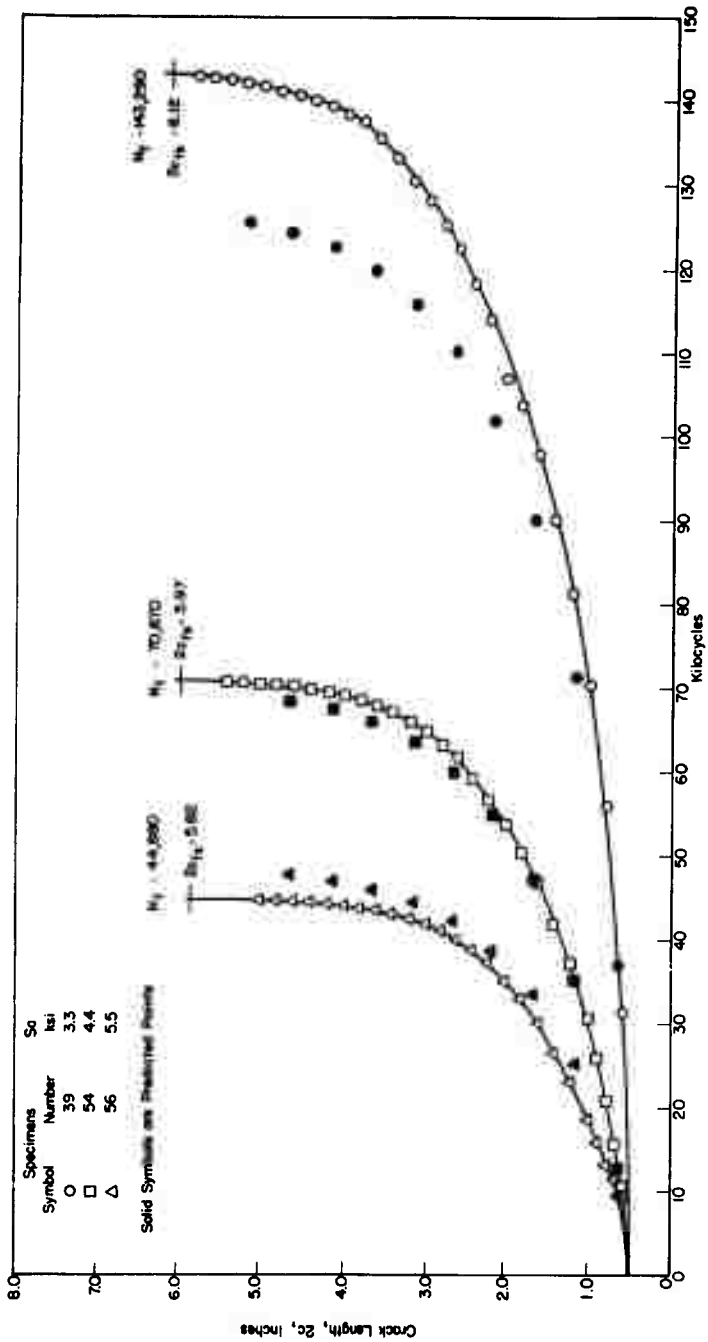

c. Mean Stress S_m = 10.0 KSI

FIGURE 14. (CONTINUED)

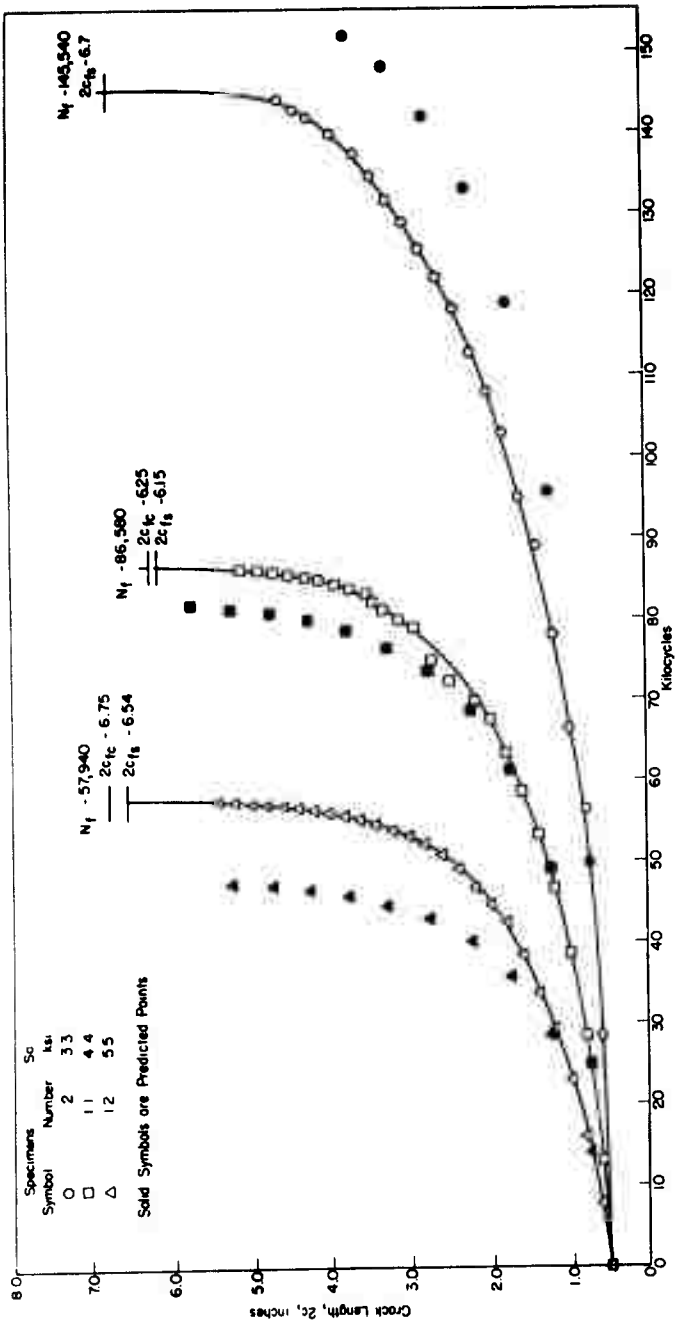

a. Mean Stress S_m = 6.8 KSI

FIGURE 15. FATIGUE-CRACK-PROPAGATION-DATA FOR 8-INCH-WIDE PANELS, 1/4 INCH THICK

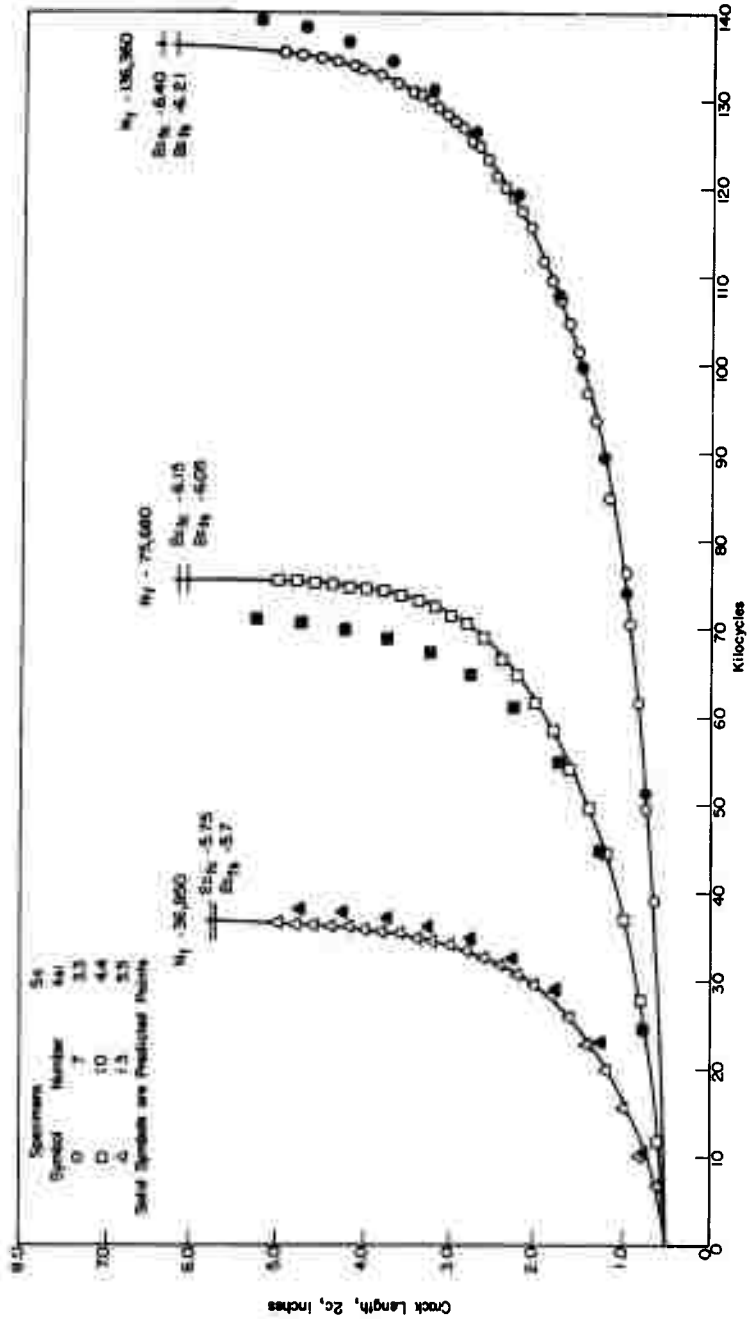

b. Mean Stress S_m = 8.4 KSI

FIGURE 15. (CONTINUED)

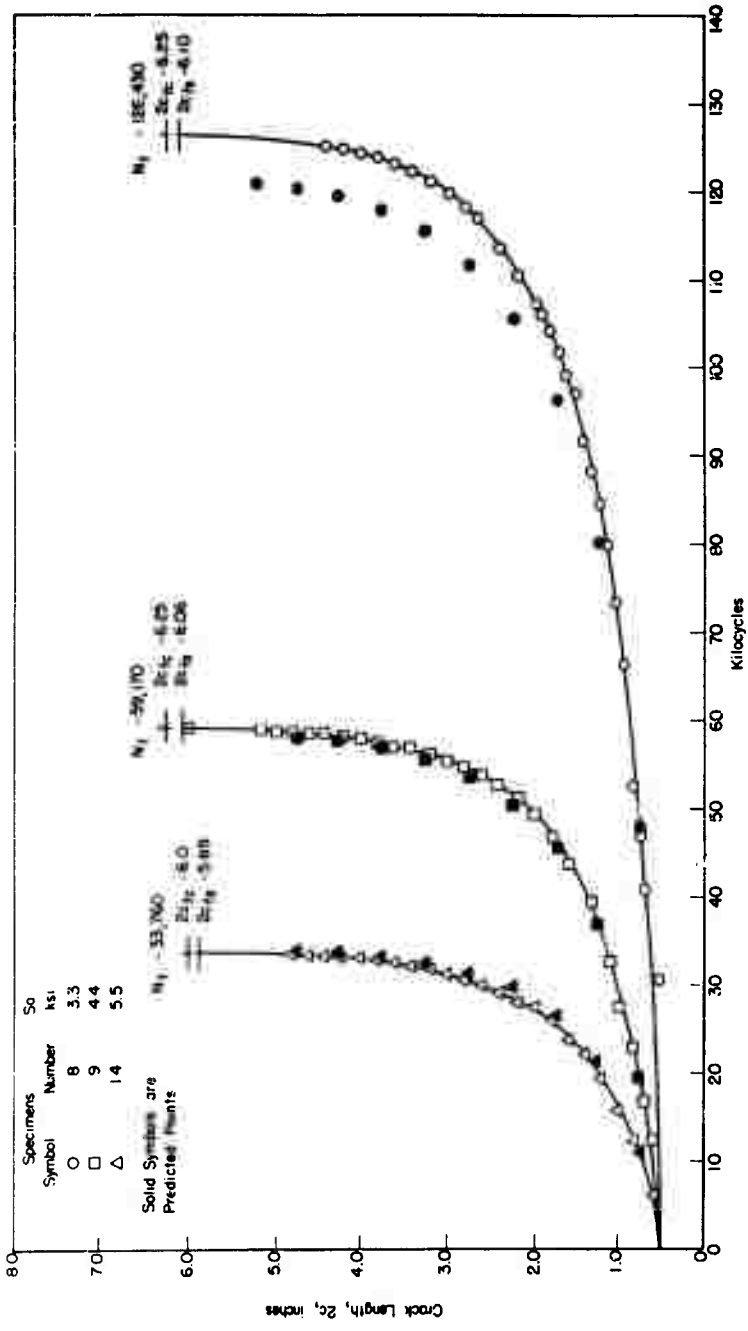

c. Mean Stress S_m = 10.0 KSI

FIGURE 15. (CONTINUED)

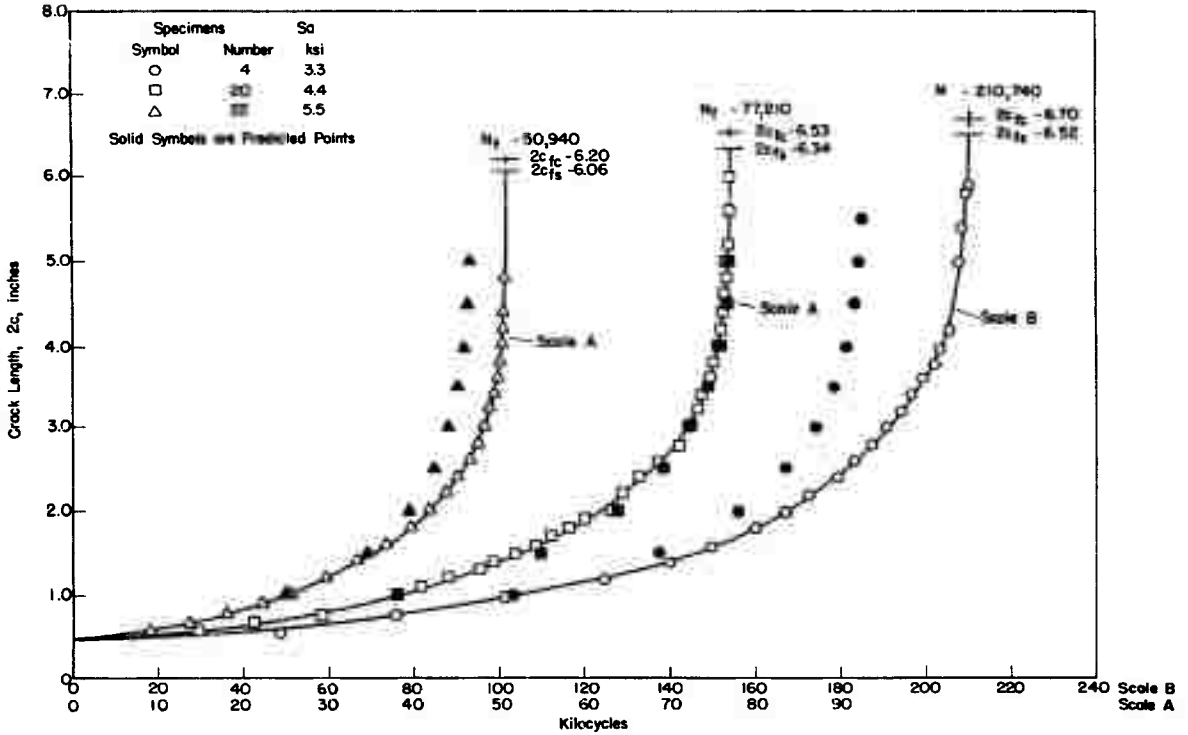

a. Mean Stress S_m = 6.8 KSI

FIGURE 16. FATIGUE-CRACK-PROPAGATION DATA FOR 8-INCH-WIDE PANELS, 1/2 INCH THICK

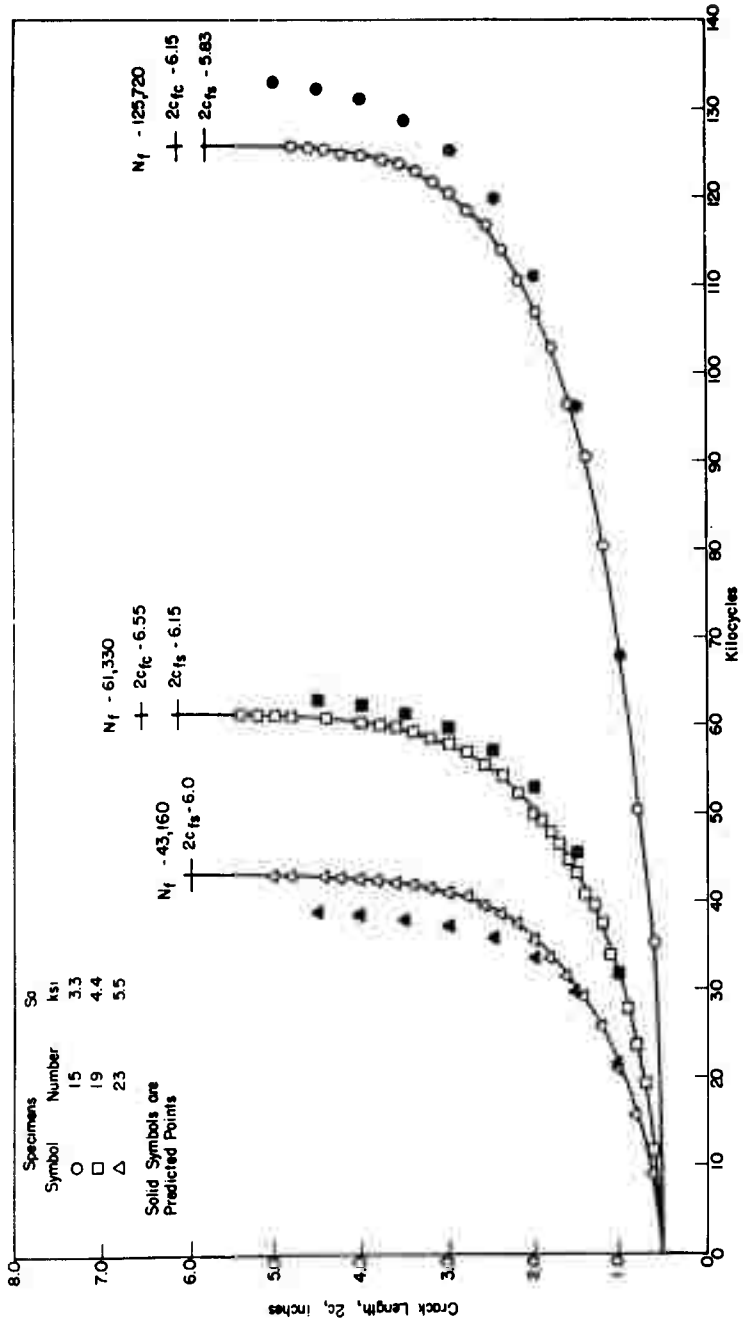

b. Mean Stress S_m = 8.4 KSI

FIGURE 16. (CONTINUED)

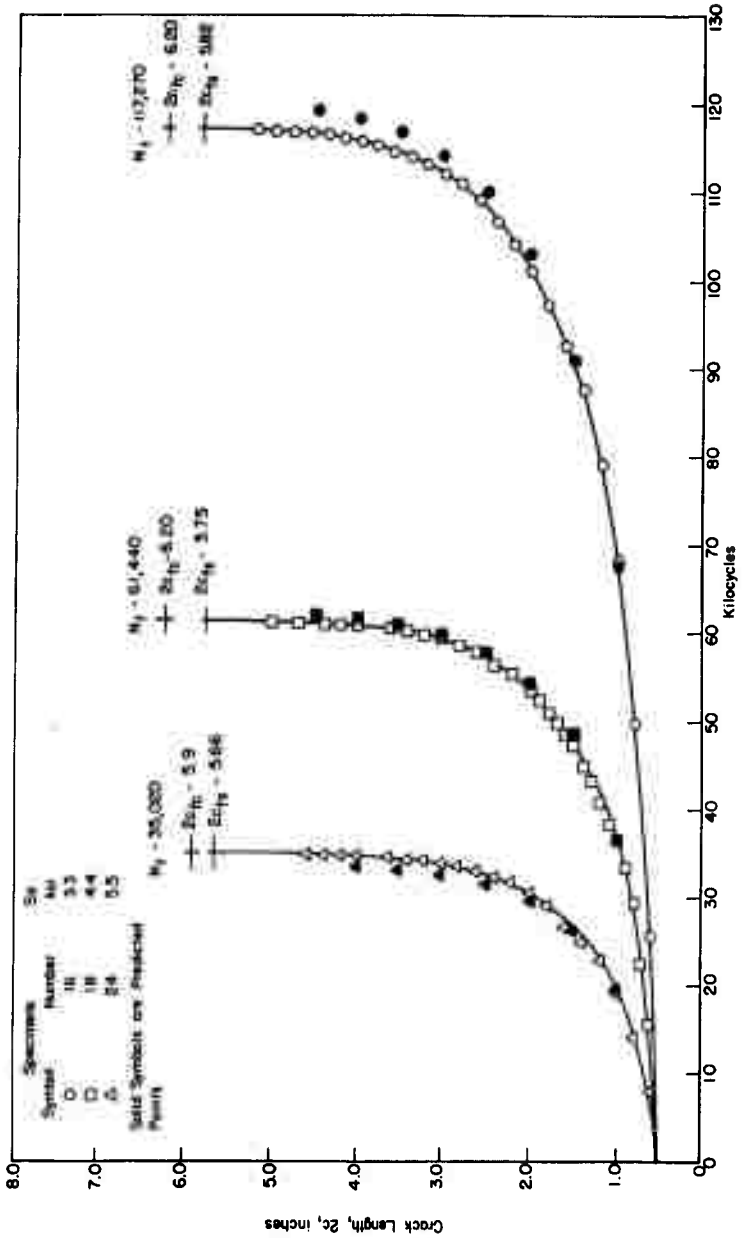

c. Mean Stress S_m = 10.0 KSI

FIGURE 16. (CONTINUED)

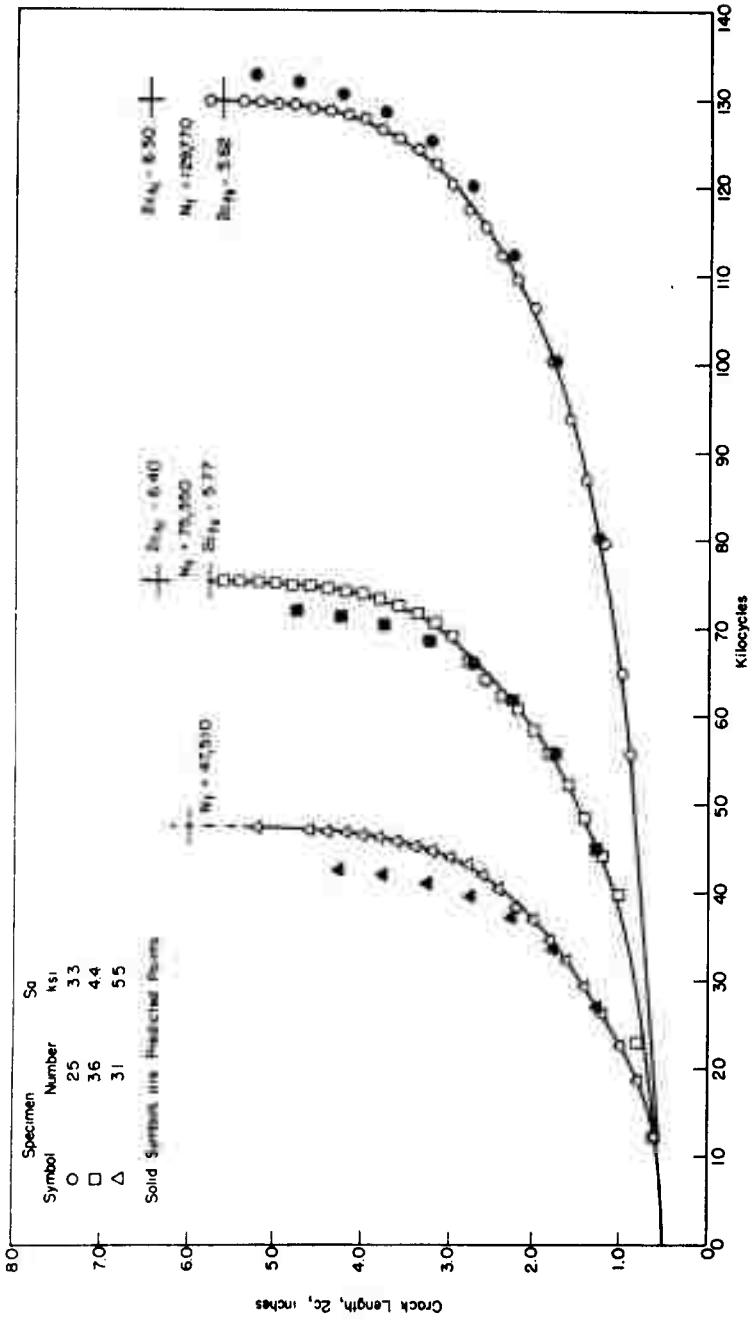

a. Mean Stress S_m = 6.8 KSI

FIGURE 17. FATIGUE-CRACK-PROPAGATION DATA FOR 8-INCH-WIDE PANELS, 1-INCH THICK

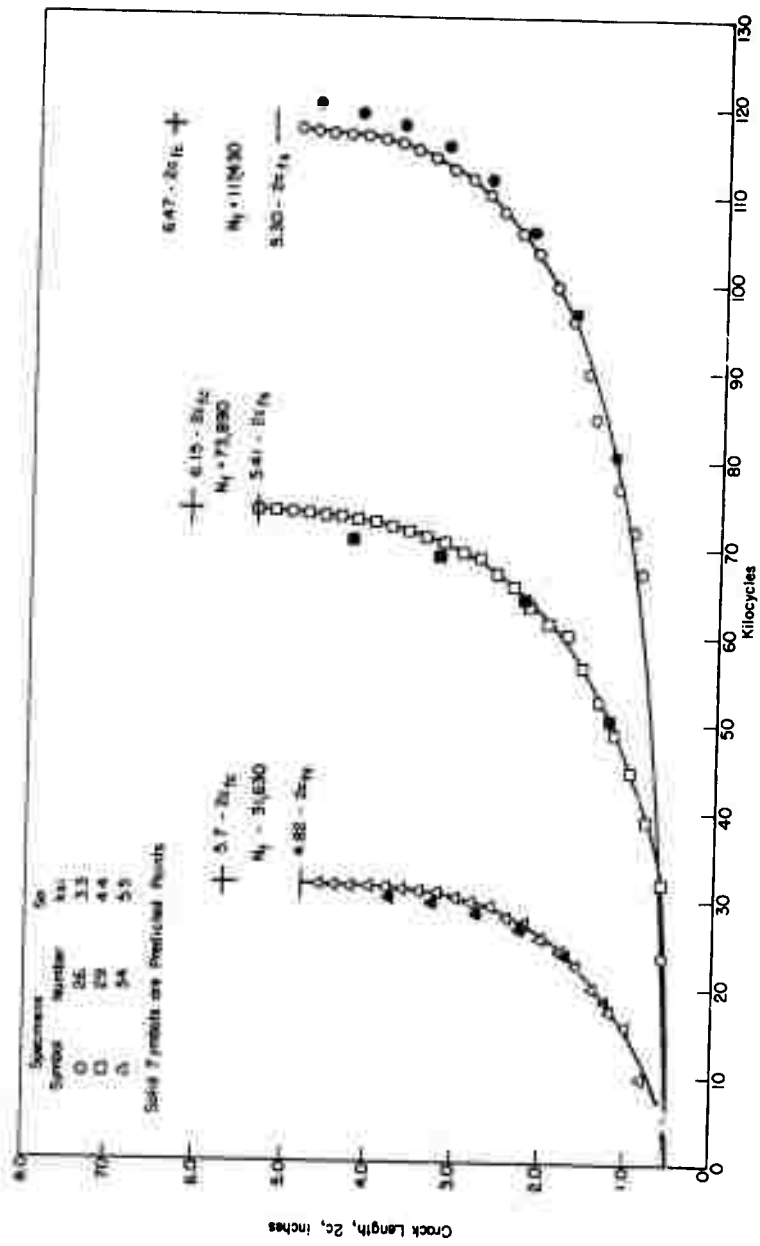

b. Mean Stress S_m = 8.4 KSI

FIGURE 17. (CONTINUED)

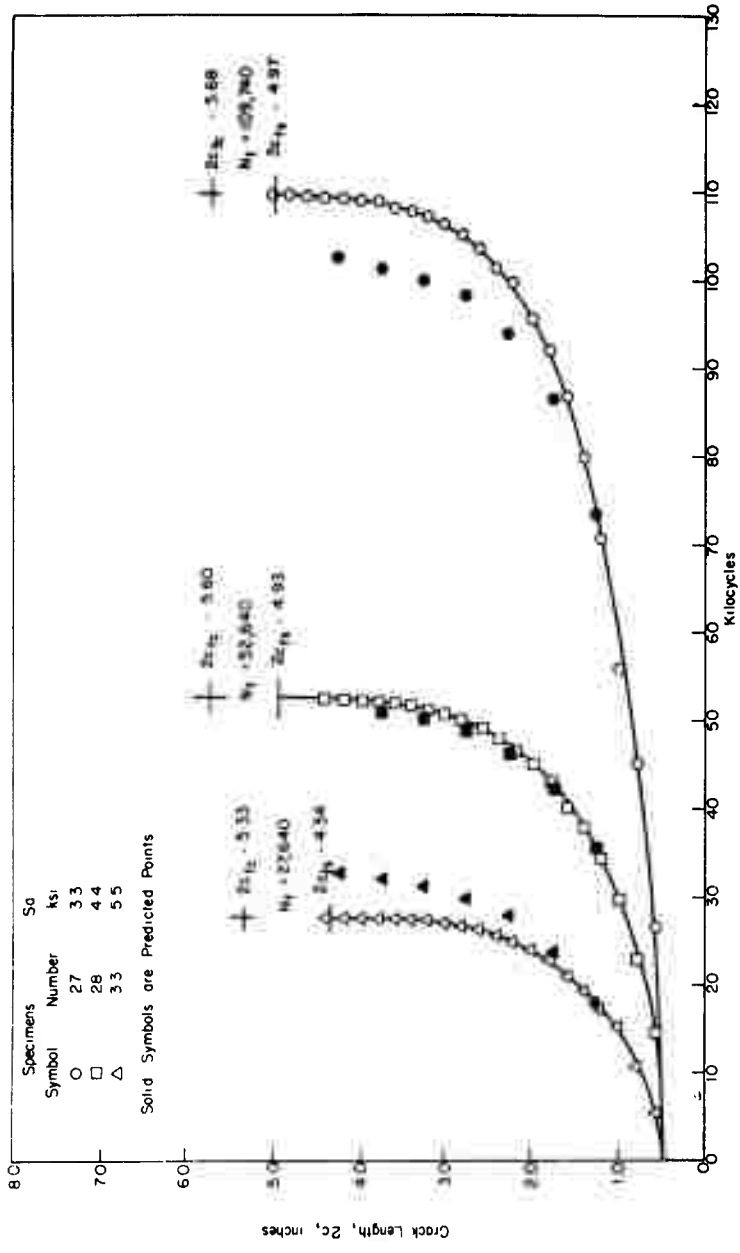

c. Mean Stress S_m = 10.0 KSI

FIGURE 17. (CONTINUED)

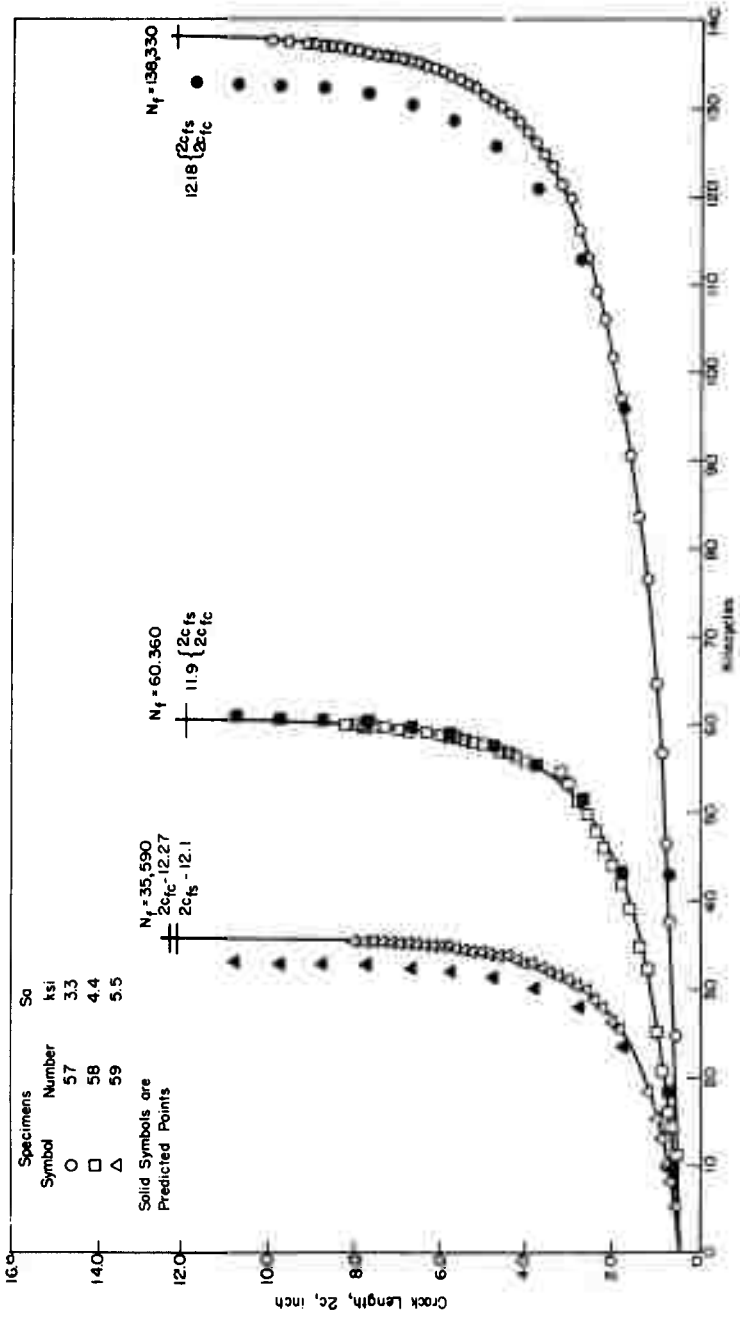

FIGURE 18. FATIGUE-CRACK-PROPAGATION DATA FOR 16-INCH-WIDE PANELS, 1/4INCH THICK, MEAN STRESS S_m = 8.4 KSI

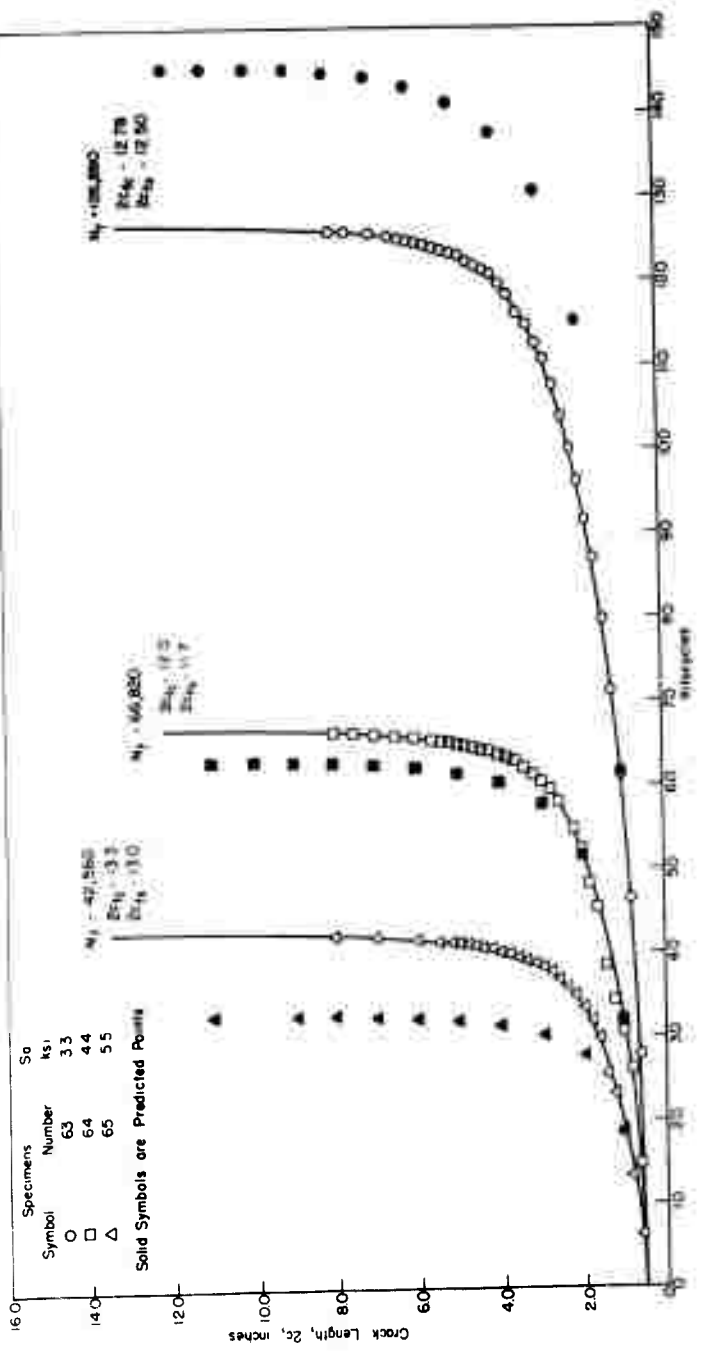

FIGURE 19. FATIGUE-CRACK-PROPAGATION DATA FOR 16-INCH-WIDE PANELS, 1/2 INCH THICK, MEAN STRESS S_m = 8.4 KSI

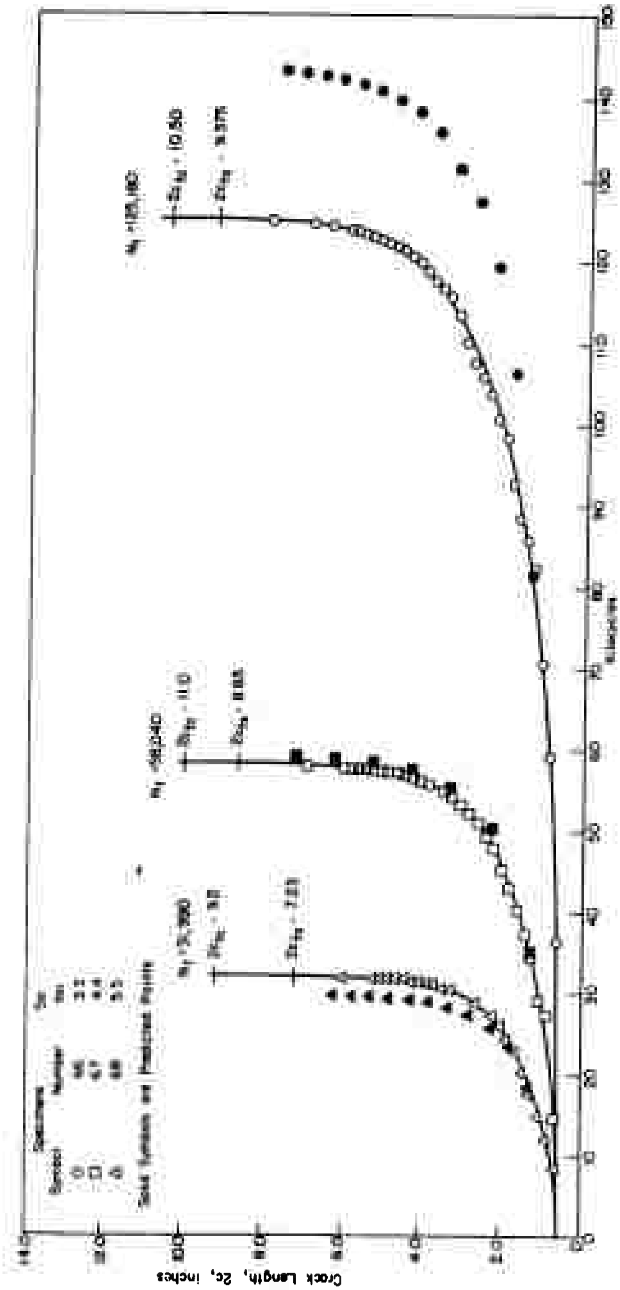

FIGURE 20. FATIGUE-CRACK-PROPAGATION DATA FOR 16-INCH-WIDE PANELS, 1 INCH THICK, MEAN STRESS S_m = 8.4 KSI

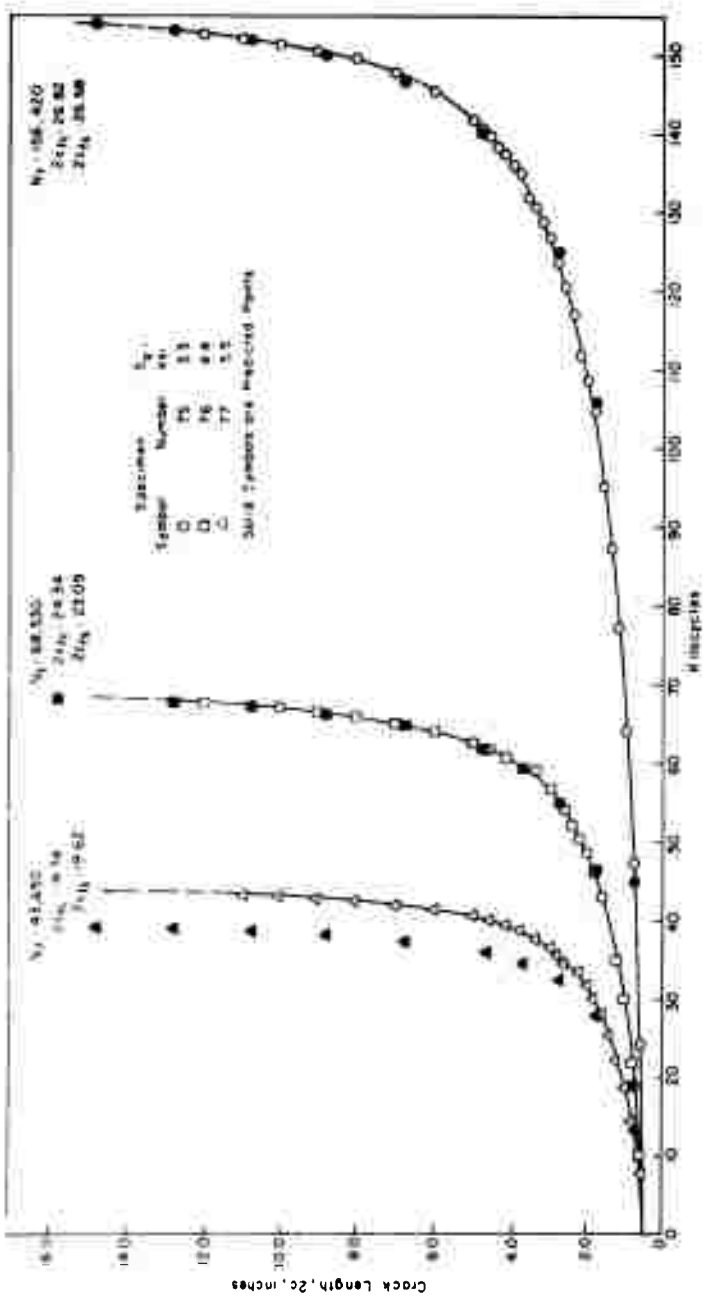

FIGURE 21. FATIGUE-CRACK-PROPAGATION DATA FOR 36-INCH-WIDE PANELS, 1/4 INCH THICK, MEAN STRESS S_m = 8.4 KSI

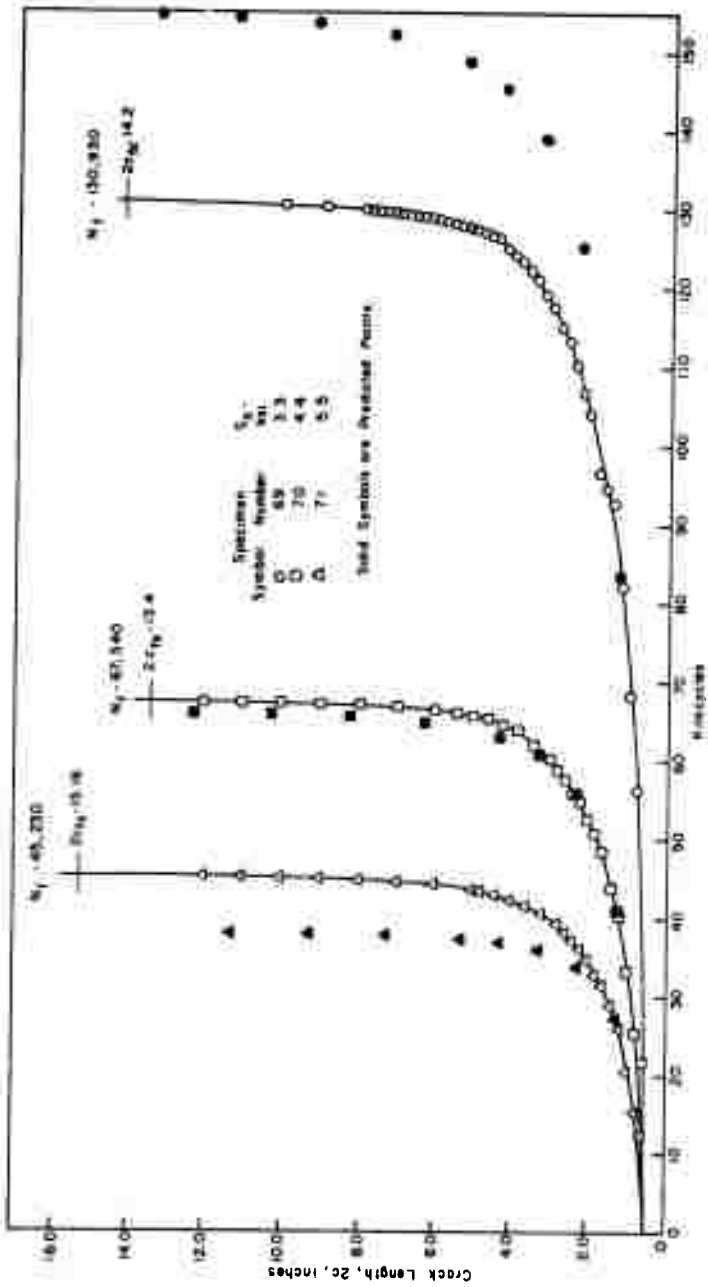

FIGURE 22. FATIGUE-CRACK-PROPAGATION DATA FOR 36-INCH-WIDE PANELS, 1/2 INCH THICK, MEAN STRESS S_m = 8.4 KSI

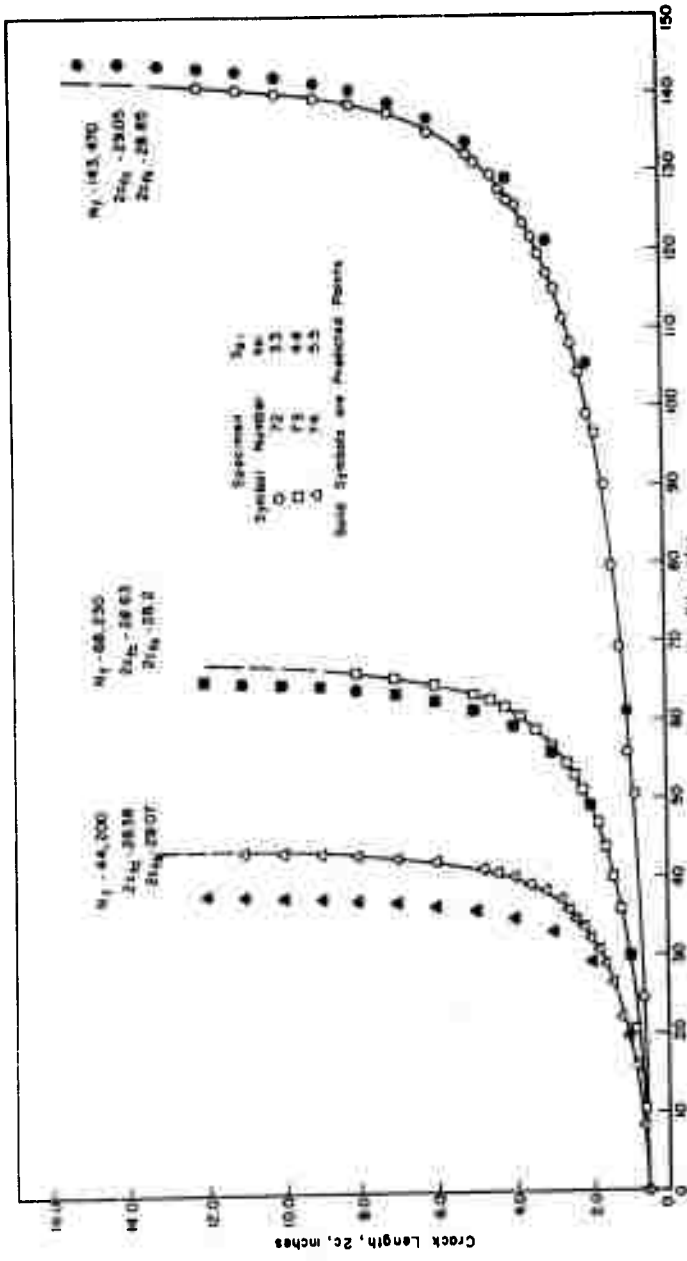

FIGURE 23. FATIGUE-CRACK-PROPAGATION-DATA FOR 36-INCH-WIDE PANELS, 1 INCH THICK, MEAN STRESS S_m = 8.4 KSI

a continuous curve originating at a length of 0.5 inch (the original EDM flaw) and terminating at the failure lifetime, N_f. The horizontal line or lines at the top of the curves represent the measured crack lengths through the center and on the surface as described above.

Figures 14, 15, 16, and 17 show the crack propagation curves for 8-inch-wide panels of 1/16-, 1/4-, 1/2-, and 1-inch thickness, respectively. A comparison of Figures 15 and 17 shows the extensive tunneling that occurs in the 1-inch-wide specimens as compared with the 1/4-inch-wide specimens. It is believed on the basis of macroscopic examination that most of this tunneling occurs very late in life.

Figures 18, 19, and 20 show the curves for 16-inch-wide panels of 1/4-, 1/2-, and 1-inch thickness, respectively.

Figures 21, 22 and 23 show the curves for 36-inch-wide panels of 1/4-, 1/2-, and 1-inch thickness, respectively.

Since in Tables 6 through 15, N_f is the total lifetime to failure for specimens notched with the EDM notch shown in Figure 4 (K_t = 15.2), based on $K_t = 1 + 2\sqrt{t/r}$, from Neuber [3]), S-N-type plots were made and are illustrated in Figures 24, 25, 26, and 27 for 1/16-, 1/4-, 1/2-, and 1-inch-thick panels, respectively. The curves on these figures are predicted curves discussed in a subsequent section.

On each figure, the data are presented two ways. The open points on the right side of each figure represent the stress – total lifetime to failure data, which includes crack initiation. The solid points on the left side of each figure represent the stress – remaining lifetime to failure after the fatigue crack has initiated and propagated to the length indicated on each figure. The indicated crack lengths are essentially the lengths needed to ensure that a through crack will be present, having propagated from the starter flaw in Figure 4.

Initial Observations

The graphs in Figures 14 through 23 show that crack propagation does not always occur as a continuous function. There are evidences that propagation may slow down for a number of cycles, or there may be a burst in propagation again for a small number of cycles. Crack-propagation laws, however, assume a continuous functional relationship. Since the fatigue-fracture profile is relatively complex as discussed in the next section, the fact that there are discontinuities in propagation is not surprising.

Both the fatigue-crack-propagation curves and the S-N data plots in Figures 24 through 27 clearly show that there is a real difference in results for 1/16-inch-thick panels compared with those for 1/4-, 1/2-, and 1-inch-thick panels. Among the three thicker panels, the distinctions are more subtle; however, they suggest that somewhat higher crack-propagation rates are associated with the thicker panels. This will be examined in considerable detail in a later section.

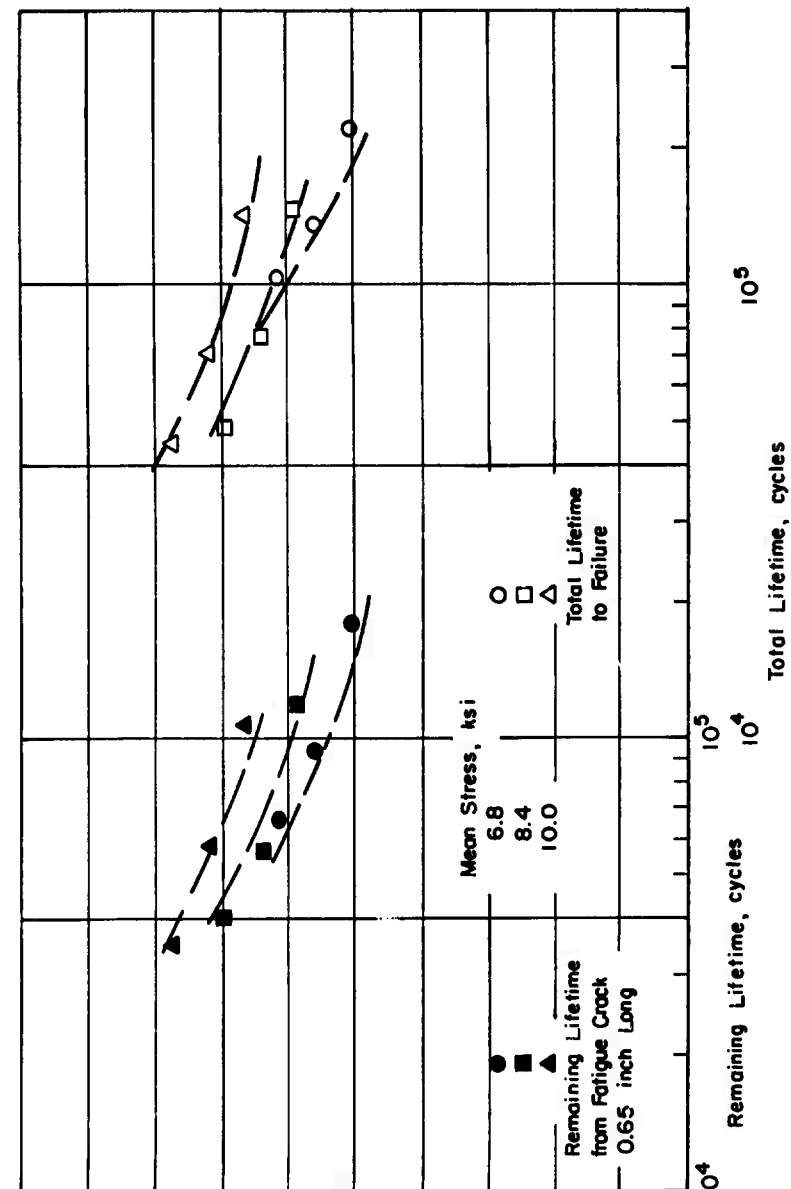

FIGURE 24. STRESS-LIFETIME GRAPHS FOR 1/16-INCH THICK PANELS, 8-INCHES WIDE, CENTER-NOTCHED WITH K_t = 15.2

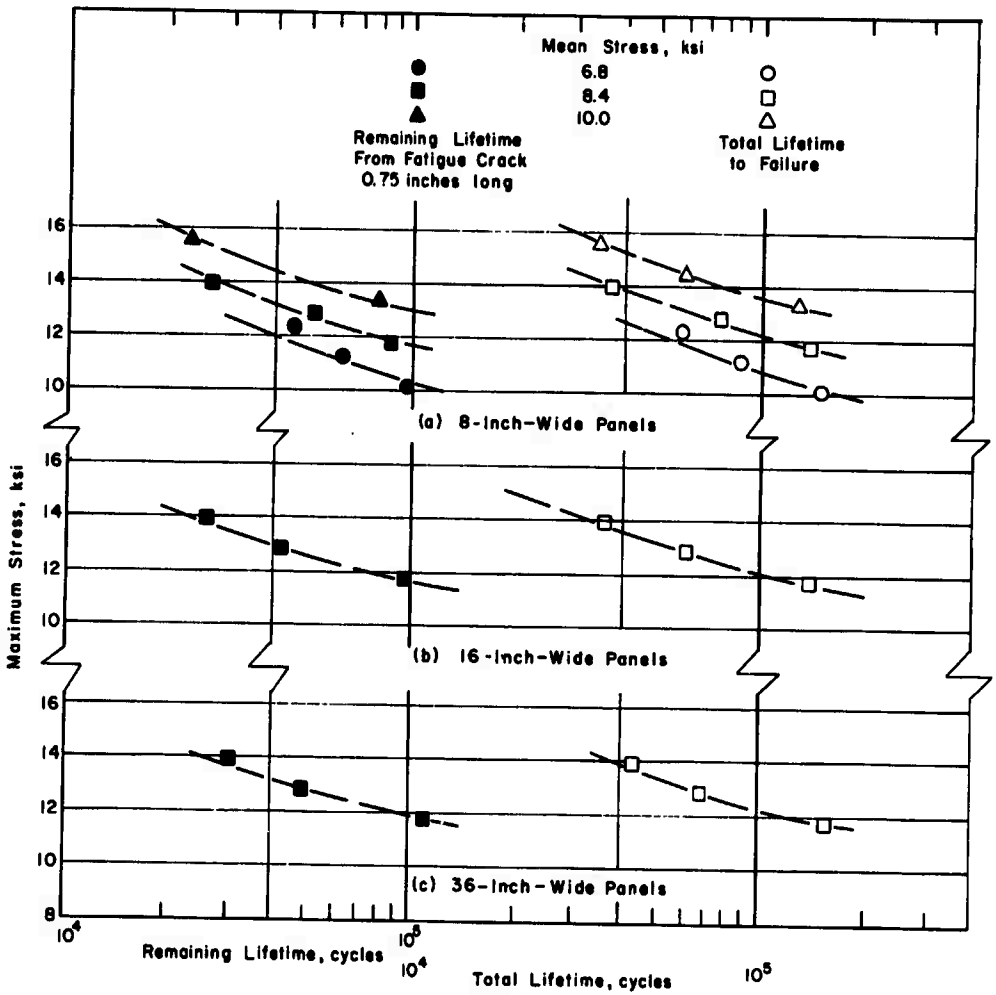

FIGURE 25. STRESS-LIFETIME GRAPHS FOR 1/4-INCH-THICK PANELS, CENTER-NOTCHED WITH K_t = 15.2

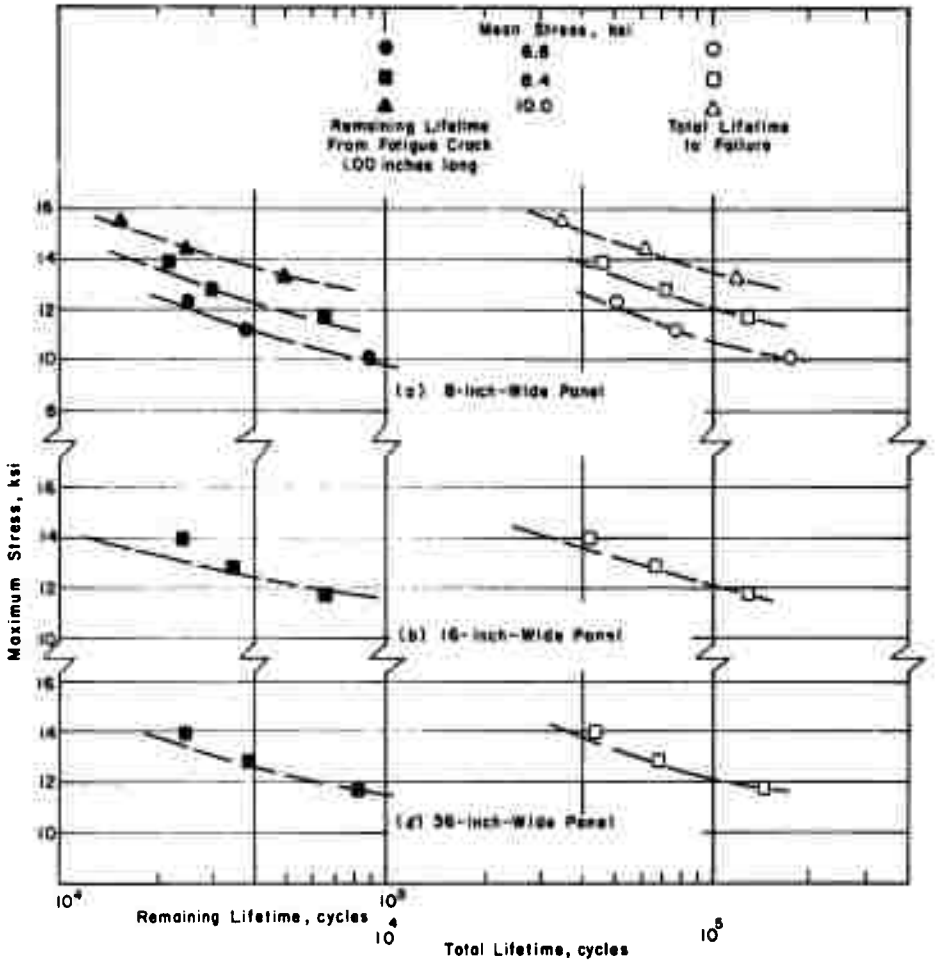

FIGURE 26. STRESS-LIFETIME GRAPHS FOR 1/2-INCH-THICK PANELS, CENTER NOTCHED WITH K_t = 15.2

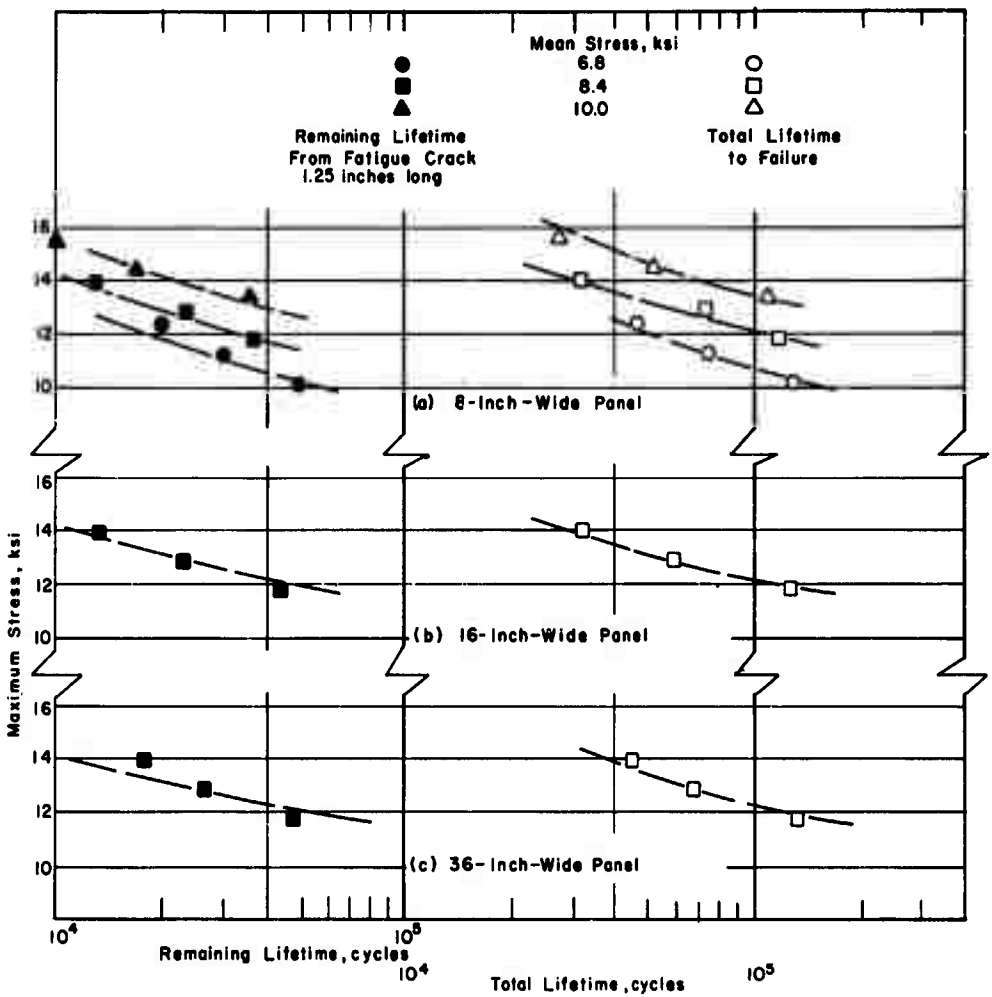

FIGURE 27. STRESS-LIFETIME GRAPHS FOR 1-INCH-THICK PANELS, CENTER NOTCHED WITH K_t = 15.2

Failure Surfaces of Fatigue-Crack-Propagation Specimens

The surfaces of the fatigue-crack-propagation specimens were quite complex. Among the four thicknesses, there were some similarities as well as notable differences. Figures 28 and 29 illustrate the major features. Generally, as the fatigue crack grew away from the starter notch, the fracture surface had a flat grainy appearance. At some distance (1) from the starter flaw (see Figure 28), a series of small ridges formed that were parallel to the sides of the specimens. The ridges generally occurred first along the midplane and then extended across the entire surface at (2). Between (1) and (2), shear lips were seen to form at both surfaces. These lengths were identified as (3) and (4).

As the fatigue crack grew, the shear lips increased in size and the small ridges combined to form fewer but much more pronounced ridges. Eventually, one ridge remained along the center plane which finally terminated when the fracture surface completed the transition to shear mode with either the slant or vee profile. The crack length at this point was identified as (5).

With the 1/16-inch-thick specimens, the symmetrical shear-lip growth that led to converging of the shear lips in the 1/4- and 1/2-inch-thick specimens did not occur. Instead, thin shear lips developed, one of which finally dominated the surface and the fracture then went into a full-slant mode, regardless of the stress level.

The final failure mode for 1/4- and 1/2-inch-thick specimens was a mixture of full slant and vee profile as shown by Sections Ea and Eb on Figure 28.

With regard to the 1-inch-thick specimens, it was interesting to note from Figure 29 that shear lips formed and grew in size until they covered over half the thickness. However, the last-to-fail portion of the specimen was flat fracture, for all widths, as was the case for the fracture specimens. In fact, surface characteristics show that accelerated crack growth leading to final failure was occurring at the fracture surface region containing the strongest shear-lip development.

Figure 30 shows photographs of the fracture surfaces of one of each of the three thicker specimens (8 inch wide). All of the features described above and shown schematically in Figures 28 and 29 are seen in these photographs. In addition, it is possible to pick out what appears to be the extent of fatigue-crack growth prior to failure, at least on the 1/4- and 1-inch-thick specimens. Both show that crack growth is occurring more rapidly along the midplane than at the surfaces. The surface of the 1-inch-thick specimen suggests that crack growth along the center may well be in bursts of varying length.

Measurements of crack lengths (1), (2), (3), (4), (5), and (6)* were made on most specimens and are listed in Table 16.

A detailed examination of Table 16 shows the following to be generally the case (there is quite a bit of scatter involved in these measurements since the distinction was many times very subjective):

*On 1/16-inch-thick specimens only, at that crack length where the fracture surface developed a full-slant mode.

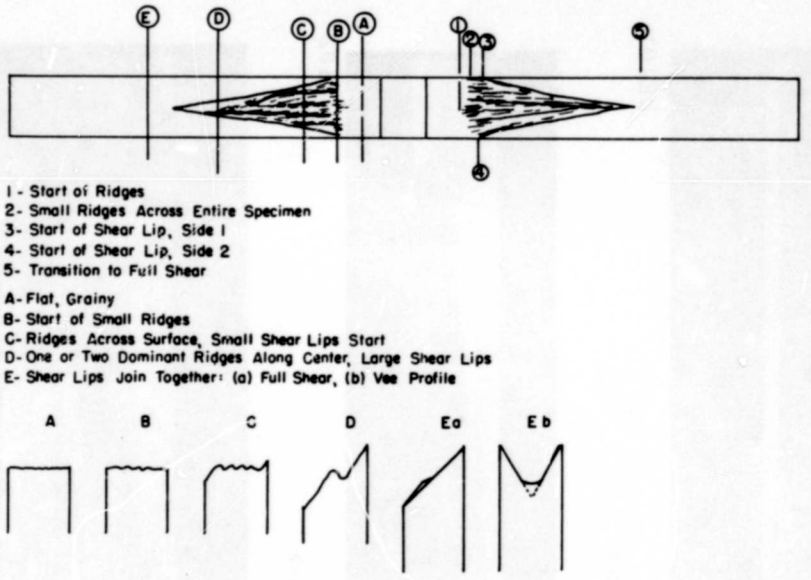

FIGURE 28. SCHEMATIC DRAWING OF FRACTURE SURFACE FEATURES, PRIMARILY 1/4- AND 1/2-INCH-THICK SPECIMENS

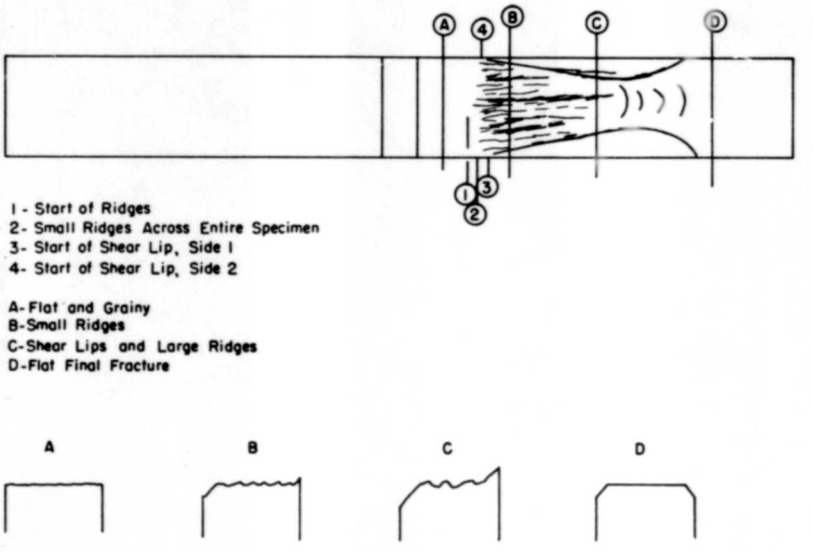

FIGURE 29. SCHEMATIC DRAWING OF FRACTURE-SURFACE FEATURES OF 1-INCH-THICK SPECIMENS

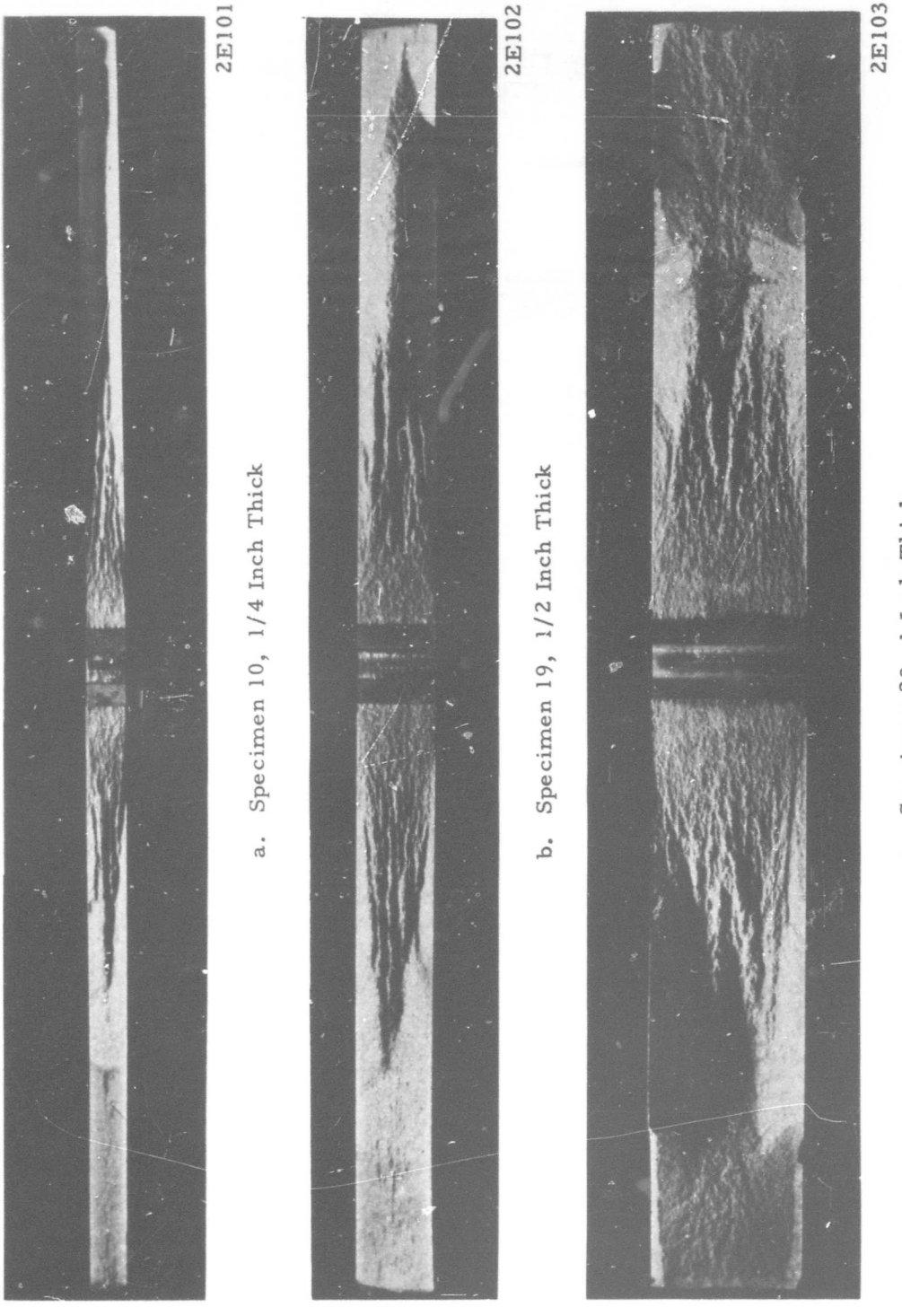

a. Specimen 10, 1/4 Inch Thick

b. Specimen 19, 1/2 Inch Thick

c. Specimen 29, 1 Inch Thick

FIGURE 30. TYPICAL FRACTURE SURFACES OF FATIGUE-CRACK PROPAGATION SPECIMENS

TABLE 16. DIMENSIONS OF FATIGUE-CRACK-PROPAGATION-SPECIMEN FAILURE-SURFACE FACETS

Specimen	S_m, ksi	S_a, ksi	Crack Lengths, inches (1)	(2)	(3)	(4)	(5)	(6)
1/16 Inch Thick, 8 Inches Wide								
56	10.0	5.5	0.91	1.04	1.28	1.34	2.35	1.54
54	10.0	4.4	0.94	0.96	1.30	1.43	2.21	1.95
39	10.0	3.3	0.88	1.18	1.64	2.21	3.79	2.34
55	8.4	5.5	1.14	1.20	1.58	1.64	2.11	2.01
41	8.4	4.4	1.77	1.84	2.54	2.75	5.49	3.47
53	8.4	3.3	1.65	1.83	1.99	2.28	4.27	2.83
43	6.8	5.5	0.68	0.80	1.35	1.36	3.82	1.54
42	6.8	4.4	0.96	1.03	1.87	1.56	4.19	2.55
1/4 Inch Thick, 8 Inches Wide								
14	10.0	5.5	0.66	0.83	0.74	0.83	3.26	
9	10.0	4.4	1.07	1.14	1.07	1.01	3.19	
8	10.0	3.3	1.15	1.22	1.51	1.64	3.70	
13	8.4	5.5	0.91	1.06	0.94	0.75	3.38	
10	8.4	4.4	1.07	1.18	1.69	1.54	4.13	
7	8.4	3.3	1.10	1.84	1.74	1.71	4.10	
12	6.8	5.5	0.78	1.24	0.91	0.88	3.75	
11	6.8	4.4	1.15	1.77	1.31	1.17	4.27	
2	6.8	3.3	1.61	1.84	2.00	1.78	4.83	
1/2 Inch Thick, 8 Inches Wide								
24	10.0	5.5	1.14	1.31	0.87	0.82	4.27	
18	10.0	4.4	1.21	1.41	1.16	0.99	5.09	
16	10.0	3.3	1.06	1.32	1.26	1.32	4.69	
23	8.4	5.5	1.15	1.46	1.18	1.08	4.71	
19	8.4	4.4	1.17	1.43	1.09	1.06	5.12	
15	8.4	3.3	1.80	2.00	1.59	1.61	4.80	
22	6.8	5.5	1.33	1.53	1.12	1.00	4.80	
20	6.8	4.4	1.55	2.16	1.78	1.63	5.19	
4	6.8	3.3	2.46	2.77	2.71	2.45	6.20	
21	6.8	3.3	2.14	2.45	1.74	2.16	5.59	
1 Inch Thick, 8 Inches Wide								
33	10.0	5.5	1.11	1.14	1.13	0.98	--	
28	10.0	4.4	0.94	1.12	1.34	1.23	--	
27	10.0	3.3	1.75	1.87	1.81	1.94	--	
34	8.4	5.5	1.11	1.20	0.92	0.98	--	
29	8.4	4.4	1.51	1.61	1.33	1.50	--	
26	8.4	3.3	1.76	2.00	2.14	2.25	--	
35	6.8	5.5	1.16	1.23	1.30	1.15	--	
36	6.8	4.4	1.18	1.34	2.21	2.09	--	
25	6.8	3.3	1.73	1.93	2.17	2.31	--	

Specimen	S_m, ksi	S_a, ksi	Crack Lengths, inches (1)	(2)	(3)	(4)	(5)	(6)
1/4 Inch Thick, 16 Inches Wide								
59	8.4	5.5	0.92	1.05	0.85	1.09	4.68	
58	8.4	4.4	1.16	1.28	1.11	1.32	5.11	
57	8.4	3.3	1.58	2.01	1.83	1.76	4.87	
1/2 Inch Thick, 16 Inches Wide								
65	8.4	5.5	1.05	1.22	1.20	1.14	4.95	
64	8.4	4.4	1.21	1.45	1.89	1.67	5.42	
63	8.4	3.3	1.61	1.90	1.80	1.92	6.35	
1 Inch Thick, 16 Inches Wide								
68	8.4	5.5	0.89	1.12	1.22	1.14	--	
67	8.4	4.4	1.41	1.71	2.14	1.93	--	
66	8.4	3.3	1.71	2.50	2.51	2.35	--	
1/4 Inch Wide, 36 Inches Wide								
75	8.4	5.5	0.81	0.99	0.91	0.94	2.15	
76	8.4	4.4	1.15	1.35	1.10	1.29	2.83	
77	8.4	3.3	1.54	1.69	1.91	1.84	4.44	
1/2 Inch Thick, 36 Inches Wide								
74	8.4	5.5	1.13	1.26	0.86	0.74	5.06	
73	8.4	4.4	1.30	1.44	1.09	1.31	6.74	
72	8.4	3.3	1.46	1.60	1.54	1.71	7.28	
1 Inch Thick, 36 Inches Wide								
71	8.4	5.5	0.98	1.26	1.21	1.43	--	
70	8.4	4.4	1.25	1.63	1.20	1.31	--	
69	8.4	3.3	1.42	1.94	2.08	2.14	--	

(1) For each one of the five facets of the fracture surface measured, (a) the length of crack at each facet was smaller, the higher the alternating stress (for a constant S_m); (b) the length of crack at each facet also was smaller, the higher the mean stress (for a constant S_a).

(2) As the panel width increased, the crack length to each facet also increased somewhat.

(3) There is some trend that as thickness increases, the crack length to similar failure surface facets increases.

The trend suggested by the first two statements appears to be in the direction suggested by Broek, et al[4] and Walker[5], namely, that completion of rotation to the shear mode should occur at about a constant value of ΔK^*. An examination of the data in Table 16 expressed as various ΔK values, depending upon the crack facet, did not negate the idea that ΔK is reasonably constant. The scatter in ΔK values did not strongly support it either. Whether these data will support Walker's thinking in regard to $\overline{\Delta K}$ on this point has yet to be tested.

There is a general belief that a fatigue crack propagating under a given stress condition should fail when the crack reaches a length critical for that stress level. To test out this belief to a first approximation, the data in Figure 11 were examined as follows. The residual-strength data given by the coordinates S_1, $2c_c/w$ in these figures were used to obtain estimates of $2c_c/w$ for each maximum stress of the nine fatigue-stress cycles used on the 8-inch-wide panels and the three fatigue-stress cycles used on the 16- and 36-inch-wide panels. This merely involved constructing a straight or curved line through data and drawing horizontal lines at all maximum stress values so that they intersected the residual-strength curve. Vertical lines from the points of intersection provided the 2c/w values that would be expected to be associated with the failure stresses. From these values, critical crack lengths were computed merely by multiplying the 2c/w by the appropriate panel width. Then, from the measured surface-fatigue-crack lengths shown in Figures 14 through 23 (as $2c_{fs}$ values), a graph was constructed showing measured surface-fatigue-crack length as a function of the critical crack length estimated from residual-strength data. Figure 31 shows the comparison. In this figure, if there is a good correlation, the plotted points should fall reasonably well along a 45-degree line. It is seen that with two exceptions the data do agree quite well. The exceptions are the two collections of data on 36-inch-wide panels for 1/4- and 1/2-inch-thick material.

Generally then, it does appear that in the fatigue-crack-propagation analyses, a useful concluding crack length for a given stress cycle is that length predicted from residual-strength data for the maximum stress of the fatigue cycle. It is recognized that the moderate-to-large amount of tunneling that occurs in the 1/2- and 1-inch specimens raises some questions, however.

* Walker says this should occur at a constant value of $\overline{\Delta K}$, an effective stress-intensity factor, that accounts for alternating stress and load ratio as discussed later in the report.

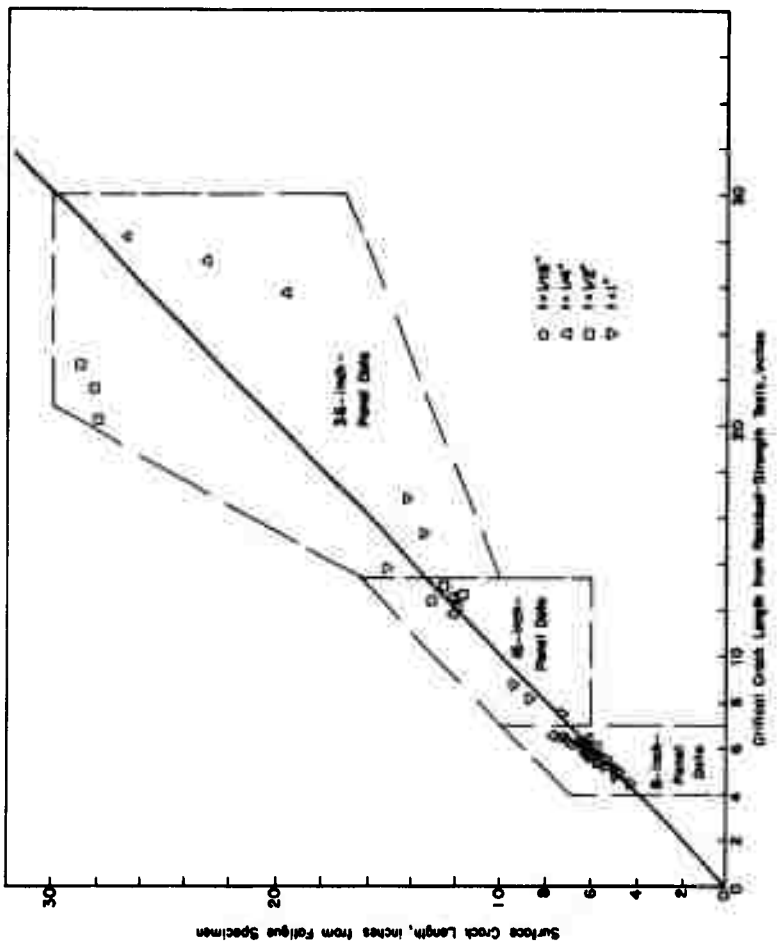

FIGURE 31. COMPARISON OF CRACK LENGTH IN FATIGUE TEST WITH CRITICAL CRACK LENGTH FROM RESIDUAL-STRENGTH TESTS

TECHNICAL EVALUATION AND DISCUSSION

Fracture Toughness and Residual Strength

The resistance of a material to the initiation and propagation of flaws and tc fracture is frequently termed the toughness of the material. Generally, this toughness is considered to be an intrinsic material characteristic that, when properly quantified, may be used to determine the residual (or remaining) strength of a flawed structural element. Since, in this program, the fracture behavior and toughness of flat, centrally cracked tension aluminum panels was studied, the following discussion will emphasize that geometric model. However, parallel discussions, observations, and arguments can be generated readily for other structural configurations.

It will be important to note that in the following discussion, toughness, or fracture toughness, is viewed as a material characteristic, while residual strength refers to the structural strength as influenced by fracture toughness, geometry, loading, and so forth. This not-always-so-obvious distinction is very important to recognize. The goal in appraising fracture toughness is to obtain a quantitative description of the material itself. Then, in residual-strength studies, this fracture-toughness quantity is applied to design situations. Of course, at this point in the discussion, this distinction is only conceptual; the purpose of the program was an elucidation of this concept.

In the most fundamental sense, the basic objective of toughness testing and residual-strength studies is to determine the relationship between gross applied stress, S, (or load) and flaw size, 2c. For flat, centrally cracked tension panels, these quantities within their geometric framework are graphically idealized in Figure 32. In this illustration, the constraint of finite size immediately suggests width as a basic parameter in the studies. Furthermore, the recognition of stress states (i.e., plane stress or plane strain) makes third-dimensional restraint, or "thickness effects", quite important. From here one can readily suggest additional parameters of temperature, environment, strain rate, etc.; however, these were beyond the scope of the current program. The remaining discussion and subsequent analysis and evaluation of data will be concerned with the basic variables, stress and flaw size, and basic parameters, width and thickness, for 7075-T7351 aluminum alloy sheet and plate.

Failure Modes in Center-Cracked Tension Panel

From both an analytical and a mechanistic point of view, it is convenient to classify center-cracked tension-panel failure modes into two general categories, namely, (1) tensile instability, and (2) energy instability, defined by the character of the stress field and the material behavior on the net critical section. In a loose sense, these categories distinguish between gross plastic behavior and gross elastic behavior, respectively, in the material at failure. Although these modes are not entirely distinct and, in fact, do interact, they are significant classifications for an evaluation of the complex field of data being considered.

Tensile Instability. Tensile instability is defined as that failure mode in which gross plastic effects are noted prior to fracture on the entire critical section. The net

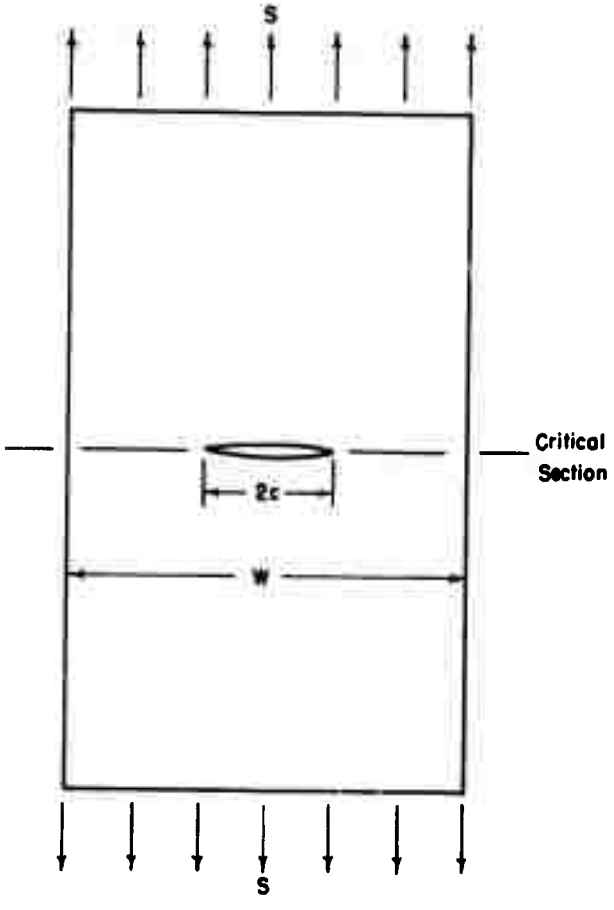

FIGURE 32. FLAT, CENTER-CRACKED TENSION PANEL

section stresses are at yield strength, or above, possibly at ultimate strength. The plastic zone extends across the entire width of the specimen. For engineering purposes, such a failure condition may be expressed as

$$\text{Tensile instability} = \sigma_{net} \sim \text{TYS, } \sigma^*, \text{ or TUS}$$

where

TYS = tensile yield strength

σ^* = some critical plastic flow stress

TUS = tensile ultimate strength.

In other words, failure has resulted from exceeding the maximum strength equilibrium of the material-structural combination.

The idealized stress profile of this mode of failure is illustrated schematically in Figure 33. The crack-tip plastic zone (PZ on figure) has engulfed the entire critical section, and the failure which is imminent will be triggered by something other than an elastic mechanism. On graphical plots of stress versus flaw-size ratio, these data appear at or above the net-section-yield line, as shown in Figure 34, indicating inelastic failure.

Energy Instability. Energy instability is that failure mode in which not all points of the cross section are in the plastic regime at the onset of fracture. As shown in Figure 35, the plastic zone does not extend completely across the critical cross section. Fracture results as a divergence from the equilibrium energy profile on the critical cross section as postulated by linear elastic fracture mechanics.[6, 7] Data of this type, schematically illustrated in Figure 36, plots as an inverse relation between stress and flaw size well below the net-section-yield line.

Interaction. To understand the interrelationship of tensile instability and energy instability more fully, it is convenient to consider the idealized superposition of the two relationships as shown in Figure 37. Tensile instability for a panel of width W is represented simply as a straight line from a gross section stress equal to TYS for 2c equal to zero to a gross section stress of zero for a 2c equal to the plate width W. Energy instability, as described by linear elastic mechanics for an infinitely wide plate, is represented by the curved line ff in Figure 37, where the curve represents explicitly one value of stress intensity, K. Although one might think that these discrete characterizations are straightforward, the modes do overlap at both extremes.

At the left, plastic-zone (PZ) development, which is the primary distinguishing factor between the two instability modes, is a continuous process increasing with applied gross stress. The plastic zone present at (a) does not suddenly expand across the critical section when the applied stress reaches (b); rather, it develops gradually and continuously between (a) and (b), amplifying the effect of the actual crack present. This transitional behavior results in the occurrence of data points in the shaded area (a,b,c) somewhat short of the idealized line (ab) for energy instability or line (bc) for tensile instability. In a similar fashion at the right-hand extreme, the finite-boundary effects

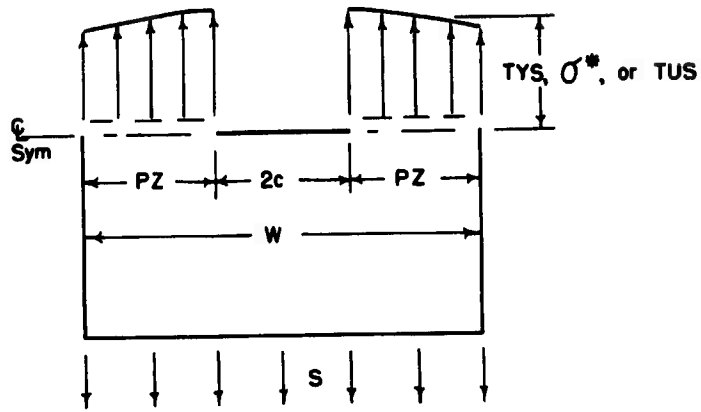

FIGURE 33. STRESS CONDITIONS WHEN FRACTURE IS IMMINENT OWING TO TENSILE INSTABILITY

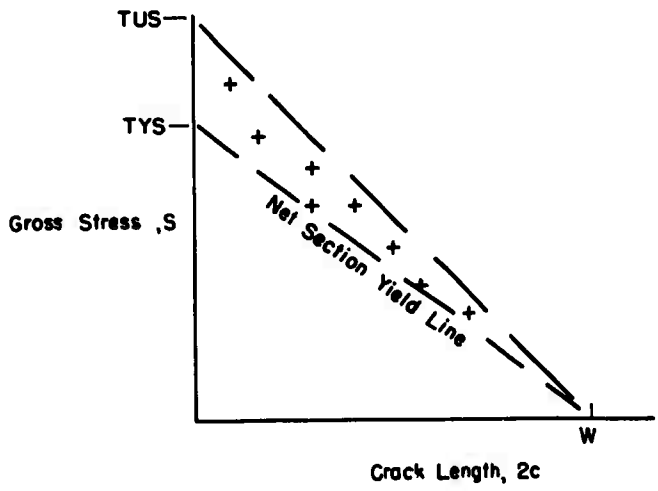

FIGURE 34. TYPICAL DATA FIELD FOR TENSILE INSTABILITY

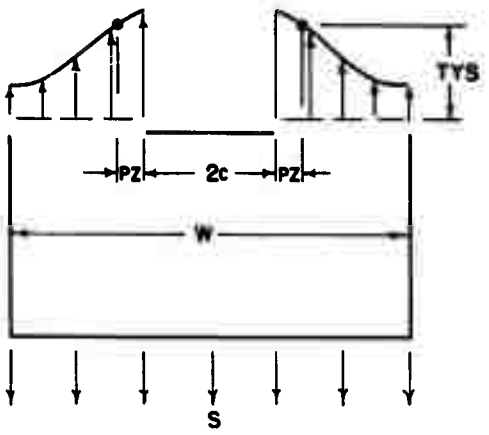

FIGURE 35. STRESS CONDITIONS WHEN FRACTURE IS IMMINENT OWING TO ENERGY INSTABILITY

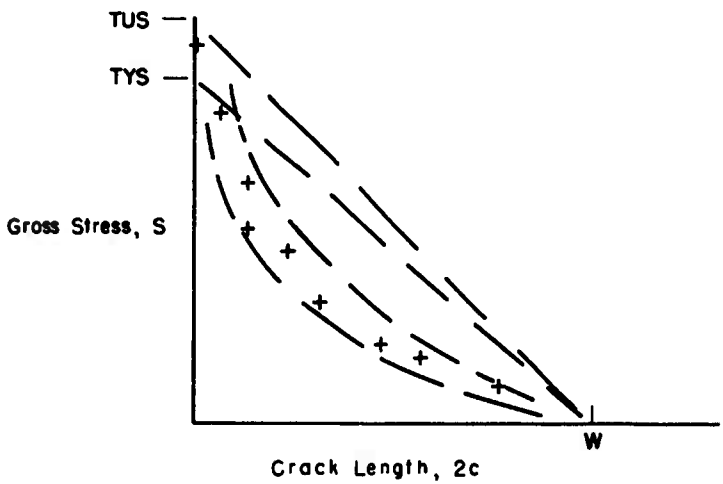

FIGURE 36. TYPICAL DATA FIELD FOR ENERGY INSTABILITY

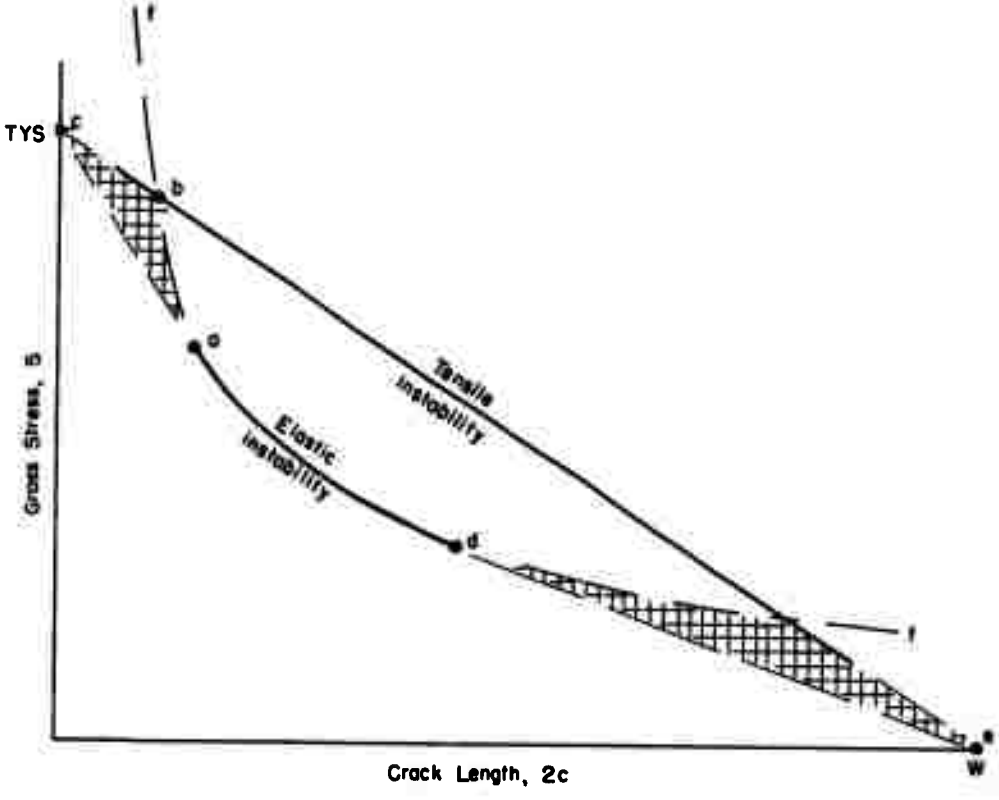

FIGURE 37. IDEALIZED SUPERPOSITION OF TENSILE- AND ENERGY-INSTABILITY CONDITIONS

depress actual data points into the shaded area below both the idealized tensile- and energy-instability lines. These observations are important for the development of a residual-strength-analysis technique later in this report.

Implicit to this categorization of fracture modes are two discrete and distinctly different fracture behavior modes. Tensile instability is predominantly a plastic mechanism on the gross section, while energy instability is largely an elastic process acting on a localized self-perpetuating front. As a result, it would be expected that no single analytical model would completely explain both behavior modes, although the two criteria may be easily interfaced to each other. There are many instances where a single analytical model appears to cover two problems; however, this is usually accomplished by "distortion" or "stretching" of either the coordinates or the data base. While this is not necessarily objectionable, it should be recognized as being semiempirical rather than rigorous.

Basic Factors in Fracture Toughness and Residual-Strength Analysis

In the following subsection, the fundamental quantities affecting fracture toughness and residual strength are discussed. Stress, flaw size, width, and thickness are the elementary quantities that have been considered in this program. However, for completeness, it is also appropriate to mention briefly additional factors which may complicate the picture.

Stress and Flaw Size. These two quantities are literally inseparable in the discussion of fracture. Without a flaw, there would be no discontinuity to disturb the stress field; without a stress field, there would be no mechanism to activate an instability at the flaw. Experience, as well as engineering intuition, always leads to the inverse relation

$$S \sim (\text{flaw size})^{-1}$$

between failure stress and flaw size. The development of linear elastic fracture mechanics[8] provided a quantification of this relation in the unique form

$$K = S\sqrt{\pi c} \quad , \tag{1}$$

where

K = stress-intensity factor

S = applied gross stress

c = flaw size, one-half crack length for center-cracked tension panel.

This latter relation, while potentially very useful, is based on certain idealized conditions that are very difficult to duplicate in finite-size structural elements and imperfectly elastic (or real) materials. As a result, practical structural experiments have not clearly discriminated the actual role of each of the several parameters influencing residual strength. In this program, an attempt was made to gain further insight into the parameters of width and thickness.

Width. The development of Equation 1 is based on the idealization of a crack or flaw in a panel of infinite extent. Of course, in real engineering structures, such a structural size is only hypothetical. A correction factor is needed to correlate fracture data obtained on finite-size elements and relate it to the reference baseline of an infinite-size panel. To account for the effects of finite width, a factor termed the finite-width correction, f(2c/W), has been used to modify Equation (1) as

$$K = S\sqrt{\pi c}\, f(2c/W) \quad , \tag{2}$$

where

2c = crack length

W = panel width.

The finite-width correction is in excess of unity, i.e.,

$$f(2c/W) \geq 1.0 \quad , \tag{3}$$

since the finite boundary tends to intensify the distribution of stresses in the area of the discontinuity. This is a more severe situation than for the equivalent flaw in an infinite-width panel. Alternatively, it may be viewed as having less section remaining to carry the cut load and, hence, a more severe loading condition.

Thickness. The effect of thickness is a bit more nebulous in its definition. The bulk restraint of thickness adjacent to the crack tip introduces a triaxial stress field which, in turn, tends to restrain plastic deformation. The extremes of thickness (i.e., plane stress, in reality, is a two-dimensional case where t = 0; and plane strain, t = ∞) are relatively easy to model analytically, but are only the extreme bound to a myriad of real, finite-thickness cases. While an evaluation of the thickness effect was one objective of this program, it is essentially an empirical study. Intimately tied to this parameter is the effect of plasticity.

Plasticity. The stress raiser at the crack tip inevitably introduces plasticity to the residual-strength problem. As suggested earlier in the discussion of tensile and energy instability, the amount of plasticity in existence on the critical section appears to be the major factor in discerning between net elastic or net plastic effects.

From an analytical perspective, plasticity can be considered as either an effective extension of the crack length or an artificial amplification of the applied gross stress. In either case, it tends to manifest itself as a relative increase in material toughness. Frequently, the influence of plasticity is appended to the crack-length term of Equations (1) and (2) as a plastic-zone radius, r, with the formulation

$$K = S\sqrt{\pi(c + r)}\, f[2(c + r)/W] \quad . \tag{4}$$

Several analytical formulations of plastic-zone sizes have been postulated. Irwin presented the relations

$$r = \frac{1}{2\pi}\left(\frac{K}{TYS}\right)^2 \tag{5}$$

for plane stress, and

$$r = \frac{1}{4\sqrt{2\pi}}\left(\frac{K}{TYS}\right)^2 \approx \frac{1}{6\pi}\left(\frac{K}{TYS}\right)^2 \tag{6}$$

for plane strain. In contrast, Dugdale derived

$$r = c\left(\sec\frac{\pi}{2}\frac{S}{TYS} - 1\right) \tag{7}$$

which for small values of S/TYS is equivalent to Equation (5), but for large S/TYS values, is significantly larger.

Interpretation and Application

The foregoing discussion on failures modes and on the principal parameters and variables involved in flaw behavior provides a framework within which the distinction between fracture toughness and residual strength can be made clearer. In the following subsection, the quantification of a material toughness index is discussed and then applied to the more general framework of residual strength. It is very important to recognize that a useful toughness index must play a dual role. It must provide a comparative rating for materials' selection and a quantitative description of damage tolerance for design applications.

Fracture Toughness. The stress-intensity factor, K, previously described, is one formulation of the conceptual toughness characteristic alluded to earlier in the report. Although it is not the only means of determining toughness, it appears to be the most amenable to design applications because it is directly stress related.

The significance of the stress-intensity factor as a parameter of energy instability is illustrated in Figure 38, repeating the essence of Figure 37. The interaction of the parametric K curves with tensile instability on the left boundary is the origin of plasticity corrections; the interaction on the right is a manifestation of finite-width effects. These multiple interactions gave rise to Equations (2) and (4), representing various refinements of the stress-intensity factor. Both are equally useful for a comparative rating of materials, provided they are utilized in a consistent fashion. It must be recognized, however, that correction factors are only approximate (i.e., none have been shown to be exact) and are most influential at the extremes of the parametric curves. They all serve to increase the value of the basic stress-intensity factor [Equation (1)], and, so to speak, bring the actual data points up into alignment with the idealized K curve. As a result, several different numerical values of K can be obtained for a specific fracture test, depending on the formulation selected or the parameters considered.

For purposes of material comparison, each formulation will provide a proper relative toughness rating within itself. However, on an absolute scale, such as is necessary for design application, the variances could lead to overly conservative or very unconservative predictions, neither of which is desirable. These aspects will be further discussed in the next subsection and in the data analysis of the experimental program.

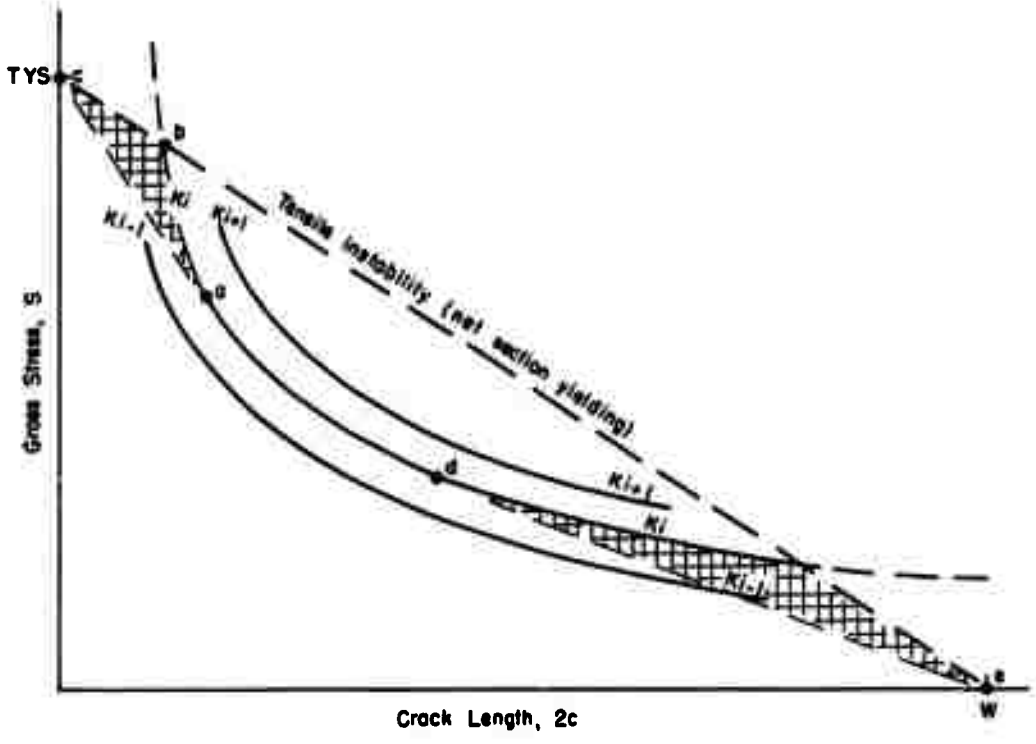

FIGURE 38. STRESS-INTENSITY FACTOR, K, AS A PARAMETER OF ENERGY INSTABILITY

Residual Strength. The residual-strength analysis considered in this report is a simple and direct means of relating stress-intensity factors to a residual-strength data format. It is based on the observation that over the central range of stresses and crack lengths, idealized elastic instability is indeed representative of fracture data, but at the extremes of stress and flaw size, analytical corrections for plasticity and width do not model the data in a reliable fashion. The technique and its analytical expressions are presented in the following paragraphs.

Although this technique may be considered an oversimplification of the ultimate method for modeling plasticity and boundary effects, it will be shown to embrace the experimental data quite well over the full range of crack lengths. This method is not a substitute for, but rather a supplement to, the stress-intensity concept. No new parameters are introduced.

The central portion (Segment a-d) of the idealized elastic-instability curve is preserved since it represents the fracture data very well in that regime. However, at the crack-length extremes (i.e., $2c = 0$, or $2c = W$), the linear extensions, c-a and d-e of Figure 38, appear to fit the experimental data better. Thus, as a convenient approximation and as a simplified representation of the data, straight-line segments are appended to the central curve by tangency conditions at Points a and d. These conditions are as follows:

(1) For tangency at Point a,

slope of c-a = slope of $K = S\sqrt{\pi c}$ at Point a

$$-\frac{TYS-S}{2c} = \frac{dS}{d(2c)} = -\frac{S}{4c}$$

$$\text{or } S = \frac{2}{3}(TYS) \quad . \tag{8}$$

(2) For tangency at Point d,

slope of d-e = slope of $K = S\sqrt{\pi c}$ at Point d

$$-\frac{S}{W-2c} = -\frac{S}{4c}$$

$$\text{or } \frac{2c}{W} = 1/3. \tag{9}$$

These conditions imply that the elastic-instability curve is effective up to two-thirds of the tensile yield strength and up to crack lengths of one-third the panel width. Beyond these limits, the straight-line projections are more realistic representations of fracture behavior.

It may next be asked, "What is the crack length 2c at which the fracture stress, S, is equal to two-thirds of the tensile yield strength?". This can be readily evaluated by the following equation:

$$S = \frac{2(TYS)}{3} = \frac{K}{\sqrt{\pi c}}$$

$$\text{or } 2c = \frac{9}{2\pi}\left(\frac{K}{TYS}\right)^2 = 1.43\left(\frac{K}{TYS}\right)^2 \quad .$$

It is interesting to note that this expression is less restrictive than the crack-length requirement,

$$2c \geq 2.5 \left(\frac{K}{TYS}\right)^2 ,$$

which has been empirically proposed[9] for a variety of fracture specimens. Thus, it does appear that a rational engineering criterion compatible with empirical evidence does exist for limiting plasticity effects.

The significance of these observations and criteria for the determination of critical stress-intensity factors may be summarized as follows:

(1) The specimen should fracture at a gross stress less than two-thirds of the tensile yield strength.

(2) The initial crack length should be less than one-third the panel width.

(3) If the first two criteria cannot be simultaneously satisfied, the material in that size range is not subject to an energy instability.

The full significance and potential of this analytical interpretation can be demonstrated by the example of a rather classical set of 2219-T87 aluminum-alloy-sheet fracture data[10] which have been used frequently to justify various analytical methods. These data represent the condition of critical instability analogous to the data coordinates ($2c_c$, S_1) of this report. Although there may be some argument as to the details of what really constitutes critical instability, the principal point in this illustration is the consistency of the data for the damage level being considered. Figure 39 presents these data points for the 18-, 24-, 30-, 36-, and 48-inch-wide panels. The data points for each width are screened in accordance with the relations

$$S \leq \frac{2}{3} \cdot TYS = 39 \text{ ksi}$$

and

$$2c \leq W/3 .$$

These latter limits are indicated on the figure for each width. The results of this screening procedure are that one data point from each of the 18-, 24-, and 36-inch panel widths is considered for analysis, that no points for the 30-inch-wide-panel data are accepted, and that four points for the 48-inch-wide-panel data are accepted. From these screened data, a stress-intensity factor is computed by Equation (1) and averaged to yield

$$K = 107 \text{ ksi-in.}^{1/2} ,$$

as a representative fracture-toughness index for this product and geometry. From this calculated index, a solid-line curve is plotted in the central portion of the figure. At the left-hand limit $\left(\frac{2}{3} \cdot TYS\right)$ of this curve, a linear tangent to TYS at zero crack length is drawn in order to approximate plastic effects. The finite-boundary limitations on the right are indicated by linear tangents to the K curve passing through the abscissa intercept corresponding to the respective panel widths. In all cases, note the good curve fit

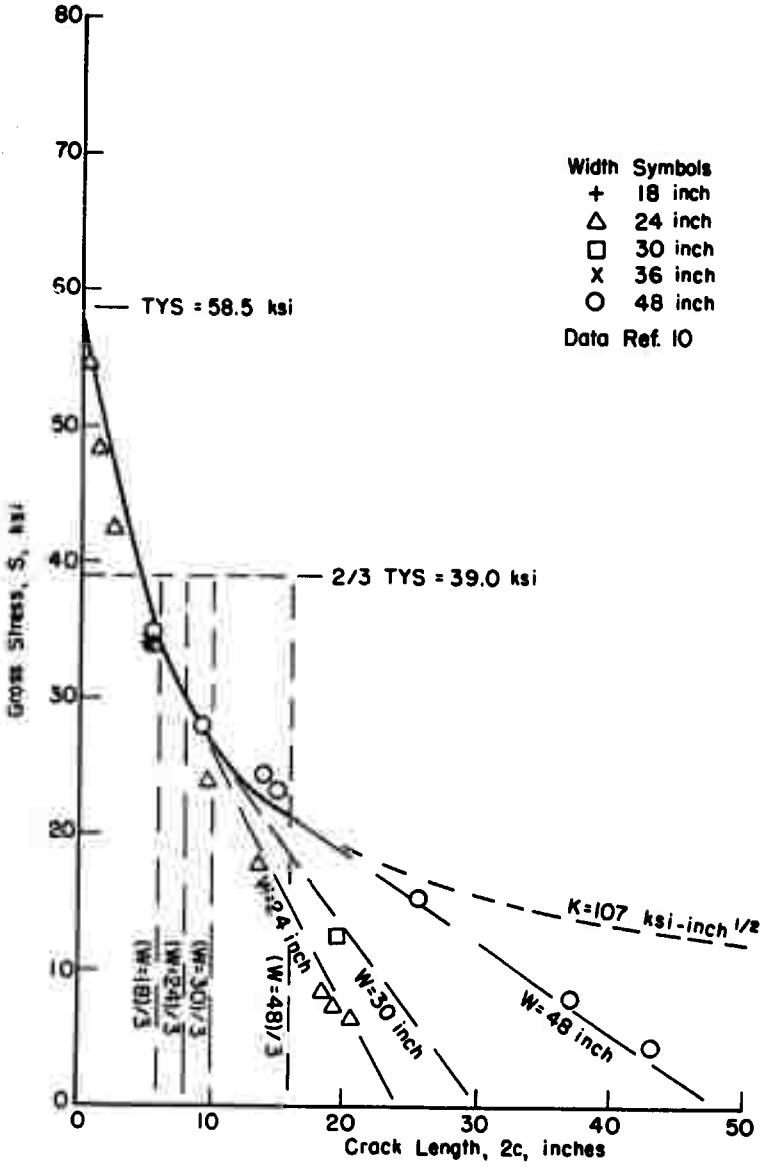

FIGURE 39. RESIDUAL STRENGTH OF PANELS OF 2219-T87 ALUMINUM ALLOY OF VARIOUS WIDTHS

that is achieved from a meager collection of screened data in the central portion of the figure. The final point of this illustration is that stress-intensity-factor indices can be simply and directly associated with the residual-strength format to relate material toughness with structural parameters.

Fracture Data Analysis and Interpretation

Fracture data may be analyzed by a variety of methods, all of which are techniques intended to be descriptive of the same phenomenon – fracture. The methods differ not so much in their expression as in their perspective. In its broadest generalization, fracture testing is usually directed toward either the characterization of the material or the characterization of the structure. In the first instance, the geometric parameters are severely constrained so as to emphasize purely mechanical behavior of the material, such as with plane-strain fracture-toughness testing. In the latter case, the combined influence of structural and material parameters is studied in more complex interactions, such as the residual-strength emphasis of this program. Thus, while the goals are similar, their scope and means of achievement are quite different.

It was the objective of the fracture-study portion of this program to determine the general fracture behavior of aluminum alloy 7075-T7351 over a range of thicknesses and widths. This has been accomplished in deriving the basic data reported in the previous section. An interpretation and discussion of these results is presented in the following subsections from several perspectives.

Notch- and Crack-Strength Analyses.

This approach to fracture characterization has evolved from the concept of notch-stress concentrations at the crack tip (considered a notch with root radius approaching zero). This development is traced in two basic steps discussed in the following subsections.

Notch-Strength Analysis (NSA).

Current concepts of notch analysis were originally presented by Neuber[3], who considered the problem in terms of elastic theory and the necessary modification for real materials. Further engineering refinements have been developed by Kuhn and Figge[11].

Essentially, stress-concentration factors on the net section are modified by size effect (a function of the Neuber constant, ρ') and plasticity. These factors are used with the ultimate strength to define the critical or allowable net section stress based on an initial flaw or crack size. The applicable equations for cracked center-notch specimens are

$$K_u = 1 + 2k_w \sqrt{\frac{c_o}{\rho'} \frac{E_1}{E}} \tag{10}$$

and

$$S_n = \frac{TUS}{K_u} , \tag{11}$$

where

c_o = one-half crack length before loading

ρ' = Neuber's constant

E = elastic modulus

E_1 = secant modulus at ultimate strength

k_w = Dixon's[12] finite-width correction = $\sqrt{(1 - 2c_o/W) / (1 + 2c_o/W)}$

TUS = tensile ultimate strength

S_n = critical net section stress = $S/(1 - 2c_o/W)$

(K_u is the effective net section stress concentration factor.)

The similarity of the right-most term to the basic formulation of the stress-intensity factor suggested[13] the consolidation of modulus values and the Neuber constant into one factor termed crack sensitivity.

Crack-Strength Analysis (CSA). An inverse measure of material toughness termed crack sensitivity was introduced by making the consolidation

$$C_m = \frac{2}{\sqrt{\rho'}} \frac{E_1}{E} \tag{12}$$

in Equation (10), with the resulting net section stress concentration factor

$$K_u = 1 + C_m k_w \sqrt{c_o} \ . \tag{13}$$

This equation may be transposed to

$$C_m = \frac{K_u - 1}{k_w \sqrt{c_o}} = \frac{\dfrac{TUS}{S_n} - 1}{k_w \sqrt{c_o}} \ , \tag{14}$$

which may be used to evaluate the crack sensitivity directly from experimental data. It is important to note that in a qualitative sense, crack sensitivity, C_m, is an inverse K value, i.e., it is inversely proportional to failure stress. High values of C_m denote brittleness; low values of C_m denote toughness.

Significance. The easily grasped physical significance of the stress-concentration-factor concept makes this technique an attractive means of expressing toughness. However, since C_m, as defined by Equation (14), is determined from the net stress, S_n, and the dimensionless aspect ratio, $2c_o/W$, panel width remains a free parameter. This lacks some of the generality sought for in other methods. Again on the positive side, this approach represents "residual" strength in its truest form. Since the method is based on initial flaw size and yet relates to failure load, it automatically compensates for the slow crack growth inherent to the rising-load test. This is in contrast to the idealized K concept which is based on a simultaneous correlation of flaw size and stress.

Data Analysis. The range and average values of the crack-sensitivity, C_m, parameter for the sheet and plate data generated on this program are shown in Figure 40. Individual values are tabulated in Appendix B. In Figure 41, the average C_m curves are plotted, along with the fracture data, on a net-section-stress format in accordance with the CSA method. It should be noted that the best fits are obtained on the wide (36-inch) panels. Furthermore, it is apparent, both from the appendix tables and the figures, that the distortion is due to the data at the high crack-aspect-ratio, $2c_o/W$, values. That is, the C_m values obtained for

$$2c_o/W \geq 0.8$$

appear to unbalance the consistency of the data at smaller aspect ratios. Thus, to be of more significant value, it appears that more restrictive criteria should be formulated for this technique.

Stress-Intensity Factors. A characterization parameter for material toughness is the stress-intensity factor which has evolved from linear elastic fracture mechanics as discussed in a previous section of this report. The general formulation of the stress-intensity factor, repeated from Equation (4), is

$$K = S\sqrt{\pi\,(c + r)}\, f[\,2(c + r)/W] \quad .$$

Specifically for the data generated on this program, the plastic-zone model of Equation (6),

$$r = \frac{1}{6\pi}\left(\frac{K}{TYS}\right)^2 \quad ,$$

and the finite-width correction,

$$f[\,2(c + r)/W] = \sqrt{\sec\frac{\pi(c + r)}{W}} \quad ,$$

were used for calculations in this section. The calculation of K for a given data point requires an iterative procedure and was cycled until the convergence of K was within 0.1 percent of the previous value. This required from three to five cycles. It should be noted that the plastic-zone-radius formulation selected is that representative of plane-strain conditions. This formulation was selected because it provides a more conservative value of K and a greater assurance of convergence within the iterative calculation. In attempting to use the plane-stress formulation on the data for the critical flaw conditions, divergence rendered the calculations useless.

The stress-intensity-factor (SIF) values derived from the data of this program are summarized in Table 17. Average SIF values, K_o and K_1, for the threshold (5 percent secant offset load) of flaw propagation data set ($2c_o$, S_3) and the maximum-load data set ($2c_1$, S_1), respectively, are presented for each thickness and width where the yield criterion was not violated. Individual values are tabulated in Appendix B. A graphical presentation of these individual values is presented in Figure 42. On the graphs in Figure 42 it should be noted that both threshold and critical stress-intensity factors are presented in a manner similar to the basic data illustrated in Figure 11. The corresponding threshold and critical values are linked by a straight line. An upper, limiting, dashed-line envelope is indicated on each figure which denotes the condition of net section yielding (NSY).

TABLE 17. SUMMARY OF AVERAGE STRESS-INTENSITY FACTORS (SIF)

Nominal Thickness, T, in.	Nominal Width, W, in.	Average 5 Percent Secant Offset SIF, K_Q, ksi-in.$^{1/2}$	Average Maximum Load SIF, K_1, ksi-in.$^{1/2}$
1/16	8	39.9	NSY
1/4	8	42.5	NSY
	16	55.7	NSY
	36	60.71	149.26
1/2	8	37.3	75.0
	16	45.0	NSY
	36	41.83	--
1	8	39.2	46.9
	16	36.3	53.4
	36	46.03	67.34

In these figures, it appears that the conditions of fracture (except for the 1-inch thickness) closely follow the net-section-yield envelope, which implies that failure conditions are beyond the realm of elastic fracture mechanics. This is a real manifestation of the tensile instability described earlier. In contrast, the data for threshold or onset of slow crack growth appear to approach a relatively more stable value of K, which implies more predominant elastic behavior. It should be recalled that one of the objectives in defining a stress-intensity factor, and then providing both plasticity and boundary corrections, is to obtain a stable material index that can be used as a design parameter. For this reason, coarse average values were also calculated for the derived data. However, these do emphasize the degeneration of the K value at the extremes of 2c/W (i.e., very low and very high aspect ratio). The net conclusion is that the present corrections for plasticity and finite width cannot totally account for crack behavior. In fact, it was this realization that motivated a look at other possibilities, such as described in the next section.

Residual Strength

The strength remaining in a panel or structural element after the occurrence of cracking or other damage is termed residual strength. A reliable description of this strength is imperative for the synthesis and analysis of design to satisfy fail-safe and/or safe-life criteria with some degree of confidence and reliability. In this section, the data derived in this program are analyzed in accordance with the residual-strength analysis described in the "Interpretation and Application" section.

For each width and thickness combination of the 7075-T73 aluminum-alloy sheet and plate tested, the derived data have been screened by Equations (8) and (9) as upper limits to valid elastic data, data unadulterated by plastic or boundary effects, for computation purposes. These criteria are

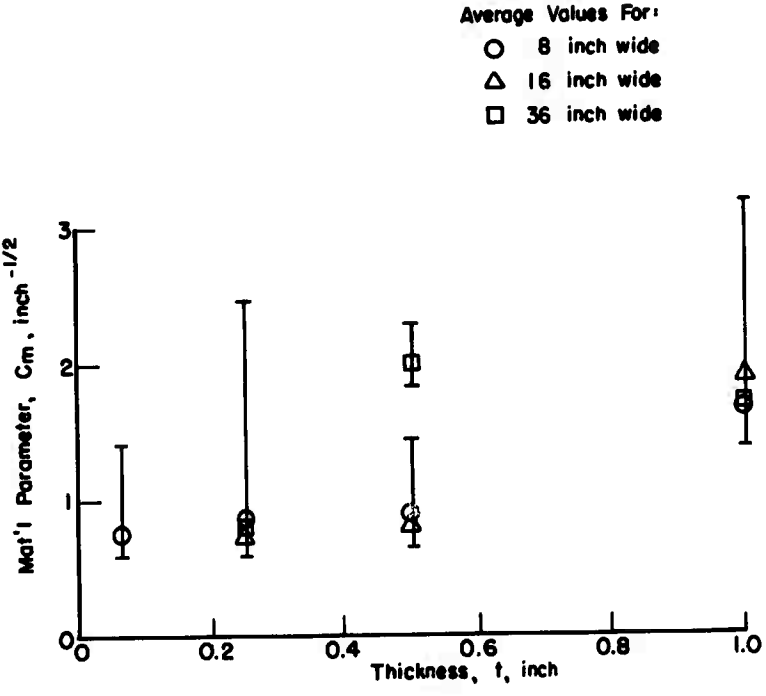

FIGURE 40. CRACK SENSITIVITY, C_m, FOR VARIOUS PANEL THICKNESSES AND WIDTHS

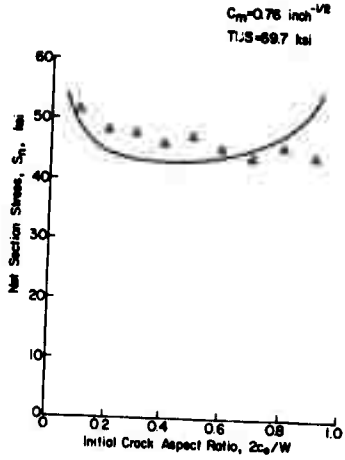

a. t = 1/16 Inch

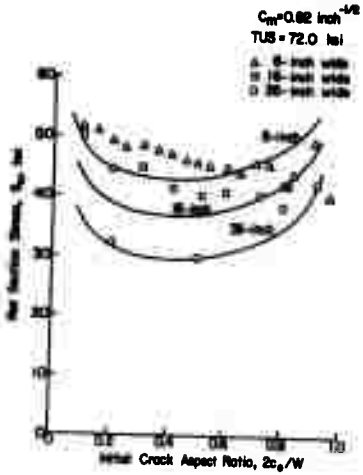

b. t = 1/4 Inch

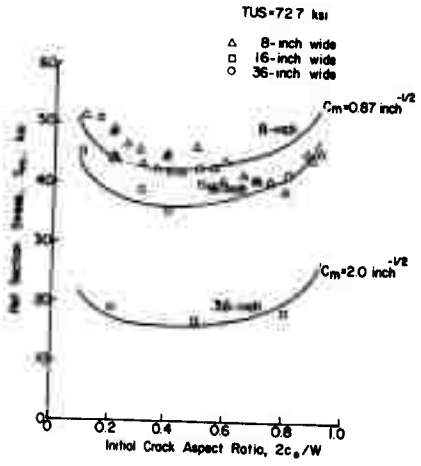

c. t = 1/2 Inch

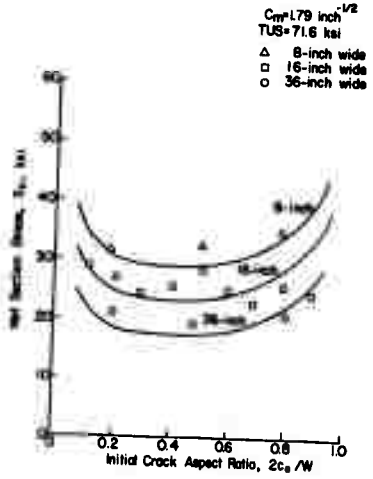

d. t = 1 Inch

FIGURE 41. FRACTURE DATA FOR 7075-T73 51 ALUMINUM ALLOY PRESENTED ON A CSA FORMAT

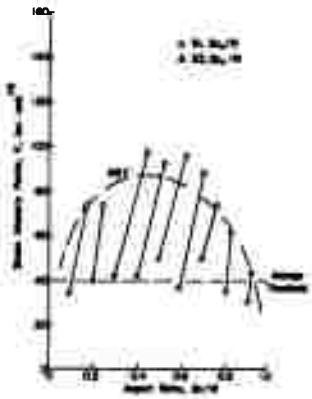

a. t = 1/16 Inch, w = 8 Inches

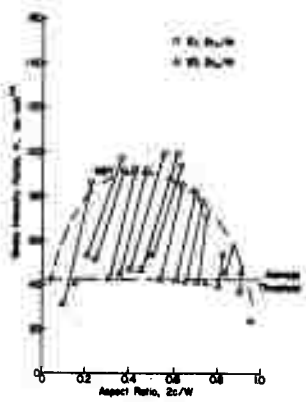

b. t = 1/4 Inch, w = 8 Inches

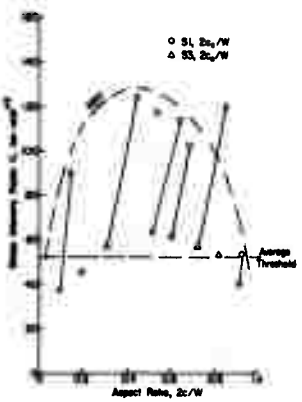

c. t = 1/4 Inch, w = 16 Inches

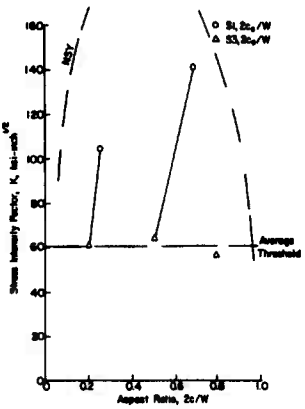

d. t = 1/4 Inch, w = 36 Inches

FIGURE 42. THRESHOLD AND CRITICAL STRESS-INTENSITY FACTORS FOR 7075-T73 51 ALUMINUM ALLOY

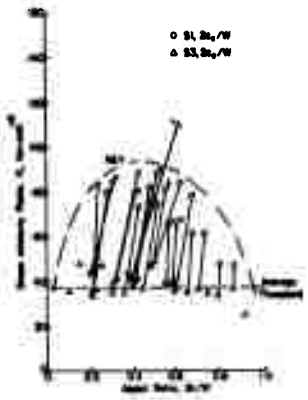

e. t = 1/2 Inch, w = 8 Inches

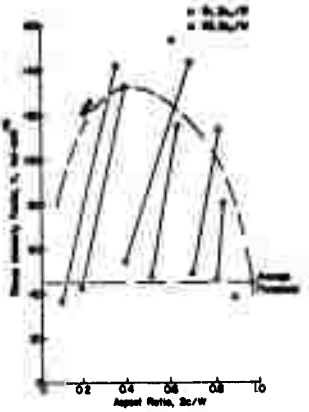

f. t = 1/2 Inch, w = 16 Inches

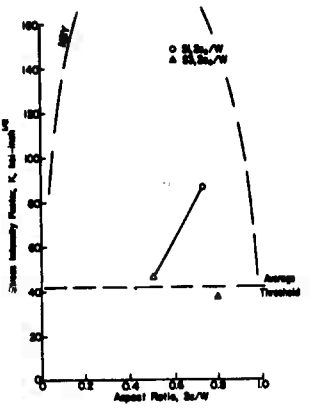

g. t = 1/2 Inch, w = 36 Inches

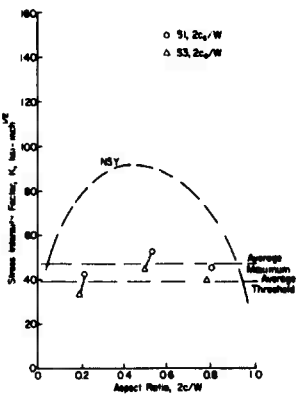

h. t = 1.0 Inch, w = 8 Inches

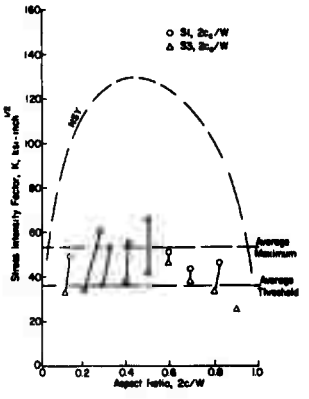

i. t = 1.0 Inch, w = 16 Inches

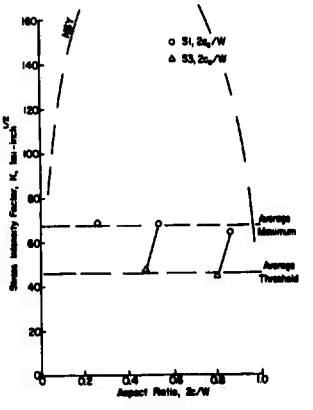

j. t = 1.0 Inch, w = 36 Inches

FIGURE 42. (CONTINUED)

$$S \leq \frac{2}{3} TYS \tag{8}$$

and

$$2c/W \leq 1/3 . \tag{9}$$

Simple stress-intensity factors are computed from the equation

$$K = S\sqrt{\pi c} \tag{1}$$

for the screened data, since in the previous section it was concluded that plastic zone and finite width corrections did not always account for crack behavior. For each thickness-width combination, an average K value is computed and is considered to be characteristic of that test series. The values are tabulated in Table 18. To illustrate the applicability and usefulness of this technique, the data generated on this program are presented in Figure 43 along with the analytical curves generated by the simplified K index.

TABLE 18. SUMMARY OF AVERAGE STRESS-INTENSITY FACTORS COMPUTED WITHIN THE CRITERIA OF THE SIMPLIFIED RESIDUAL-STRENGTH ANALYSIS

Nominal Thickness, T, in.	Nominal Width, W, in.	5 Percent Secant Offset SIF, K_0	Maximum Load SIF, K_1
1/16	8	37	68
	8	41	NSY
1/4	16	45	92
	36	59	99
	8	38	70
1/2	16	39	NSY
	36	43	--
	8	32	41
1	16	33	52
	36	43	66

The results of this analysis point out the excellent modeling of data that can be achieved by the proposed residual-strength-evaluation technique. In most all cases, the closeness and consistency of data representation are superior to those of the other models discussed.

A final, but very significant, set of illustrations relevant to this technique is presented in Figures 44 and 45. First consider Figure 44. For each thickness (1/4, 1/2, and 1 inch), fracture data for all three (8-, 16-, and 36-inch) panel widths are incorporated on a single display. The data on each plot are screened and analyzed in accord with the criteria of Equations (8) and (9). Additionally, the data from the lesser widths (i.e., 8 and 16 inches) which have crack lengths, 2c, greater than one-third their

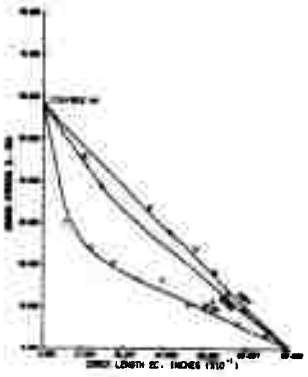

a. t = 1/16 Inch, w = 8 Inches

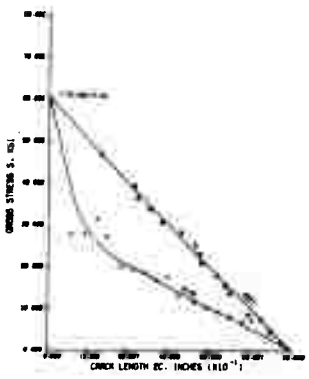

b. t = 1/4 Inch, w = 8 Inches

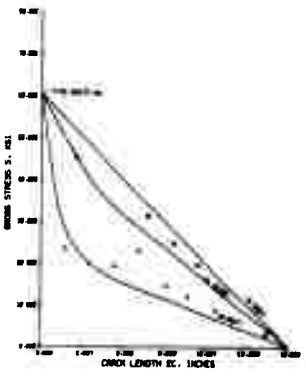

c. t = 1/4 Inch, w = 16 Inches

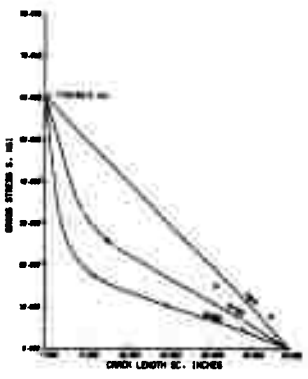

d. t = 1/4 Inch, W = 36 Inches

FIGURE 43. RESIDUAL-STRENGTH GRAPHS FOR 7075-T73 51 ALUMINUM ALLOY

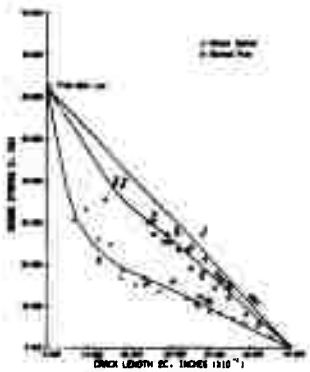

e. t = 1/2 Inch, w = 8 Inches

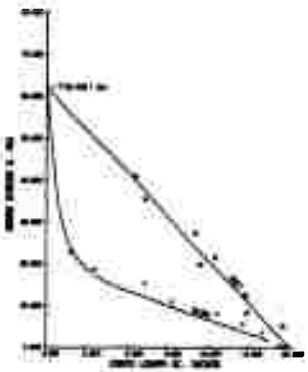

f. t = 1/2 Inch, w = 16 Inches

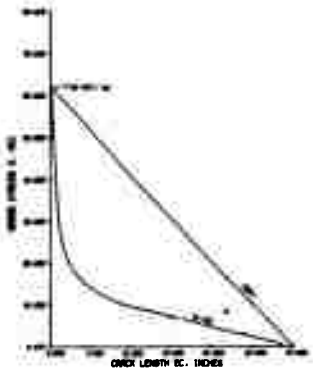

g. t = 1/2 Inch, w = 36 Inches

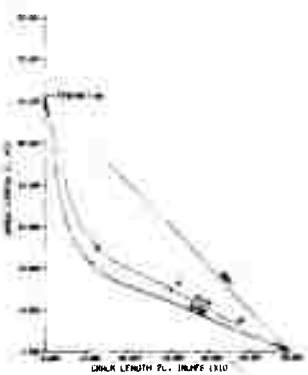

h. t = 1.0 Inch, w = 8 Inches

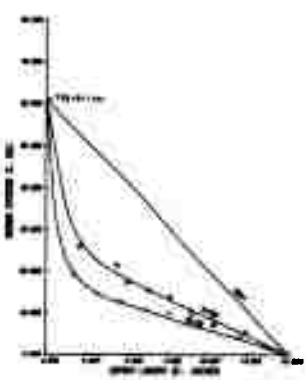

i. t = 1.0 Inch, w = 8 Inches

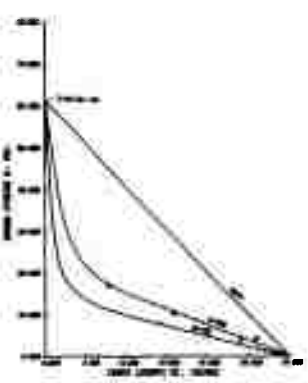

j. t = 1.0 Inch, w = 8 Inches

FIGURE 43. (CONTINUED)

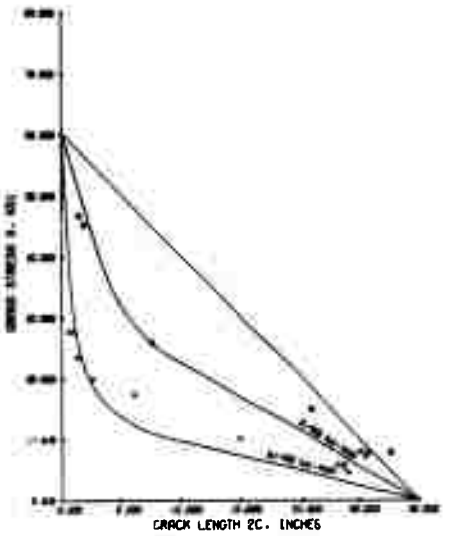

a. t = 1/4 Inch, w = 36 Inches

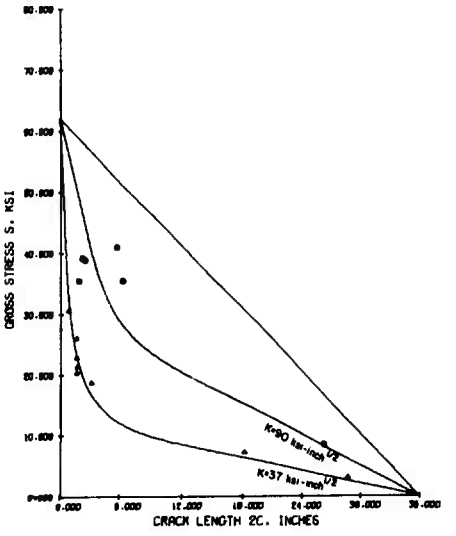

b. t = 1/2 Inch, w = 36 Inches

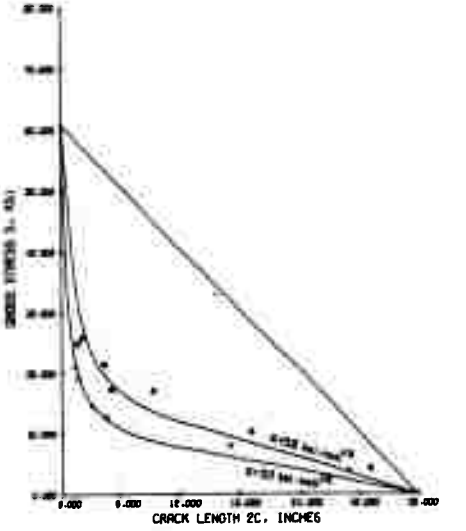

c. t = 1/2 Inch, w = 36 Inches

FIGURE 44. COMBINED RESIDUAL-STRENGTH GRAPHS FOR 7075-T73 51 ALUMINUM ALLOY

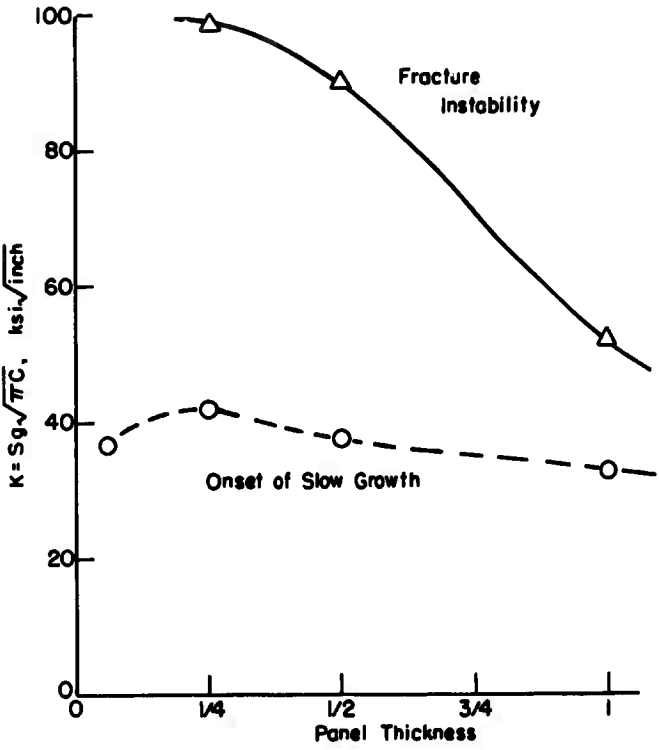

FIGURE 45. EFFECT OF THICKNESS ON FRACTURE CRITERIA OF CENTRALLY NOTCHED 7075-T7351 ALUMINUM-ALLOY PANELS

respective widths have been deleted for clarity in the display. Obviously, from the method described, these data points lie on the linear segment directed downward to the abscissa intercept of 8 or 16 inches and would only clutter the basic illustration of a K data fit.

It is interesting to note in these three figures that the fracture-toughness indices associated with both the threshold and fracture conditions decrease with increasing thickness. It is also significant to note that the data fit appears to improve with increasing thickness. This is attributed to the more distinct and more abrupt response and detection of specimen behavior in the thicker sections.

Figure 45 illustrates quantitatively the qualitative statement of the previous paragraph relative to the effect of thickness on the two fracture criteria. It is seen in the figure that as thickness increases from t = 1/4 inch, the K values associated with instability and onset of slow growth decrease. In fact the fracture instability curve approaches that for onset of slow growth. The implication is that for some thickness greater than 1 inch, failure will occur essentially without slow growth, further implying that the K value at that thickness will be K_{1c}.

Fatigue-Crack Propagation

It is recognized that flaws may exist in new aircraft components as an inadvertent metallurgical defect by virtue of the fact that real materials and production processes are used. Also, flaws may initiate as a consequence of service. Growth of the flaws by the repeated stress environment can be expected to occur since operating stress levels of aircraft are similar to those that are known to cause fatigue-crack propagation in laboratory specimens of the basic materials. It becomes necessary then to know something of the effects of geometric variables and stress variables in order to provide the insight to establish inspection intervals in real structure, and to predict remaining life of a component in which a recognizably finite-length flaw has been found.

These considerations have led to the development of many crack-propagation relations, some of which are empirical formulations and some of which are based upon continuum mechanics development. A few of these relations are discussed in this report. One has been singled out for extensive evaluation of the data.

Fatigue-Crack-Propagation Relations

Frost and co-workers have been early contributors to an understanding of fatigue-crack propagation. Their research[14-19] has suggested that the rate of fatigue-crack propagation is related to the instantaneous crack length, ℓ, as follows:

$$d\ell/dN = K\ell^{*}. \qquad (15)$$

This equation suggests that there should be a linear relationship between ln ℓ and N. This, in fact, is shown to be the case in Frost's work. However, Frost conceded initially that the relation was applicable only for short cracks and subsequently concluded that the relation applied for crack lengths where propagation was on a plane normal to

*In this section ℓ is sometimes used synonymously with 2c. It is the crack length.

the tensile stresses causing crack growth. From extensive research, Frost and co-workers concluded that K in Equation (15) could be a function of alternating stress, S_a, or could be a function of S_a and the mean stress, S_m, depending upon the material. Their generalized equation was

$$d\ell/dN = (P + Q\, S_m)\, S_a^3\, \ell \ . \tag{16}$$

All of their work supports the use of the exponent 3 on S_a.

Schijve and his co-workers[20-24] over a period of years have indicated that the rate of crack propagation, $d\ell/dN$, is not linear with ℓ as indicated by Frost, but rather that

$$d\ell/dN \approx C\, \ell^n \ , \tag{17}$$

where n has a value greater than 1. They also recognized, on the basis of their extensive studies of 2024 and 7075 aluminum sheet, that there was a complex effect of S_a and S_m on $d\ell/dN$. Their work led to the general relation

$$\frac{d\ell}{dN} = C_1\, e^{-c2R}\, S_{max}{}^3\, \ell^{3/2} \left(1 + 10\, \frac{\ell^2}{w^2}\right) \ , \tag{18}$$

reported to be useful for small ratios of crack lengths to panel width (ℓ/w). It is seen in Equation (18) that $S_{max}\, \ell^{1/2}\, (1 + 10\, \ell^2/w^2)^{1/3}$ approximates the stress intensity of a center-cracked panel. In other words, Equation (18) has some similarity to the Paris and Erdogan relation[25]

$$d\ell/dN \approx c\, K_{max}^n \ , \tag{19}$$

where n was considered to be 4 for many materials. The important difference between Paris' original idea and Equation (18) is that Broek and Schijve's relation recognizes the importance of load ratio, R, in addition to maximum stress.

At this point, it is relevant to point out that in this country since about 1960, following the insights of Hardrath and McEvily[26] and Paris, Gomez, and Anderson[27], fatigue-crack-propagation relations and data displays have employed stress intensity more often than stress. This usage carries the implied assumption that the fatigue stresses provide essentially an elastic stress field adjacent to the crack, which may not always be the case. It is, however, a convenient measure of the stress state around a crack tip since in some forms, the stress intensity includes the gross stress from external loads and the geometric interplay between crack length and component geometry. Relations developed involving stress intensity have included the use of K_{max} (associated with the maximum gross stress in a stress cycle), K_a, K_m, and ΔK associated, respectively, with the alternating stress, the mean stress, and the total range of stress ($\Delta K = 2K_a$).

One of these relations involving stress intensity was suggested by Forman, Kearney, and Engle[28] after noting that the Paris equation does not account for load-ratio effects on crack growth nor for accelerated crack growth as the stress-intensity approaches the critical value associated with failure. Also, they did not consider that Equation (18) from Broek and Schijve[21] would account for the acceleration in crack growth either. Their empirical expression assumes that the rate of crack propagation

is proportional to ΔK to some power n, and that the rate of crack propagation becomes very large as the stress intensity of the growing crack approaches K_c or K_{Ic}, whichever is applicable. This relation also provided for the effect of load ratio and is as follows:

$$d\ell/dN = \frac{C(\Delta K)^n}{(1 - R) K_c - \Delta K} \quad . \tag{20}$$

Their paper provides confirming evidence, based upon test data retrieved from the literature, that the equation is useful. More recently, Hudson[29] showed that the above relation was particularly good in accounting for load-ratio effects.

Erdogan[30] has developed a continuum model for fatigue-crack growth based upon a consideration of dislocation movement in the plastic zone ahead of a fatigue crack. He rationalized that crack-growth rate is a function of the maximum plastic-zone size (p_{max}), related to the total number of dislocations that could possibly contribute to crack extension, and also a function of the range of plastic-zone size (p_r), related to the fraction of the total number of dislocations contributing to crack growth:

$$\frac{d\ell}{dN} = A\, p_{max}^{\alpha_1}\, p_r^{\alpha_2} . \tag{21}$$

Analytical estimates for p_{max} and p_r were obtained using Dugdale's technique and the assumption of small-scale yielding, so that Equation (21) became

$$\frac{d\ell}{dN} = B\, K_{max}^{2\alpha_1}\, K_r^{2\alpha_2} \quad . \tag{22}$$

Since load ratio, R, is K_{min}/K_{max}, Equation (21) can be rewritten as

$$\frac{d\ell}{dN} = C \left(\frac{1}{1 - R}\right)^{2\alpha_1} \Delta K^{2(\alpha_1 + \alpha_2)} \quad , \tag{23}$$

where K_r and ΔK each is the range of stress intensity.

Thus, Erdogan's expression again seeks to describe analytically the experimental observation that load ratio, R, does influence crack-propagation rate. C, α_1, and α_2 are obtained experimentally.

Walker[5] has started with an expression in terms of stress and crack length, identical to Equation (22) from Erdogan, i.e.,

$$\frac{d\ell}{dN} = f\left(C(S_{max}\sqrt{\ell})^c\, (\Delta S\sqrt{\ell})^b\right) \quad . \tag{24}$$

By letting $1 - m = c/c + b$, $m = b/c + b$, and $n = c + b$, the above equation becomes

$$\frac{d\ell}{dn} = f\left(C(S_{max})^{1-m}\, \Delta S^m \sqrt{\ell}\right)^n \quad . \tag{25}$$

He then noted that

$$S_{max}^{1-m} \cdot \Delta S^m = S_{max}\,(1 - R)^m \quad , \tag{26}$$

which he defined as an effective stress $\bar{S}$. Therefore, Equation (26) reduces to

$$\frac{d\ell}{dN} = f\left(\bar{S}\sqrt{\ell}\right) = f\left(\bar{\Delta}K\right) \quad . \tag{27}$$

Walker's $\bar{\Delta}K$ is termed an effective stress intensity that in a sense performs the same function as Erdogan's and Forman's equations in accounting for load ratio effects. The equation is not complete, however, since Walker has chosen not to express the explicit functional relation between $d\ell/dN$ and $\bar{\Delta}K$. Walker has shown that notched-specimen-fatigue data at various load ratios can be normalized by use of Equation (26). His work shows for several materials that the value of m from crack-propagation data is equal to the value of m from notched-fatigue data and suggests that m is a kind of material parameter.

Data-Interpretation Methods

The crack-growth data obtained in the test program consisted of observations of crack length and cumulative cycles. Since, generally, it was expected that long central cracks would be tolerated by the material at the stresses involved, measurements usually were made in crack-length increments of 0.20 inch; sometimes an increment of 0.10 inch was used.

Examination of Figures 14 through 23 shows that crack growth is not always a continuous process. Thus, if one uses directly the crack-propagation data to obtain $\Delta\ell/\Delta N$, then between observations, the resulting $d\ell/dN$ values frequently will show quite a bit of scatter about some mean growth rate line. Therefore, in the first portion of the computer analysis, the following steps were accomplished. From the coordinate pairs covering a test, the computer examined the first four data pairs, established the coefficients for a fourth-order equation through the points, and computed for the interval between the second and third data pair the crack length, K_{max}, K_{min}, ΔK, and $d\ell/dN$ for life intervals associated with 2500-cycle increments. The computer then examined the second through fifth data pair similarly in order to obtain similar computations between the third and fourth data pair. The procedure was repeated until all groups of data pairs had been examined. This technique smoothed out some of the gross irregularities in instantaneous $d\ell/dN$ values, but not all. The output from the computations for each specimen was a tabulation of crack length (ℓ), K_{max}, K_{min}, ΔK, and $d\ell/dN$ for 2500-cycle increments over the lifetime range.

In these computations, all stress-intensity values were computed using $K = S_g\sqrt{\pi\ell/2 \sec \pi\ell/2w}$. Although this expression contains the width correction, it does not contain a plastic-zone correction. Since the gross section stresses were quite low, it was believed that the plastic-zone correction would not be necessary.

Additionally, a plotting routine permitted the automatic plotting of certain relations among the data that included ln ℓ versus N, $d\ell/dN$ and ln $d\ell/dN$ versus K_{max}, ΔK, ln K_{max}, and ln ΔK. Examination of these graphs suggested that for limited crack lengths it might be possible to develop a crack-rate equation similar to that of Frost. Also, it appeared from other plots and for other limited ranges of crack length that linear relations could be established between ln $d\ell/dN$ and ln K_{max} or ln ΔK as well as other combinations. In fact, a more detailed analysis was made of the data for 1/4-inch-thick material using Frost's approach.

The analysis started with an examination of the relationship between ln ℓ and N. Also, the same data were evaluated to explore the relationship between ln $d\ell/dN$ and ln ΔK.

The Frost type of analyses suggested that for the 1/4-inch-thick material and for a crack length from about 0.75 inch to about 2.0 inches, a relation of the form $d\ell/dN = c\,\ell$ might be possible, where c is an expression containing S_a to some power and S_m.

It also was found that the scale selection for the graphs of ln $d\ell/dN$ versus ln ΔK could be adjusted so that the data for a given load ratio could be approximated "reasonably well" by two straight-line segments. It appeared that it would be possible to formulate a complex relation between $d\ell/dN$, ΔK, and R, since these data generally were layered in accordance with load ratio. The steepest slopes on the ln $d\ell/dN$ versus ln ΔK graph were for the test stresses with the highest positive load ratio. As load ratio approached R = 0, the slopes decreased, displacing the curves to the right. There was some reluctance to carry these analyses to completion. Figure 46 shows the computer-drawn graph of ln $d\ell/dN$ versus either ln ΔK (Figure 46a) or ΔK (Figure 46b). Both graphs suggest that a continuous function should be sought that contains the reversed curvature shown in the two graphs at a ΔK of about 15 ksi $\sqrt{\text{inch}}$. This characteristic for Specimen 2 was seen in most of the other computer-drawn graphs for other specimens.

Of the various equations described briefly in the previous section, only the empirical equation of Forman, et al,[28] could provide such a curve. The remainder of this portion of the report contains a discussion of the evaluation of the Forman-type equation using the data from this program. Once again, this equation is

$$\frac{d\ell}{dN} = \frac{C(\Delta K)^n}{(1 - R)\,K_c - \Delta K} \quad . \tag{28}$$

It is necessary to determine the constant C and exponent n from the data. A decision was needed relative to which value of K_c to use. Figure 31 shows the comparison between the crack length observed on the fatigue-fracture surface to the estimated crack length that one would predict (on the basis of fracture data shown in Figure 11) if the gross failure stress had been the same as each fatigue-test stress. The figure shows essentially a one-to-one correspondence for the two lengths regardless of panel width or thickness. This suggested the simple expedient of using the fracture data of Figure 11 to establish, for the nine maximum test stresses and load ratios, the estimated crack aspect ratios, 2c/W (or ℓ/w). From each value of ℓ/w and for the appropriate $S_{g_{max}}$, a K_c was computed using

$$K_c = S_{g_{max}} \sqrt{\frac{\pi\ell}{2}} \cdot \sqrt{\sec \pi\ell/2w} \quad , \tag{29}$$

which is the same formula used to compute the ΔK values obtained for each crack-propagation specimen as described above.

As discussed earlier in the fracture-toughness-analysis section, some doubt can be raised concerning the use of Equation (29) since the graphs of Figure 11 clearly show that for many combinations of thickness and panel width, failure occurs at or slightly above net section yielding. Since, in the fatigue tests, cracks did propagate to a length where net section yielding could occur, and since all ΔK values were similarly computed, it appears in the computation procedure that the terminal point, i.e., K_c, was

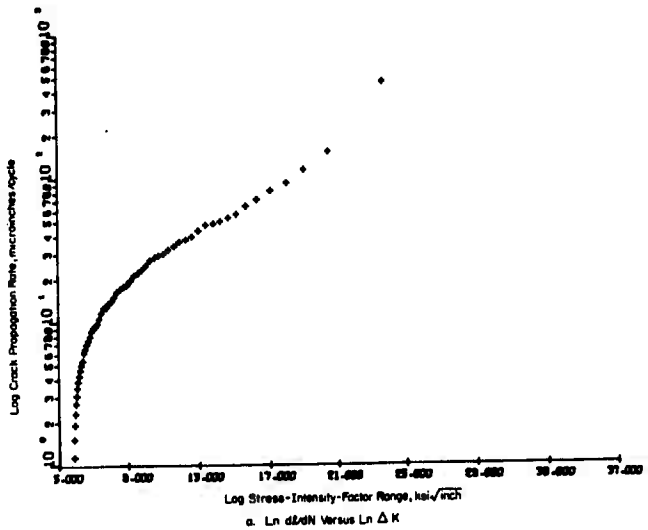

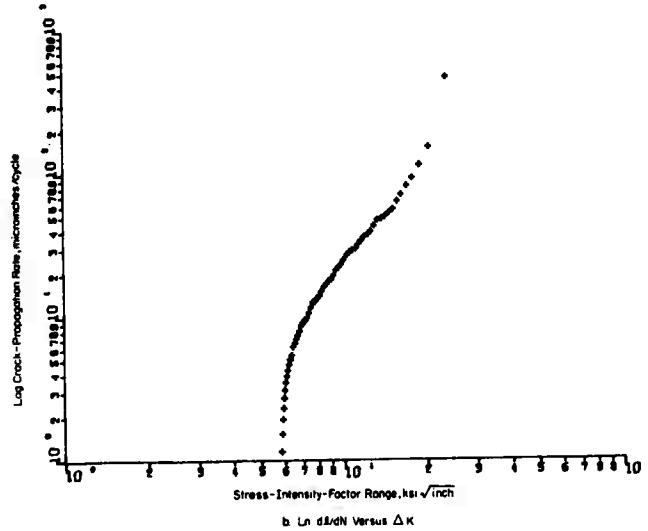

FIGURE 46. COMPUTER PRINT-OUT OF CRACK-PROPAGATION DATA FOR SPECIMEN 2

compatible with the ΔK values for long cracks as well as short cracks. In design engineering there is precedent for this procedure. The use of $S = \frac{Mc}{I}$ or $\frac{Tc}{J}$ to compute the fracture moduli in bending and torsion (modulus of rupture) as well as to compute yield conditions and elastic stresses is one such example. Actually, for each thickness and panel width, the decision was made to use an average value of K_c for all nine test stress levels, since the range in maximum stress for the series was so narrow.

This approach was tried out first on the 1/4-inch-thick specimens, considering the 8-, 16-, and 36-inch-wide panels separately. Using the data for the 1/4-inch-thick, 8-inch-wide panel as an example, the following steps were taken:

(1) For each of the nine stress ratios, R, corresponding to the nine combinations of S_a and S_m, the data pairs $d\ell/dN$, ΔK from the original printout were used in program CRACK to compute for each specimen its value of C and n. CRACK performs a least-squares regression on the data pairs to provide the best value for C and n for each specimen.

(2) From this computation, the values of C and n were examined and were found to vary as shown below:

Specimen	S_m, ksi	Sn, ksi	n	C
2	6.8	±3.3	2.192	1.208E-9[a]
11	6.8	±4.4	2.822	3.032E-12
12	6.8	±5.5	2.468	8.200E-11
7	8.4	±3.3	2.977	8.752E-13
10	8.4	±4.4	3.140	1.566E-13
13	8.4	±5.5	2.568	4.601E-11
8	10.0	±3.3	3.275	5.579E-14
9	10.0	±4.4	2.920	1.517E-12
14	10.0	±5.5	2.511	7.728E-11

(a) E-9 = 10^{-9}, etc.

Thus, in order to provide one value of n and C for the group of data, some averaging of the computed values was needed. A mathematical analysis of Equation (28) indicated that it was appropriate to compute n as the arithmetic mean and C as the geometric mean of the tabulated values as is illustrated in Appendix C.

(3) For the 1/4-inch-thick, 8-inch-wide panels, C and n were computed to be 6.139E-12 and 2.76, respectively. Using an average value K_c = 67.7 ksi $\sqrt{\text{inch}}$, and the above values of C and n, in Equation (28), values of $d\ell/dN$ were computed for selected values of ΔK from $\Delta K = 3$ to $\Delta K \approx (1 - R) K_c$.

(4) Steps (1), (2), and (3) then were carried out using the data for the 1/4-inch-thick, 16- and 36-inch-wide panels where K_c was computed to be 92.2 and 136.4 ksi $\sqrt{\text{inch}}$ for 16- and 36-inch-wide panels, respectively.

From Steps (1) through (4) and the $d\ell/dN$, ΔK data pairs, Figure 47 has been constructed. On each graph of Figure 47 are plotted the test data, evaluated as described early in this section on ln $d\ell/dN$, ΔK coordinates. The graphs in Figure 47 for the 8-inch-wide panels contain, in addition to the data, two curved lines. The dashed line is the result of Step (1) computation for each specimen. Examination of each graph shows that the dashed curve appears to fit the data quite well, suggesting that Equation (28) may be quite good in representing fatigue-crack-propagation data. The solid curve in each graph represents the average curve from Step (3) calculations. Examination of the nine graphs shows that the use of the average values of C, n, and K_c provides somewhat less of a good fit than did the individual values; however, this is considered a necessary penalty in obtaining a more generally useful equation.

In Figures 48 and 49 for the 16- and 36-inch-wide panels, only the data points and the average curve are shown. There is excellent agreement between the data and the average curves.

In order to assess how satisfactory this equation might be in predicting the remaining life, one additional set of computations was made using the equations for the 1/4-inch-thick, 8-inch-wide panel obtained for each specimen in Step (1) and for the family of specimens in Step (3).

This computation was to determine the number of cycles to failure for each specimen, assuming a crack existed that was 0.75 inch long. From Figure 15, the actual remaining life was determined for each specimen for comparison with the computed value.

The computation scheme for Program LIFE is illustrated schematically in Figure 50. The essential feature for a given specimen was to determine by computer $d\ell/dN$ and ℓ for selected values of ΔK using Equation (28). Then the reciprocals of the $d\ell/dN$ values could be paired with each ℓ to construct a $dN/d\ell$ versus ℓ plot. Computation of the area under the curve from some initial value of ℓ (say 0.75 inch) to a value of ℓ consistent with $\Delta K = (1 - R) K_c$ would be the predicted remaining lifetime to failure.

The entire operation was programmed and the computer printed out predicted failure lifetimes for each specimen for initial cracks ranging in length upwards from 0.75 inch in increments of 0.25 or 0.50 inch.

Table 19 shows the results of this set of computations for the 1/4-inch-thick, 8-inch-wide panels. In the table, there are three lifetime columns of interest. The first of these is the actual lifetime remaining obtained from the curves on Figure 15, given a crack 0.75 inch long. The second lifetime column is a predicted lifetime using the values of C and n for the specimen obtained in Program CRACK. The deviations from the actual lifetimes are in the adjacent column. They show that the deviations, without regard to sign, agree with actuality within about 5.0 percent on the average. Following that column, are two columns based upon predictions made with Equation (28) using the mean values of C and n. It is seen that the average deviation has increased when using the mean values. It was considered, however, that the equation was providing an

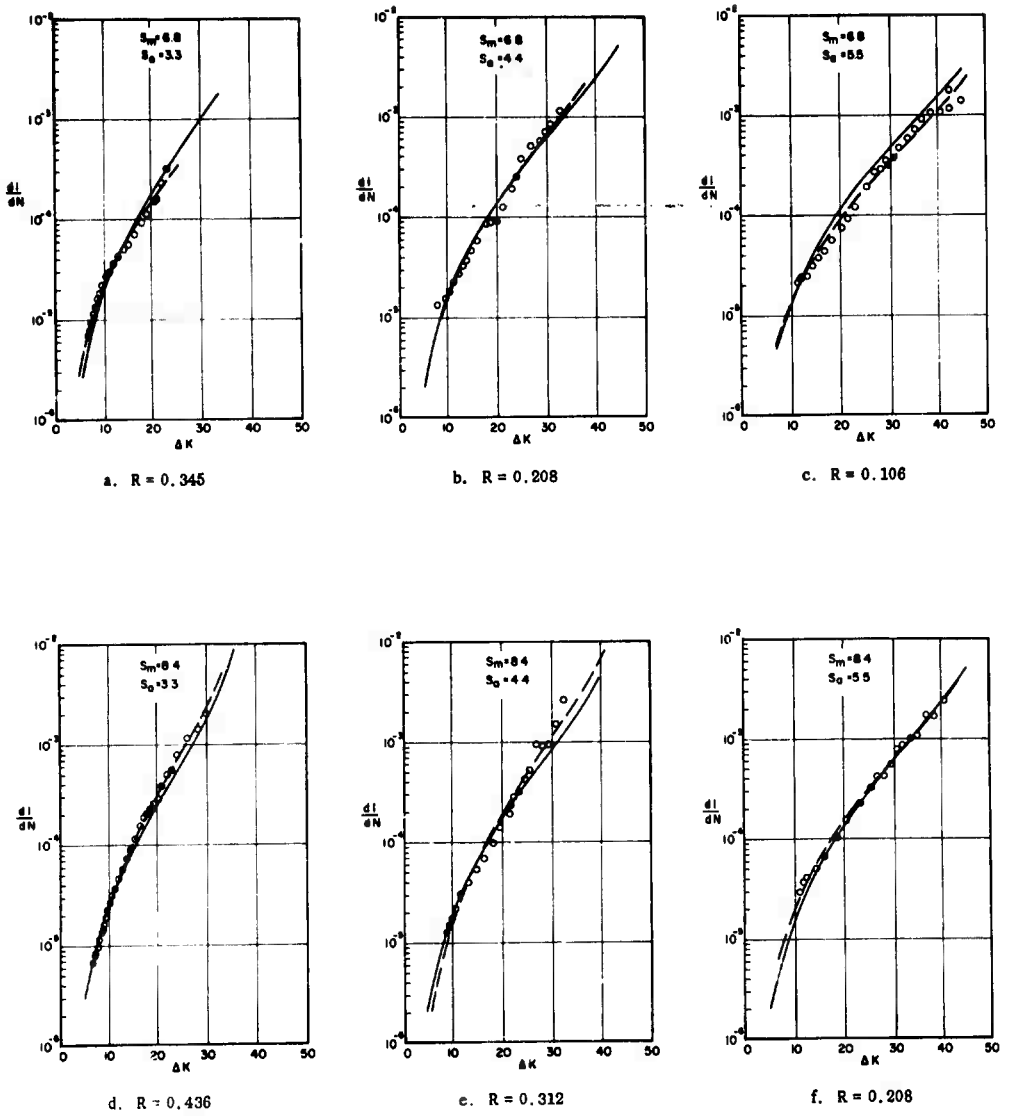

a. R = 0.345

b. R = 0.208

c. R = 0.106

d. R = 0.436

e. R = 0.312

f. R = 0.208

FIGURE 47. FATIGUE-CRACK-PROPOGATION RATE AS A FUNCTION OF ΔK FOR 1/4-INCH-THICK, 8-INCH-WIDE PANELS

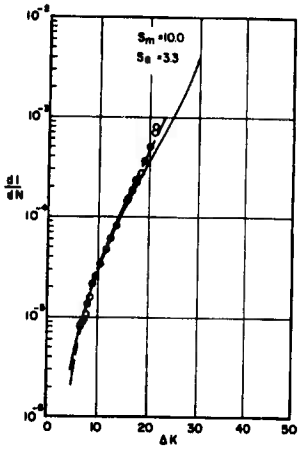

g. R = 0.504

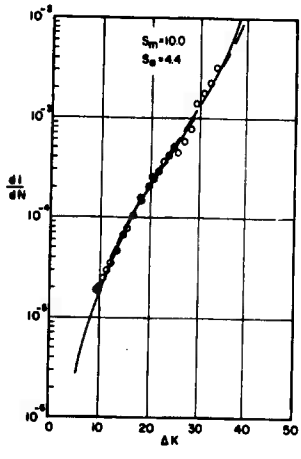

h. R = 0.389

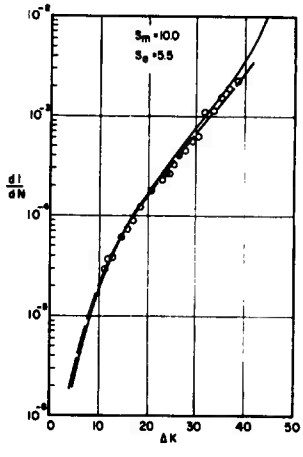

i. R = 0.290

FIGURE 47. (CONTINUED)

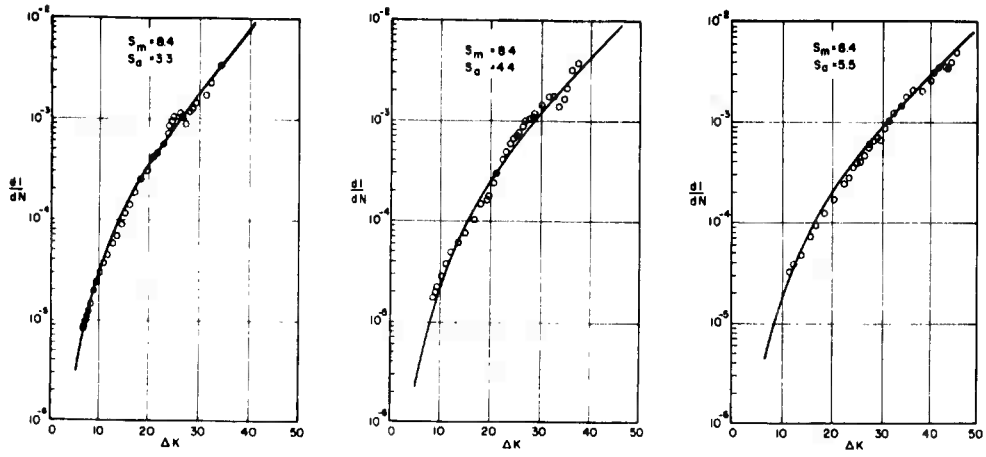

a. R = 0.436 b. R = 0.312 c. R = 0.208

FIGURE 48. FATIGUE-CRACK-PROPOGATION RATE AS A FUNCTION OF ΔK FOR 1/4-INCH-THICK, 16-INCH-WIDE PANELS

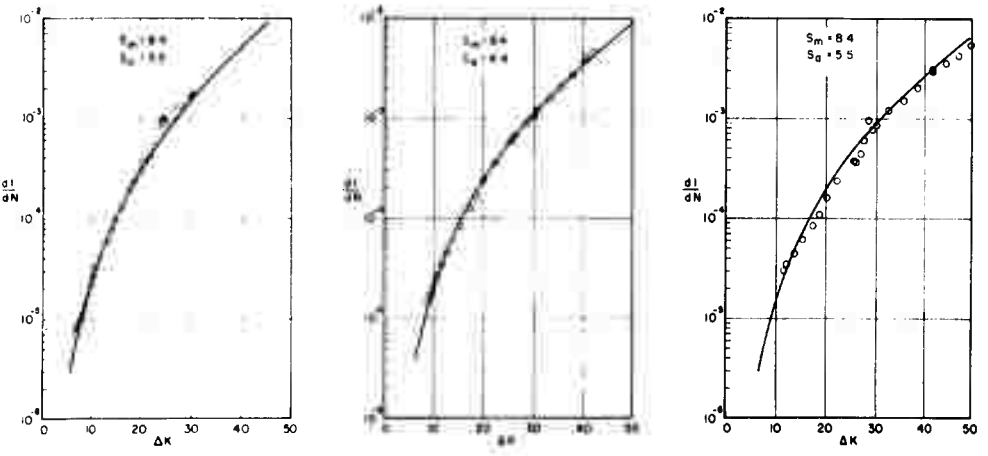

a. R = 0.436 b. R = 0.312 c. R = 0.208

FIGURE 49. FATIGUE-CRACK-PROPOGATION RATE AS A FUNCTION OF ΔK FOR 1/4-INCH-THICK, 36-INCH-WIDE PANELS

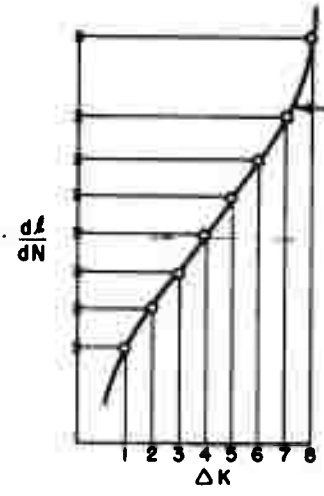

$$\frac{da}{dN} = \frac{C(\Delta K)^n}{(1-R)K_c - \Delta K}$$

1. For each ΔK_i, compute $\left(\frac{da}{dN}\right)_i$
2. For each ΔK_i, compute a_i using $\Delta K = 2S_o\sqrt{\frac{\pi a}{2}\sec\frac{\pi a}{2W}}$
3. In each $\left(\frac{da}{dN}\right)_i$, compute reciprocal, ie., $\left(\frac{dN}{da}\right)_i$
4. Plot data pairs $\left(\frac{dN}{da}, a\right)_{i=1}^{i=8}$
5. Compute the area under the curve from $a = 0.75$ inch to a (where $\Delta K = (1-R)K_c$)
6. The resulting value is the remaining life, N

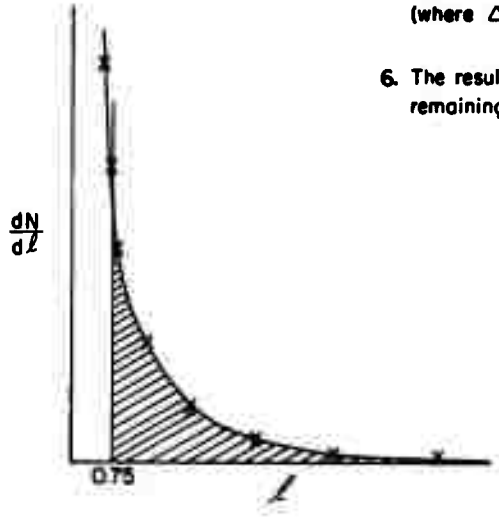

FIGURE 50. SCHEMATIC DIAGRAM OF REMAINING LIFE CALCULATION

excellent predictive tool. Consequently, the crack-propagation data for the remaining test conditions were handled in a similar manner.

TABLE 19. COMPARISON OF ACTUAL AND PREDICTED LIFETIMES TO FAILURE OF 1/4-INCH-THICK, 8-INCH-WIDE PANELS WITH AN INITIAL CRACK OF 0.75 INCH LONG

Specimen	Lifetime Remaining for Panel With 0.75-inch Crack				
	Actual Cycles	Predicted[a] Cycles	Deviation, percent	Predicted[b] Cycles	Deviation, percent
2	95,540	101,740	+6.55	109,500	+14.60
11	61,580	58,740	-4.62	57,000	-7.45
12	44,900	40,140	-10.60	33,600	-25.20
7	84,860	83,750	-1.31	88,800	+4.64
10	51,180	49,250	-3.77	46,800	-8.55
13	26,150	24,280	-7.15	27,800	+6.31
8	78,430	74,910	-4.49	73,200	-6.67
9	39,670	37,230	-6.15	39,000	-1.69
14	22,960	22,850	-0.48	23,300	+1.48
		Average Deviation, %	5.01		8.51

(a) Based on individual values of C and n for each specimen.

(b) Based on average C and n values for the group of specimens.

Incidentally, in Figure 15 and in other such figures for the other thicknesses, the solid symbols for each specimen mark points along predicted crack-propagation curves, assuming a crack was discovered with a length of 0.65 inch, 0.75 inch, 1.0 inch, and 1.25 inch for the 1/16-, 1/4-, 1/2-, and 1-inch-thick panels.

Fatigue-Crack-Propagation Evaluation

Using the methods reviewed in the previous section, the data for the remaining thicknesses have been evaluated in a similar fashion. For each thickness and panel width, the computations have been made and mean values of C and n have been determined in each case. The results of the evaluation are presented and discussed in this section.

For the 1/16-inch-thick material, only 8-inch-wide panels were tested. Mean values of C and n were computed to be 1.77E-9 and 2.138, respectively, using an average K_c of 66.8 ksi$\sqrt{\text{inch}}$. Figure 51 contains graphs of ln $d\ell/dN$ versus ΔK for each load ratio. In addition to the data points, the continuous curve represents Equation (28) using the mean values of C and n. In a number of cases, there is quite a divergence between the data points and the curves as a consequence of the averaging of C and n. Program LIFE was used, together with the curves of Figure 14, to provide an estimate of

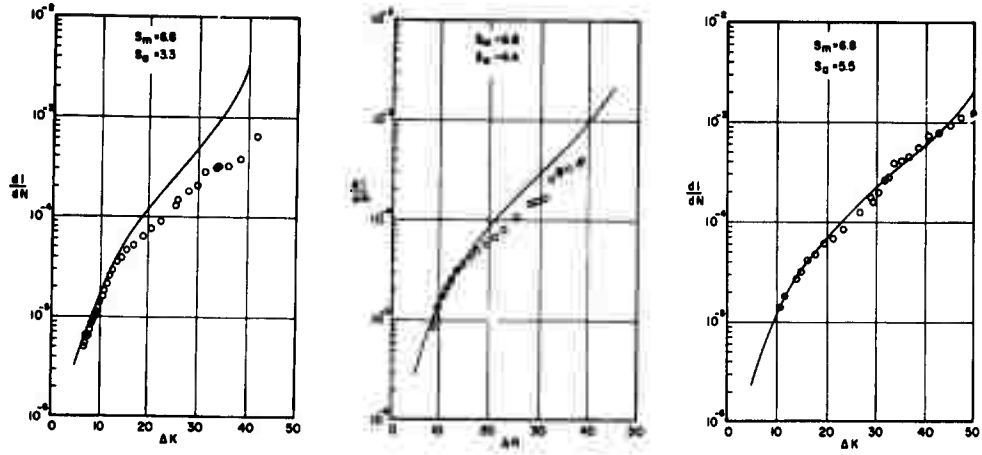

a. R = 0.345 b. R = 0.208 c. R = 0.106

d. R = 0.436 e. R = 0.312 f. R = 0.208

FIGURE 51. FATIGUE-CRACK-PROPAGATION RATE AS A FUNCTION OF ΔK FOR 1/4-INCH-THICK, 16-INCH-WIDE PANELS

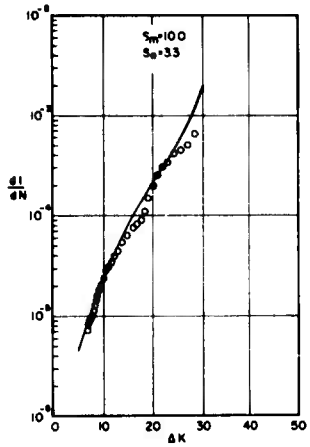

g. R = 0.504

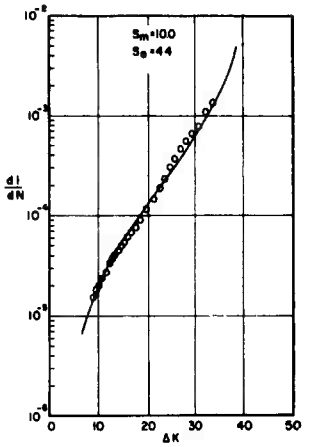

h. R = 0.389

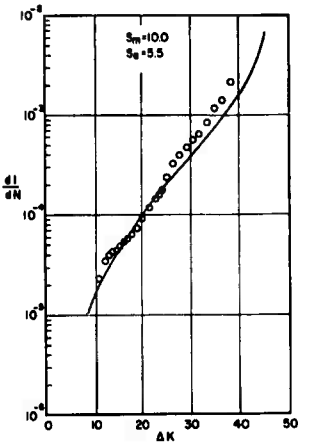

i. R = 0.290

FIGURE 51. (CONTINUED)

remaining life, based on a fatigue-crack initially 0.65 inch long. The comparison with actual remaining lifetimes is shown in Table 20. The table also shows that the average deviation in predicted life from actual life is 13.5 percent, which is about 50 percent larger than the average deviation for the 1/4-inch-thick panels. The greatest deviation is almost 25 percent, the same as that for the 1/4-inch-thick panels.

TABLE 20. COMPARISON OF PREDICTED LIFETIME TO FAILURE WITH ACTUAL LIFETIME TO FAILURE FOR 1/16-INCH-THICK PANELS CONTAINING A FATIGUE CRACK 0.65-INCH LONG

Specimen	S_m	S_a	N_f	$N_{0.65}$	Life Remaining, cycles		Deviation, percent
					Actual	Predicted	
46	6.8	3.3	221,690	43,000	178,690	135,000	-24.4
42	6.8	4.4	135,810	43,000	92,810	83,600	-9.9
43	6.8	5.5	103,160	37,000	66,160	56,300	-14.9
53	8.4	3.3	146,230	26,500	119,730	108,700	-9.2
41	8.4	4.4	76,650	20,000	56,650	68,300	+20.6
55	8.4	5.5	48,690	8,200	40,390	46,400	+14.6
39	10.0	3.3	143,290	37,000	106,290	89,000	-16.3
54	10.0	4.4	70,870	13,000	57,870	56,300	-2.7
56	10.0	5.5	44,880	9,500	35,380	38,600	+9.1
					Average Deviation, %		13.5

Although the resulting evaluation of the 1/4-inch-thick material in 8-inch-wide panels has been illustrated and described in the previous section, the results of the LIFE Program computations were not given for the two wider panels. Table 21 lists the pertinent information for all three panel widths. From the table it can be seen that Equation (28) appears to be quite useful for all three panel widths.

The data for the 1/2- and 1-inch-thick panel were evaluated in a similar manner. The results are shown in Figures 52 through 54 for t = 1/2 inch, and in Figures 55 through 57 for t = 1.0 inch. Tables 22 and 23 once again provide comparisons of remaining life. Generally, the series of figures and the tables show that there is somewhat greater divergence between predicted and actual remaining lives for specimens with these thicknesses than for 1/4-inch-thick specimens. Part of the reason for this is that the $d\ell/dN$ - ΔK curves for the thicker panels did not extend into low $d\ell/dN$ values. This is an important area in which to have good agreement, since for moderate to long-lived specimens, most of the crack-propagation lifetime is used up at these low rates.

The comparisons discussed above represent an average deviation of about 13 percent between all predicted lives and actual lives, with a maximum deviation of about 50 percent. In addition to the above data comparisons, Figures 24 through 27 show another way to evaluate the predictive capability of Equation (28). The figures show all of the data plotted on S-N coordinates. The data points are test lifetimes. The curves

TABLE 21. COMPARISON OF PREDICTED LIFETIME TO FAILURE WITH ACTUAL LIFETIME TO FAILURE FOR 1/4-INCH-THICK PANELS CONTAINING A FATIGUE CRACK 0.75-INCH LONG

Specimen	S_m	S_a	N_f	$N_{0.75}$	Life Remaining From 0.75" Crack, cycles		Deviation, percent
					Actual	Predicted	
				8 Inch Wide			
2	6.8	3.3	145,540	50,000	95,540	109,500	+14.60
11	6.8	4.4	86,580	25,000	61,580	57,000	-7.45
12	6.8	5.5	57,900	14,000	44,900	33,600	-25.20
7	8.4	3.3	136,360	51,500	84,860	88,800	+4.64
10	8.4	4.4	75,680	24,500	51,180	46,800	-8.55
13	8.4	5.5	36,850	10,700	26,150	27,800	+6.31
8	10.0	3.3	126,430	48,000	78,430	73,200	-6.67
9	10.0	4.4	59,170	19,500	39,670	39,000	-1.69
14	10.0	5.5	33,760	10,800	22,960	23,300	+1.48
				16 Inch Wide			
57	8.4	3.3	138,330	43,000	95,330	89,900	-5.70
58	8.4	4.4	60,360	18,200	42,160	42,600	+1.04
59	8.4	4.4	35,590	9,500	26,090	23,400	-10.3
				36 Inch Wide			
75	8.4	3.3	156,420	45,000	111,420	110,400	-0.92
76	8.4	4.4	68,530	19,000	49,530	49,500	0.00
77	8.4	5.5	43,650	13,200	30,450	26,100	+14.30
						Average Deviation, %	7.25

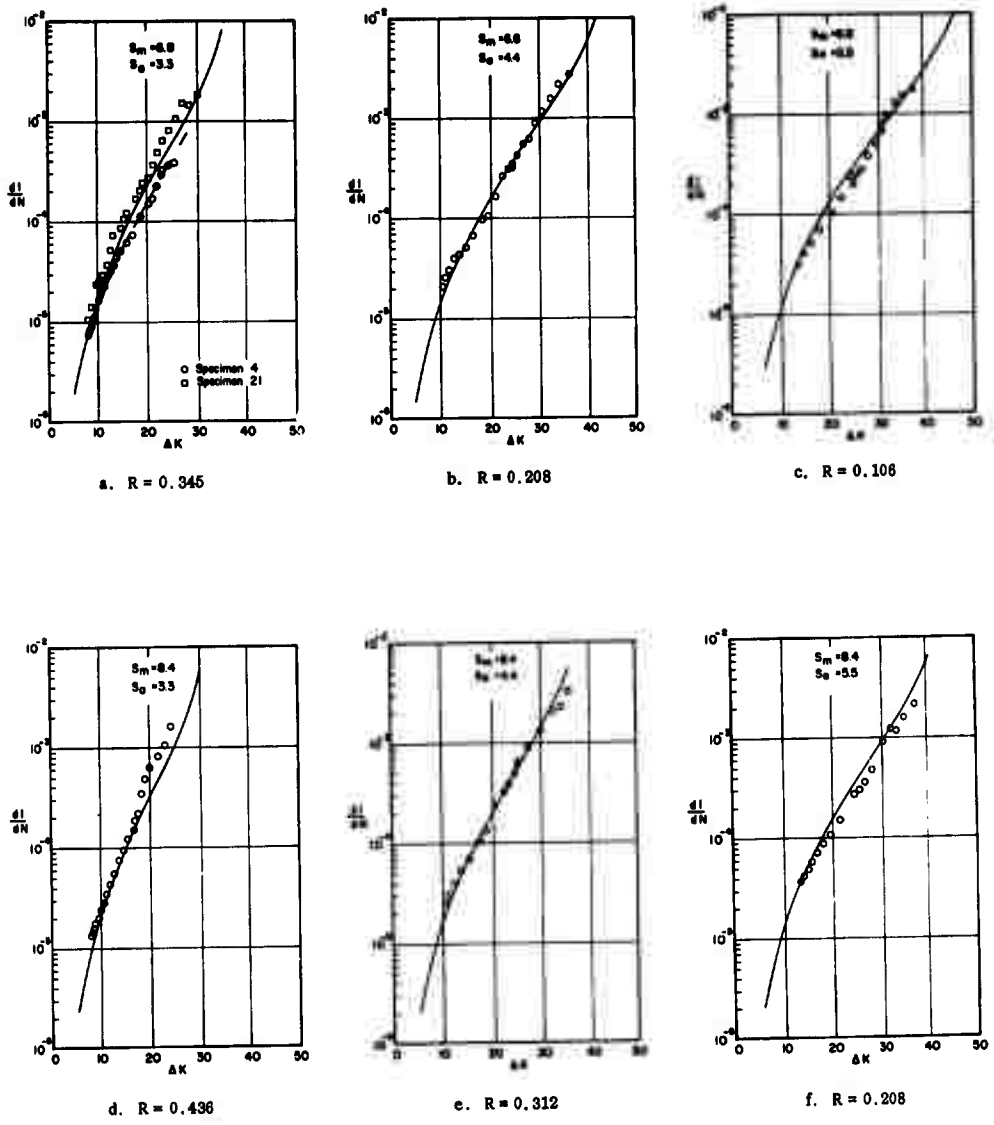

a. R = 0.345

b. R = 0.208

c. R = 0.106

d. R = 0.436

e. R = 0.312

f. R = 0.208

FIGURE 52. FATIGUE-CRACK-PROPOGATION RATE AS A FUNCTION OF ΔK FOR 1/2-INCH-THICK, 8-INCH-WIDE PANELS

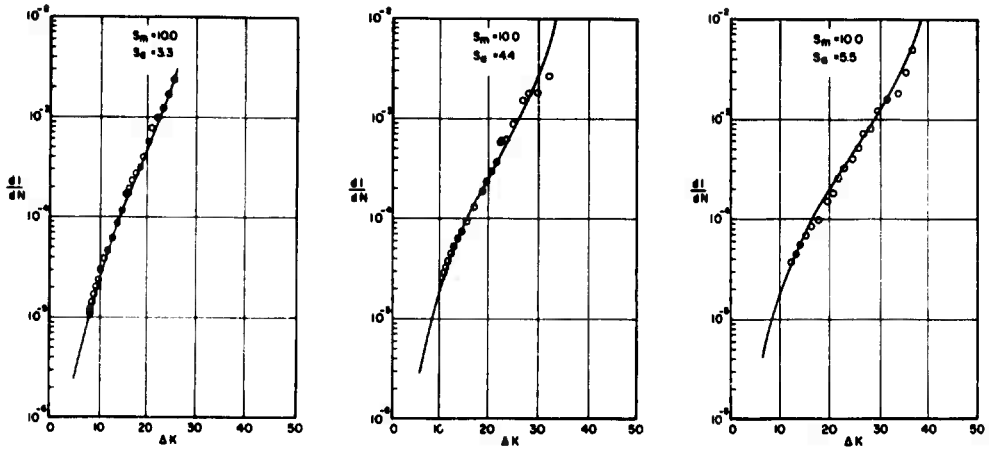

g. R = 0.504 h. R = 0.389 i. R = 0.290

FIGURE 52. (CONTINUED)

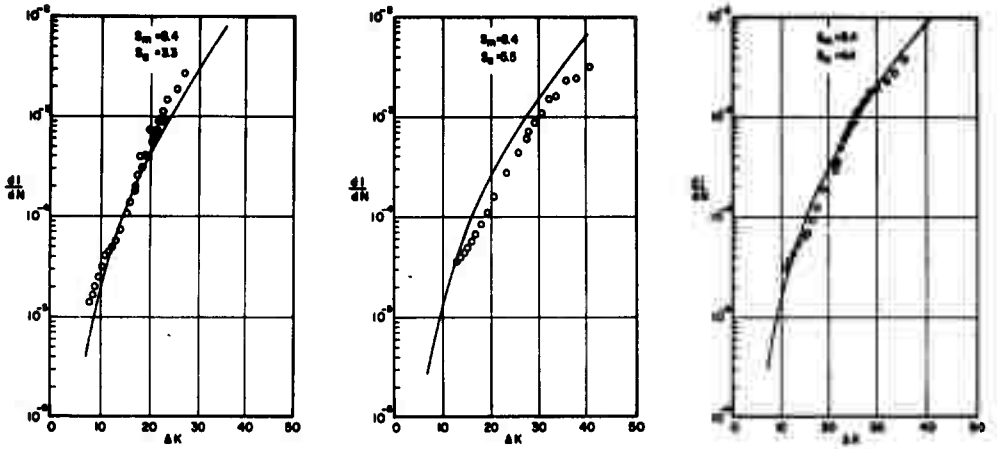

a. R = 0.436 b. R = 0.312 c. R = 0.208

FIGURE 53. FATIGUE-CRACK-PROPOGATION RATE AS A FUNCTION OF ΔK FOR 1/2-INCH-THICK, 16-INCH-WIDE PANELS

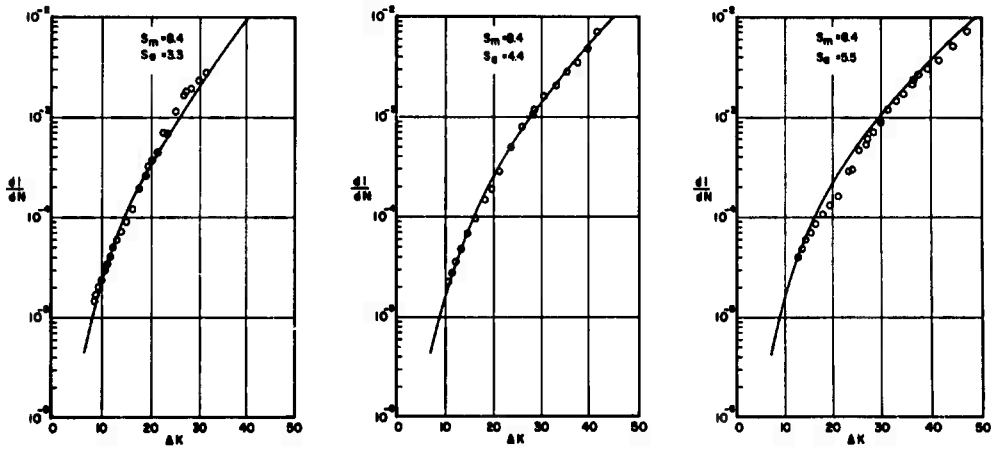

a. R = 0.436 b. R = 0.312 c. R = 0.208

FIGURE 54. FATIGUE CRACK PROPOGATION RATE AS A FUNCTION OF ΔK FOR 1/2-INCH-THICK, 36-INCH-WIDE PANELS

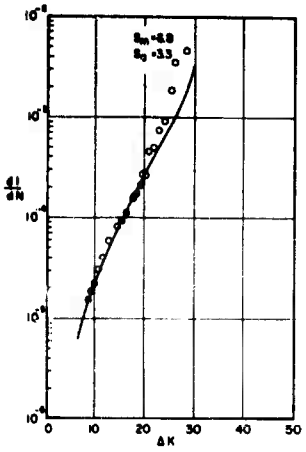

a. R = 0.345

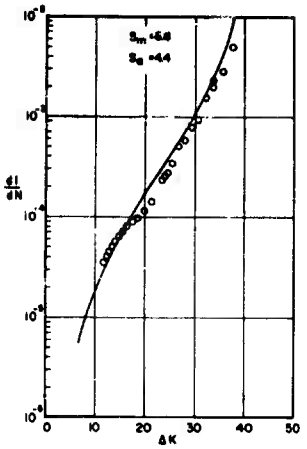

b. R = 0.208

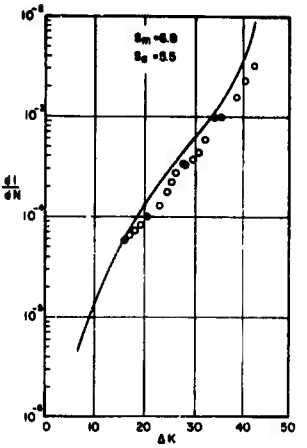

c. R = 0.106

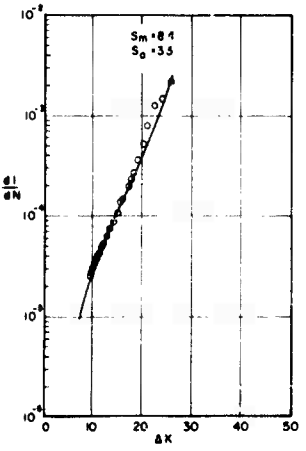

d. R = 0.436

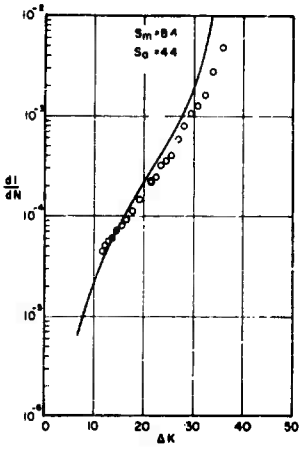

e. R = 0.312

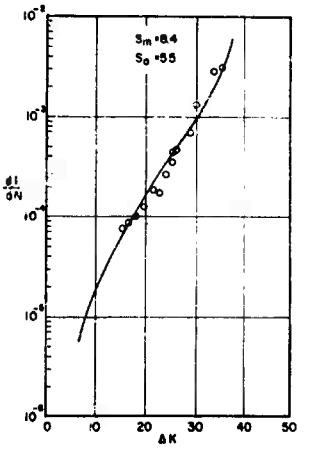

f. R = 0.208

FIGURE 55. FATIGUE-CRACK-PROPOGATION RATE AS A FUNCTION OF ΔK FOR 1-INCH-THICK, 8-INCH-WIDE PANELS

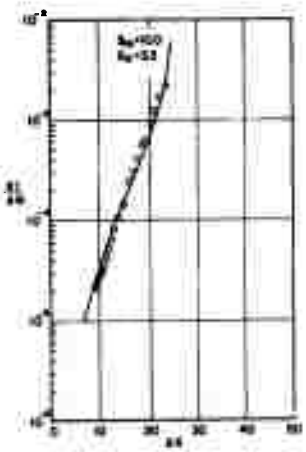

g. R = 0.504

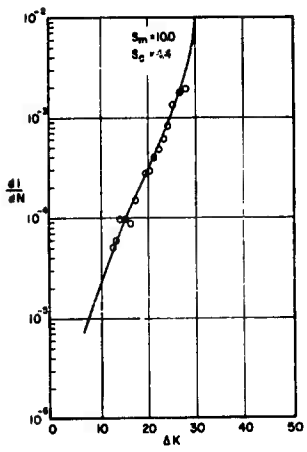

h. R = 0.389

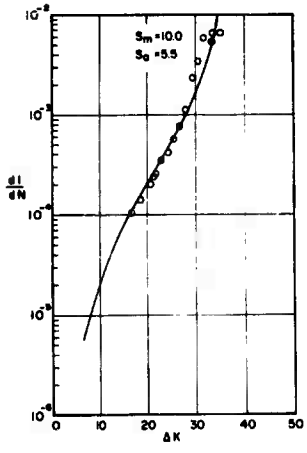

i. R = 0.290

FIGURE 55. (CONTINUED)

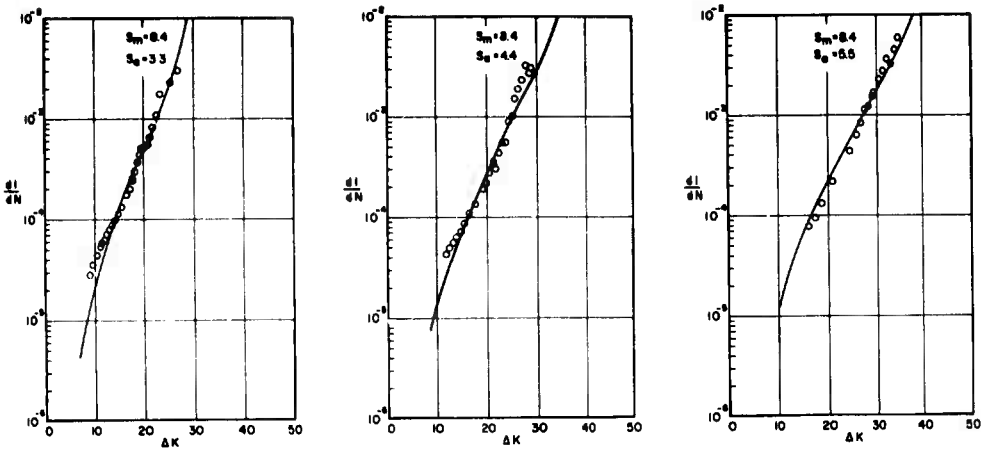

a. R = 0.436 b. R = 0.312 c. R = 0.208

FIGURE 56. FATIGUE-CRACK-PROPOGATION RATE AS A FUNCTION OF ΔK FOR 1-INCH-THICK, 16-INCH-WIDE PANELS

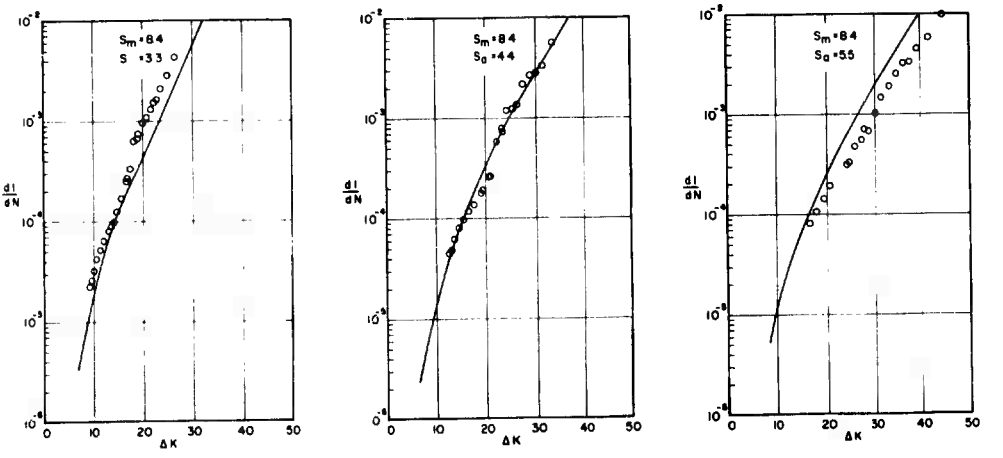

a. R = 0.436 b. R = 0.312 c. R = 0.208

FIGURE 57. FATIGUE-CRACK-PROPOGATION RATE AS A FUNCTION OF ΔK FOR 1-INCH-THICK, 36-INCH-WIDE PANELS

TABLE 22. COMPARISON OF PREDICTED LIFETIME TO FAILURE WITH ACTUAL LIFETIME TO FAILURE FOR 1/2-INCH-THICK PANELS CONTAINING A FATIGUE CRACK 1.0-INCH LONG

Specimen	S_m	S_a	N_f	$N_{1.0}$	Life Remaining, cycles		Deviation, percent
					Actual	Predicted	
				8 Inch Wide			
4 & 21 (avg.)	6.8	3.3	173,540	89,000	84,540	82,600	-2.30
20	6.8	4.4	77,210	38,000	39,210	39,500	+0.74
22	6.8	5.5	50,940	25,000	25,940	21,700	-16.4
15	8.4	3.3	125,720	68,000	57,720	65,400	+13.3
19	8.4	4.4	61,330	31,700	29,630	31,600	+6.76
23	8.4	5.5	43,160	21,600	21,560	17,500	-18.8
16	10.0	3.3	117,270	67,500	49,770	52,500	+5.48
18	10.0	4.4	61,440	36,700	24,740	25,600	+3.47
24	10.0	5.5	35,020	19,500	15,520	14,210	-8.44
				16 Inch Wide			
63	8.4	3.3	126,890	61,500	65,390	84,000	+29.1
64	8.4	4.4	66,820	32,200	34,620	30,900	-10.75
65	8.4	5.5	42,560	18,800	23,760	13,900	-41.50
				36 Inch Wide			
72	8.4	3.3	143,470	61,000	82,470	84,000	+1.86
73	8.4	4.4	68,230	29,800	38,430	35,900	-6.58
74	8.4	5.5	44,200	19,800	24,400	18,200	-25.4
						Average Deviation, %	12.7

TABLE 23. COMPARISON OF PREDICTED LIFETIME TO FAILURE WITH ACTUAL LIFETIME TO FAILURE FOR 1-INCH-THICK PANELS CONTAINING A FATIGUE CRACK 1.25-INCH LONG

Specimen	S_m	S_a	N_f	$N_{1.25}$	Life Remaining, cycles		Deviation, percent
					Actual	Predicted	
			8 Inch Wide				
25	6.8	3.3	129,770	80,300	49,470	52,800	+6.54
36	6.8	4.4	75,350	45,000	30,350	27,200	-10.38
31	6.8	5.5	47,510	27,200	20,310	15,700	-22.70
26	8.4	3.3	117,430	80,500	36,930	40,100	+8.60
29	8.4	4.4	73,890	50,200	23,690	20,800	-12.20
34	8.4	5.5	31,630	18,400	13,230	12,000	-9.30
27	10.0	3.3	109,740	73,500	36,240	30,700	-15.30
28	10.0	4.4	52,640	35,500	17,140	16,000	-6.65
33	10.0	5.5	27,640	17,400	10,240	15,700	+53.20
			16 Inch Wide				
66	8.4	3.3	125,180	81,500	43,680	61,800	+41.40
67	8.4	4.4	58,040	35,000	23,040	24,200	+5.05
68	8.4	5.5	31,990	18,500	13,490	11,310	-16.16
			36 Inch Wide				
69	8.4	3.3	130,930	83,500	47,430	71,200	+43.9
70	8.4	4.4	67,340	41,000	26,340	24,900	-5.47
71	8.4	5.5	45,230	27,300	17,930	10,700	-40.3
						Average Deviation, %	19.8

on each of these figures represent predicted lives. The agreement between test data and prediction is outstanding.

It appears then that an equation of the form $\frac{d\ell}{dN} = \frac{C\ \Delta K^n}{(1 - R)\ K_c - \Delta K}$ can usefully predict lifetimes remaining in cracked panels. Some further thoughts on this point are discussed in a later section.

This program was initiated partly to examine the influence of thickness and width on fatigue-crack propagation. The information in Table 24 provides a summary of the average values of C and n obtained during the analysis of data for each combination of thickness and width. In the table are the values of C and n and the average K_c value used for each set of calculations. An examination of the table suggests that the values of C and n vary with thickness and width, but not always consistently. The trend of C and n is usually to increase as thickness increases for each width. Also, the trend of C and n is to increase as width increases for each thickness. In both cases, the C and n values for 1/2-inch-thick, 16-inch-wide panels are too high to fit within the stated trends. An examination of the equation shows that $d\ell/dN$ would be expected to increase with increasing C and n. It is evident though that the values of K_c will influence this also.

TABLE 24. COMPUTED VALUES OF C AND n

FOR $\frac{d\ell}{dN} = \frac{C(\Delta K)^n}{(1-R)\ K_c - \Delta K}$

Plate Characteristics				
t, in.	w, in.	K_c, ksi$\sqrt{in.}$	C*	n
1/16	8	66.8	1.770E-9	2.134
1/4	8	67.7	6.139E-12	2.760
1/4	16	92.2	2.252E-13	3.179
1/4	36	136.4	3.867E-14	3.409
1/2	8	58.0	5.377E-13	2.995
1/2	16	101.0	4.631E-17	4.075
1/2	36	96.7	8.478E-15	3.524
1	8	50.7	1.396E-11	2.644
1	16	55.0	7.890E-16	3.677
1	36	70.5	1.259E-17	4.155

*E-9 = 10^{-9}, etc.

Some additional insight can be obtained by examining the $d\ell/dN$ versus ΔK data plots, wherein certain of the data have been overlaid. Figure 58 shows three of the overlays that were made from the data for the 8-inch-wide panel; Figure 59 data for the 16-inch-wide panel; and Figure 60, data for the 36-inch-wide panel. One can see from

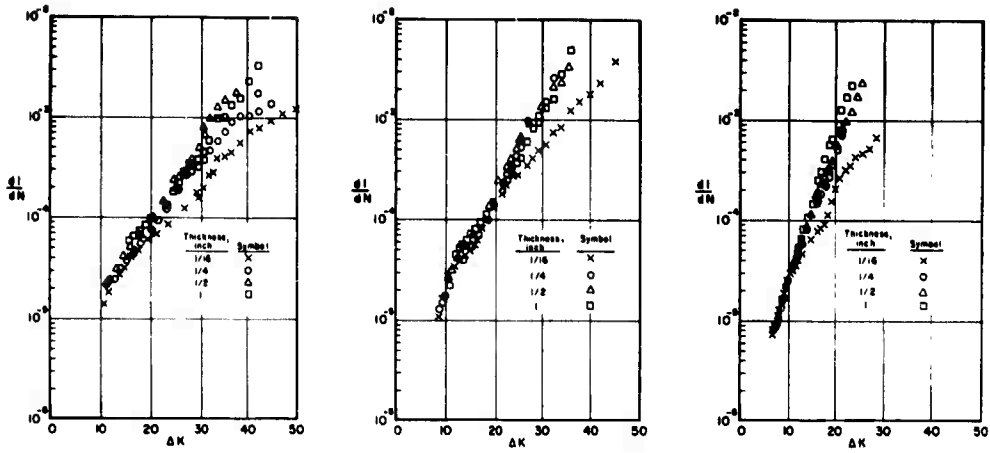

a R = 0.106 b. R = 0.312 c. R = 0.504

FIGURE 58. EFFECT OF THICKNESS ON FATIGUE-CRACK-PROPOGATION RATE FOR 8-INCH-WIDE PANELS

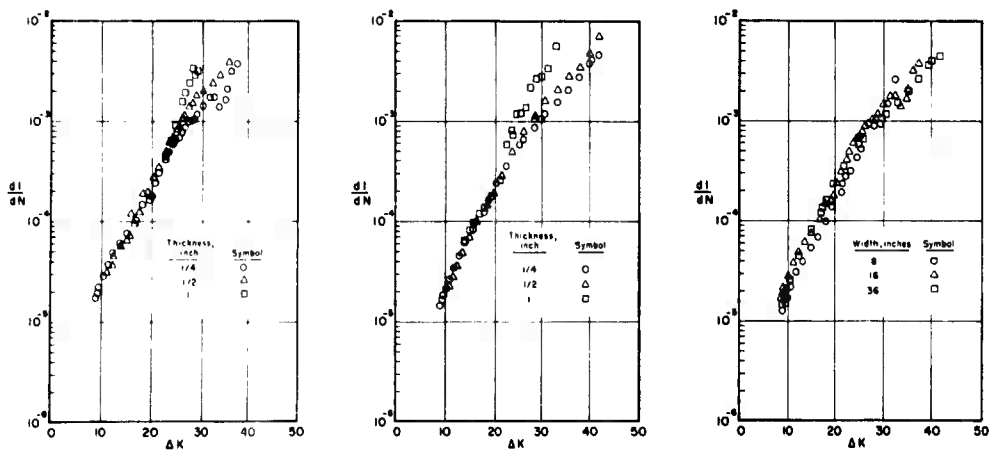

a. 16-Inch-Wide Panels b. 36-Inch-Wide Panels

FIGURE 59. EFFECT OF THICKNESS ON FATIGUE-CRACK-PROPAGATION RATE OF WIDE PANELS AT R = 0.312

FIGURE 60. EFFECT OF WIDTH ON FATIGUE-CRACK PROPAGATION FOR 1/4-INCH-THICK PANELS

this series of figures that there is a small but consistent effect of thickness on fatigue-crack-propagation rate for thicknesses in the range 1/4 to 1 inch. The panels of greater thickness have a somewhat higher propagation rate. With regard to the 1/16-inch-thick panels, the rate of crack propagation always is less than that of the thicker materials. The figures show also for rates below about 10^{-4} in./in./cycle that the crack growth for 1/4-, 1/2-, and 1-inch-thick panels are essentially the same. At these low growth rates, the crack is propagating primarily on a plane normal to the tensile stress, although shear-lip formation may have initiated. The real divergence above 2×10^{-4} in./in./cycle begins to reflect to some extent the difference in residual strength among the panels of various thicknesses.

Similar displays were made of the data to examine sheet-width effects. Realistically, one would say that over the range of crack lengths measured, there was almost no effect of specimen width when the data are organized to express crack-propagation rate in terms of stress intensity. Figure 59 shows a summary overlay for 1/4-inch-thick specimens of the three widths tested at 8.4 ± 4.4 ksi. The figure suggests that all the data could reasonably be considered together, at least to $d\ell/dN = 10^{-3}$ in./in./cycle. The form of the crack-propagation equation suggests that the data would begin to diverge at propagation rates higher than 10^{-3} in./in./cycle. This is because the equation predicts a curve that is vertically asymptotic at $\Delta K = (1 - R) K_c$ for each width panel, in accordance with the assumption that $d\ell/dN \rightarrow \infty$ when $K_{max} \rightarrow K_c$. The fitting factors (i.e., C and n) must vary to accommodate the assumption. This suggests that the crack-propagation equation may not be quite correct, even though this work has demonstrated that it predicts remaining life quite well.

Another feature of the analysis bears comment. In all of this discussion of fatigue-crack propagation, stress intensity has been defined with the width correction factor as $K = S_g \sqrt{\pi \ell / 2 \sec \pi \ell / 2w}$. In the section on fracture toughness and residual strength, the finally suggested residual-strength analysis employs stress intensity without any corrections, i.e., as $K = S_g \sqrt{\pi \ell / 2}$. While there is a difference between the two, they are not incompatible. In view of the fact that stress intensity has been used in the crack-propagation analysis as a mathematical tool rather than as a precise description of stress condition, it should not matter which K is used. Once data are available for stress cycles higher than those evaluated in this program, the reevaluation will be done using the uncorrected K.

CONCLUDING REMARKS

In this program, panels of 7075-T7351 of various thicknesses and widths were provided with a center notch and tested to failure by a monotonically increasing load or by a load cycle that was repeated many times. The former test provided residual-strength data whereas the latter test provided fatigue-crack propagation data. Both types of data were extensively analyzed and discussed in previous sections of this report. There were several significant results of these analyses.

First, it is apparent that there are at least two distinct and important bench marks in crack behavior during the rising-load test. The first bench mark is at onset of slow growth. At this load, a flaw initially present will begin to grow slowly as the load is increased. The second bench mark is the critical instability at failure. At this load, unstable and rapid crack growth occurs that results in complete failure. The loads and

gross section stresses at which these bench marks occur are distinctly different. For example, for instability at failure, in several instances, the gross failure stresses were high enough that net section yielding was the critical fracture criterion. Only in the very wide or thick plates was elastic instability a failure criterion. However, in all cases, slow growth initiated in the elastic range. It therefore was well represented by a stress-intensity value.

Both of these load levels have important significance for design considerations as well as for establishing and delineating thin-sheet-testing standards.

A second significant result is the development of a generalized residual-strength analysis that provides a data format consistent with and in terms of stress-intensity factors. It serves a dual purpose of identifying a fracture-toughness property for thin and transition-thickness material, and of presenting design data and developing fracture-prediction methods for structural applications. This analysis also provides screening criteria for residual-strength data and has significance in establishing testing standards.

A third significant result is the identification and evaluation of an empirical expression that appears to be quite useful in predicting crack propagation and the remaining lifetime of a panel containing a fatigue crack. The expression attempts to recognize that residual strength of a panel is associated with a flaw length which represents the terminal point in fatigue-crack propagation.

In terms of quantitative results on 7075-T7351 alloy, the data analysis has shown that there is a transition in failure characteristics within the thickness range of 1/4 to 1 inch that influences the fracture strength of center-notched panels of this alloy. The stress intensity for instability decreases as material thickness increases. Not only that, but the K value for instability approaches that of the threshold of slow growth. The implication is that for some thickness greater than 1 inch, failure will occur essentially without slow growth, further implying that the K value at that thickness will be K_{Ic}.

In regard to fatigue-crack propagation, this program has shown, over the limited stress range studied, that in the thickness range 1/4 to 1 inch, there is a very small effect of thickness on fatigue-crack propagation at propagation rates below about 10^{-4} in./in./cycle. A thickness effect at higher rates (for identical ΔK, $d\ell/dN$ is greater, the greater the thickness) is believed to reflect the reduced fracture resistance of the thicker materials. In comparison with the 1/4 to 1-inch-thick material, 1/16-inch-thick sheet had substantially lower rates of crack propagation for all comparable crack lengths.

The question of the effect of plate width has not been completely answered by this study since crack-growth measurements were not followed to the instability length. However, for crack lengths up to about 10 inches in 16- and 36-inch-wide panels and up to about 6 inches in 8-inch-wide panels, the rates of crack propagation up to a rate of approximately 10^{-3} in./in./cycle at similar values of ΔK are essentially the same. Additional experiments are needed to determine whether this is the case at even higher cracking rates.

REFERENCES

(1) Military Specification Series MIL-A-8860 (ASG), "Airplane Strength and Rigidity – General Specification for", May 18, 1960; includes MIL-A-8861 (ASG), "Airplane Strength and Rigidity – Flight Loads," and MIL-A-8866 (ASG), "Airplane Strength and Rigidity – Reliability Requirements, Repeated Loads, and Fatigue".

(2) Srawley, J. E., Jones, M. H., and Brown, W. F., Jr., "Determination of Plane Strain Fracture Toughness", Materials Research and Standards, 7 (6), 262-266 (June, 1967).

(3) Neuber, H., Theory of Notch Stresses: Principles for Exact Stress Calcualtion, J. W. Edwards, Ann Arbor, Michigan (1946).

(4) Broek, D., de Rijk, P., and Sevehuysen, P. J., "The Transition of Fatigue Cracks in Alclad", NLR Report 2100, National Aeronautical Research Institute, Amsterdam, Holland, August, 1965.

(5) Walker, K., "The Effect of Stress Ratio During Crack Propagation and Fatigue for 2024-T3 and 7075-T6 Aluminum", Effects of Environment and Complex Load History on Fatigue Life, ASTM STP No. 462, 1-14 (1970).

(6) Griffith, A. A., "The Phenomena of Rupture and Flow in Solids", Trans. Roy. Soc. (London), 221, 163-198 (1920).

(7) Irwin, G. R., "Fracture", Handbuch Der Physik, Vol. VI, Springer, Berlin (1958).

(8) Irwin, G. R., "Analysis of Stresses and Strains Near the End of a Crack Traversing a Plate", J. Appl. Mech., 21, 361-364 (1957).

(9) Brown, W. F., Jr., and Srawley, J. E., "Plane Strain Crack Toughness Testing of High Strength Metallic Materials", ASTM STP No. 410 (1966).

(10) Eichenburger, T. W., "Fracture Resistance Data Summary", Boeing Company Report No. D2-20947 (June, 1962).

(11) Kuhn, Paul, and Figge, I. E., "Unified Notch-Strength Analysis for Wrought Aluminum Alloys", NASA TD-D-1259 (1962).

(12) Dixon, J. R., "Stress Distribution Around Central Crack in a Plate Loaded in Tension; Effect of Finite Width of Plate", J. Roy. Aero. Soc., 64, 141-145 (1960).

(13) Kuhn, Paul, "Residual Strength in the Presence of Fatigue Cracks", Presentation to the AGARD Structures and Materials Panel, 1967.

(14) Frost, N. E., and Dugdale, D. S., "The Propagation of Fatigue Cracks in Sheet Specimens", J. Mech. Phys. Solids, 6, 92-110 (1958).

(15) Frost, N. E., "A Relation Between the Critical Alternating Propagation Stress and Crack Length for Mild Steel", Proc. Inst. Mech. Eng., 173 (35), 811-827 (1959).

(16) Frost, N. E., and Denton, K., "Effect of Sheet Thickness on the Rate of Growth of Fatigue Cracks in Mild Steel", J. Mech. Eng. Sci., 3 (4), 295-298 (1961).

(17) Frost, N. E., "Effect of Mean Stress on the Rate of Growth of Fatigue Cracks in Sheet Materials", J. Mech. Eng. Sci., 4 (1), 22-34 (1962).

(18) Frost, N. E., and Denton, K., "The Fatigue-Crack Propagation Characteristics of Titanium and Two Titanium Alloys", Metallurgia, 70, 113-120 (September, 1964).

(19) Frost, N. E., and Greenan, A. F., "Effect of a Tensile Mean Stress on the Alternating Stress Required to Propagate an Edge Crack in Mild Steel", J. Mech. Eng. Sci., 9 (3), 234-240 (1967).

(20) Schijve, J., "Fatigue-Crack Propagation in Light Alloy Sheet Materials and Structures", Advances in Aeronautics and Astronautics, 3, 387 (1962).

(21) Broek, D., and Schijve, J., "The Influence of the Mean Stress on the Propagation of Fatigue Cracks in Aluminum Alloy Sheet", National Aeronautical Research Institute, Amsterdam, TR M2111, January, 1963.

(22) Schijve, J., and Jacobs, F. A., "Fatigue-Crack Propagation in Unnotched and Notched Amuminum Alloy Specimens", National Aeronautical Research Institute, Amsterdam, TR M2128, May 1964.

(23) Broek, D., and Schijve, J., "The Influence of Sheet Thickness on Crack Propagation", Aircraft Engineering, 38 (31) (November, 1966).

(24) Schijve, J., "Significance of Fatigue Cracks in Micro-Range and Macro-Range", in Fatigue Crack Propagation, ASTM STP No. 415, 415 (1967).

(25) Paris, P. C., and Erdogan, F., "A Critical Analysis of Crack Propagation Laws", J. Basic Engineering, Transactions, ASME, 85, 528 (1963).

(26) Hardrath, H., and McEvily, A. J., "Engineering Aspects of Fatigue-Crack Propagation", Proceedings of the Crack Propagation Symposium, Vol. 1, Cranfield, England, 1961, pp 231-270.

(27) Paris, P. C., Gomez, M. P., and Anderson, W. E., "A Rational Analytic Theory of Fatigue", The Trend in Engineering, 13 (1), 9-14 (1961).

(28) Forman, R. G., Kearney, V. E., and Engle, R. M., "Numerical Analysis of Crack Propagation in Cyclic-Loaded Structures", J. Basic Engineering, Transactions, ASME, 89, 459-464 (1967).

(29) Hudson, C. M., "Effect of Stress Ratio on Fatigue-Crack Growth in 7075-T6 and 2024-T3 Aluminum Alloy Specimens", NASA TN D-5390, August, 1969.

(30) Erdogan, F., "Crack Propagation Theories", NASA CR-901, October, 1967.

APPENDIX A

PRELIMINARY TESTS

APPENDIX A

PRELIMINARY TESTS

APPENDIX A

PRELIMINARY TESTS

In this appendix are presented details of the preliminary series of tests and their interpretation. For brevity, all information common to these tests and the main body of tests has been included in the main text.

Test Details

Material

All specimens were machined from 7075-T7351 aluminum alloy 1/4-inch sheet or 1-inch plate. Tensile tests were performed and the results for the 1/4-inch sheet and 1-inch plate are listed in Table A-1, as are the Alcoa figures.

TABLE A-1. VERIFICATION TEST DATA FOR TENSILE PROPERTIES OF 7075-T7351 ALUMINUM ALLOY

Battelle Room-Temperature Tensile-Test Results			
Specimen	Thickness, in.	2 Percent Yield Strength, psi	Ultimate Tensile Strength, psi
1	0.2512	60,295	71,040
2	0.2500	60,745	71,220
3	0.2503	60,385	71,130
4	0.2510	60,025	71,015
5	0.2505	60,465	71,160
Average		60,383	71,113
1	1.0370	65,535	75,190
2	1.0380	65,550	75,450
3	1.0370	64,865	75,140
4	1.0368	65,610	75,770
5	1.0380	64,550	74,835
Average	1.0380	65,222	75,277

Alcoa Tensile Test Results (75 F)

Tensile Strength . . . . . 73,000 psi
Yield Strength . . . . . 63,000 psi

Specimen Configuration and Fabrication

The specimens were machined from 1/4-inch sheet and 1-inch plate to the desired thickness so that rolling effects upon material-property variation were minimized. It was necessary to use 1/4-inch sheet for specimens 1/4 inch thick and less because of the machining and handling difficulties associated with 1-inch plate machined to less than 1/4 inch thick at the reduced section.

The 1/4-inch-thick specimens were made from both 1/4-inch sheet and 1-inch plate to observe deviations in fracture and fatigue-crack-propagation behavior due to processing.

The overall dimensions and profile types of the specimens are presented in Figure A-1. Profile Types 2 and 4 represent offset specimens. The offset was employed to determine whether there were any differences in properties with respect to the location of the reduced section and to note whether there were machining effects. Specimens 1/4, 1/8, and 1/16 inch thick were machined according to Profile 1 in Figure A-1. Specimens 3/8, 1/2, 5/8, 3/4, 7/8, and 1 inch thick were machined according to Profile 3 of Figure A-1. Two 1/8-inch-thick offset specimens were machined according to Profile 2 and two 1/2-inch-thick specimens were machined according to Profile 4.

The specimens were blanked in the mill before shipping to Battelle. Fabrication was accomplished using standard machining operations. The initial through-the-thickness flaw was machined using electric discharge machining. The dimensions and shape of the initial flaw are shown in Figure 4 in the main body of the report.

Test Procedures

Fatigue-Crack Propagation. Two preliminary tests were conducted to determine the stress level to be employed for the crack-growth studies. The initial stress levels were selected in accordance with operational stress levels applied to naval aircraft. However, it was found that by employing these levels, the fatigue crack made a transition from the flat to the slant mode of propagation before the desired crack length of W/3 was reached. Consequently, a lower value of stress had to be employed in the crack-growth studies. The values of stress finally arrived at were a mean stress of 8000 psi and an alternating stress of 5000 psi. It was found that this stress level was low enough to prevent the transition from the flat to the slant mode of propagation. The specimens were subjected to sinusoidal loading such that the peak value of load gave a corresponding peak gross stress of 13,000 psi and a minimum load value that resulted in a 3000-psi stress level.

On the basis of previous investigations of aluminum alloys, it was assumed that 7075-T7351 was insensitive to loading frequency. The specimens were always tested at the highest possible frequency while maintaining consistent load accuracy by visually monitoring the load cycle on an oscilloscope and by using limit detectors that restrict machine operation to the desired accuracy. The limit detectors were set to give upper and lower load accuracies of 1.5 percent full scale for the load range used. The fatigue loading was terminated using the remote on-off switch when the crack reached a length of 2.6 inches.

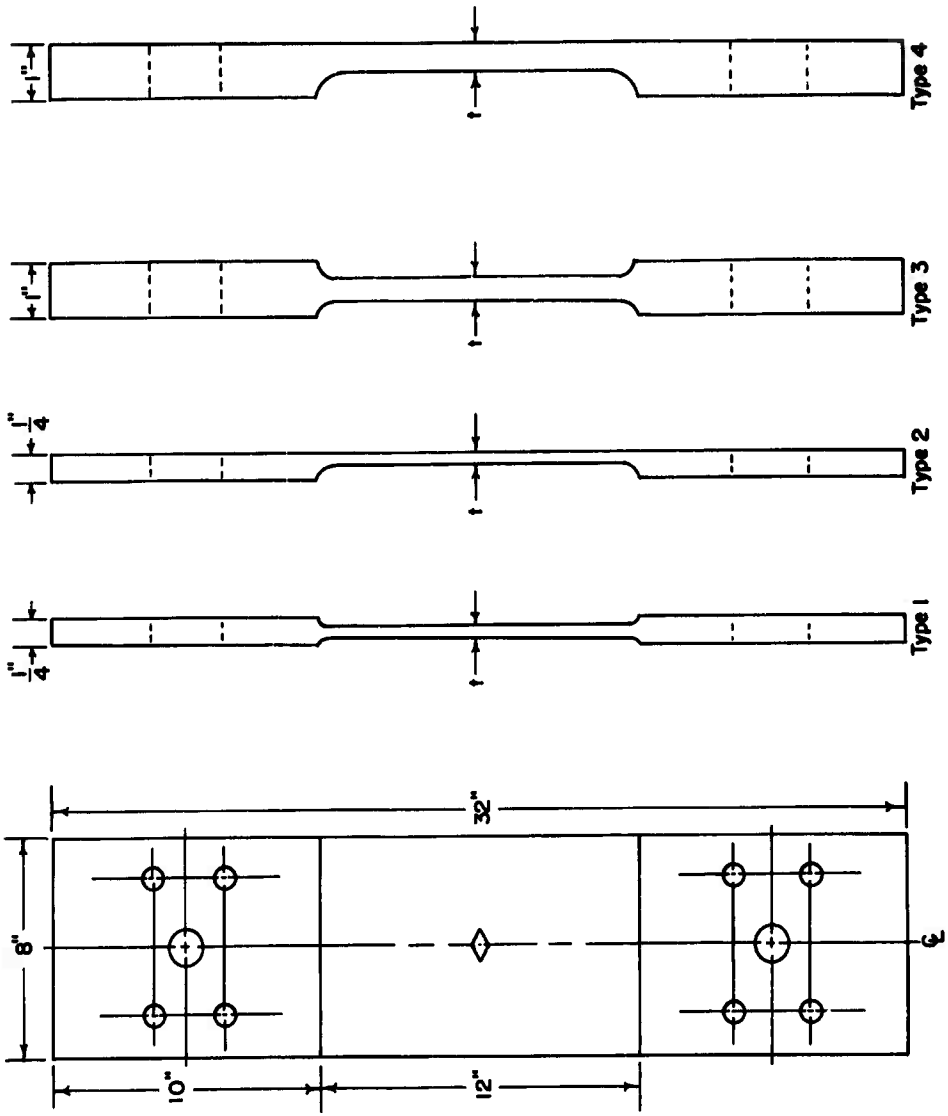

FIGURE A-1. DETAILS OF ALTERNATIVE SPECIMEN CONFIGURATIONS

Fracture. After fatigue cracking was completed, the plastic grid was removed and a compliance gage was inserted into the crack opening. The gage was aligned with a telescope. The fracture tests for Specimens 1 through 21 were conducted at a strain rate of 0.005 in./in./min until failure occurred. The tests on Specimens 22 through 27 were conducted using a constant loading rate to fracture. The loading rate was selected such that it produced a strain rate of 0.005 in./in./min in the elastic portion of the deformation. The constant-load-rate tests were conducted because it was observed that immediately after pop-in on the constant strain tests, the load dropped off. This drop-off in load is associated with a delay in the hydraulics when pop-in occurs. It was reasoned that a structure does not see a loading situation where the load drops off at pop-in, and thus it was decided to conduct tests at a constant load rate to determine whether this type of loading would affect the results.

The compliance-gage output was the X-axis input to an X-Y recorder with the X-axis recording the load level. The COD-load curves comprised the record of the fracture tests. This plot, in conjunction with viewing the fracture surface, was used to analyze the results.

Experimental Results

Fatigue-Crack Propagation Results

Figure A-2 is a graphical display of the basic crack-propagation data. The crack length as a function of the number of load cycles is plotted for the spectrum of thicknesses.

From Figure A-2, the crack growth rate, d(2c)/dN, for a given crack length was obtained by graphical differentiation. It was plotted as a function of crack length for 1-, 3/8-, and 1/16-inch-thick specimens. These thicknesses were selected because of possible interest in them for the main program. Figure A-3 represents the crack-growth rate versus crack-length data plotted on arithmetic coordinates.

Fracture Results

Basic Data. The results of the fracture tests are presented in Table A-2. For each specimen, Table A-2 contains the following information (reading left to right): specimen number; thickness, t; gross area, Ag; maximum fracture load, P_1; pop-in load, P_2; 5 percent secant offset load, P_3; gross stresses S_1, S_2, and S_3; and the stress-intensity factors K_1, K_2, and K_3 based on P_1, P_2, and P_3, respectively.

Stress-Intensity Factors. The fracture-data analysis was based on the concepts of linear elastic fracture mechanics using for a center-notched, through-the-thickness flaw,

$$K = S_g \sqrt{\pi c \sec(\pi c/W)} \quad . \qquad \text{(A-1)}$$

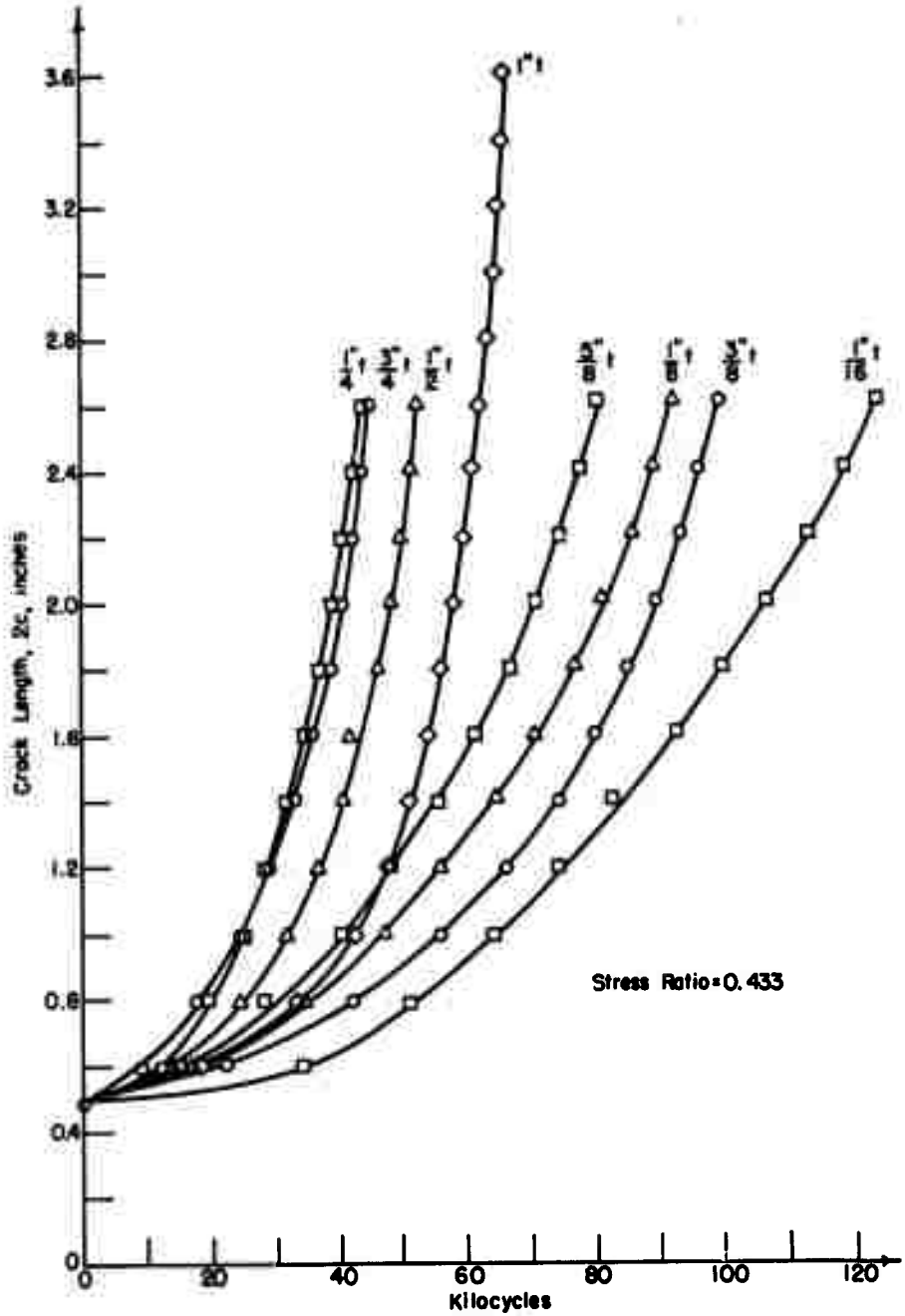

FIGURE A-2. CRACK LENGTH VERSUS CYCLES FOR PANELS OF VARYING THICKNESSES

BATTELLE MEMORIAL INSTITUTE – COLUMBUS LABORATORIES

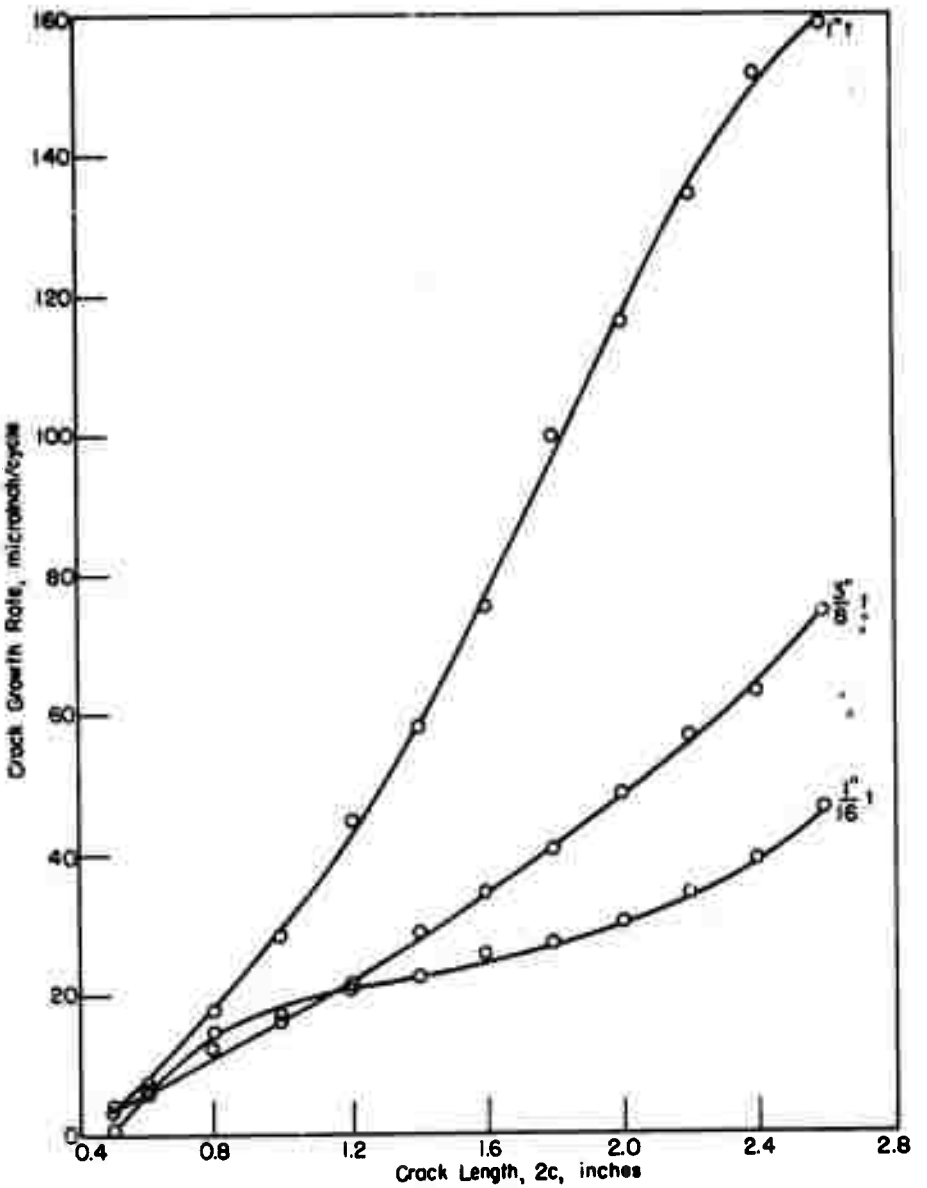

FIGURE A-3. CRACK GROWTH RATE AS A FUNCTION OF CRACK LENGTH AND THICKNESS

TABLE A-2. FRACTURE-TOUGHNESS DATA

Specimen	Thickness, in.	Gross Area, Ag, sq in.	Maximum Load, P_1, kip	Pop-In Load, P_2, kip	5 Percent Secant Offset Load, P_3, kip	S_1, ksi	S_2, ksi	S_3, ksi	K_1, ksi$\sqrt{in.}$	K_2, ksi$\sqrt{in.}$	K_3, ksi$\sqrt{in.}$
5	1/16 sheet	0.503	14.0	12.5	10.5	27.8	24.9	20.9	60.4	53.8	45.2
8	1/16 sheet	0.523	--	--	--	--	--	--	--	--	--
4	1/8 sheet	0.982	35.1	--	28.0	35.7	--	28.5	77.0	--	61.5
7	1/8 sheet	0.973	35.0	--	28.5	36.0	--	29.3	77.6	--	63.3
6	1/8 offset-sheet	0.993	35.7	--	28.2	35.7	--	28.4	76.8	--	61.4
9	1/8 offset-sheet	1.025	36.7	--	28.9	35.8	--	28.2	77.4	--	60.9
1	1/4 sheet	1.998	71.0	--	55.0	35.1	--	27.6	75.8	--	59.6
2	1/4 sheet	2.007	68.5	50.0	50.0	34.1	25.0	25.0	73.6	54.0	54.0
3	1/4 sheet	2.015	72.5	64.0	56.0	36.0	31.8	27.8	77.6	68.7	60.0
19	1/4 plate	1.996	51.5	--	--	25.8	--	--	55.8	--	--
26	1/4 plate	2.006	69.0	--	64.5	34.5	--	32.3	74.5	--	69.7
10	3/8 plate	2.983	109.1	--	63.0	36.6	--	21.1	78.9	--	45.5
14	3/8 transverse plate	2.967	70.5	52.5	67.0	23.8	17.7	22.6	51.5	38.2	48.9
15	1/2 plate	4.018	135.0	76.0	106.0	33.6	18.9	26.4	72.5	40.8	57.0
25	1/2 plate	3.985	128.5	72.0	100.0	32.4	18.1	25.1	70.0	39.0	54.2
27	1/2 offset-plate	4.005	122.0	68.0	120.0	30.6	17.0	30.0	66.0	36.7	64.7
20	1/2 offset-plate	3.985	123.0	120.0	100.0	30.9	30.1	25.1	66.7	65.0	54.2
12	5/8 plate	4.977	156.2	88.0	120.0	31.4	17.7	24.1	67.9	38.2	52.0
24	5/8 plate	4.986	154.7	91.0	120.0	31.0	--	24.1	67.0	--	52.0
16	3/4 plate	6.026	--	104.0	146.0	--	17.2	24.3	--	37.0	52.5
22	3/4 plate	6.006	184.0	103.0	136.5	30.7	17.2	22.8	66.3	37.1	49.1
17	7/8 plate	6.952	188.5	121.0	146.5	27.1	17.4	21.1	58.5	37.5	45.5
21	7/8 plate	6.975	178.5	117.5	142.0	25.6	16.8	20.4	55.3	36.4	44.0
11	1 plate	8.045	--	138.0	--	--	17.2	--	--	37.2	--
13	1 transverse plate	8.050	134.0	119.0	128.0	16.6	14.8	15.9	36.0	32.0	34.4
18	1 plate	8.078	210.5	123.0	152.0	26.6	15.4	18.8	57.4	33.1	40.6
23	1 plate	8.229	216.0	144.0	152.5	26.2	17.6	18.5	56.6	37.9	39.9

Figure A-4 is a plot of the stress-intensity factor based upon maximum load versus thickness. Figure A-5 shows the stress-intensity factor based on the 5 percent secant offset load as a function of thickness, and Figure A-6 is a plot of stress-intensity factor based on pop-in load versus thickness. From Figures A-4, A-5, and A-6, it is noted that the K values for the transverse specimens are significantly lower than those for the longitudinal specimens.

Discussion

Fracture

The effects of thickness upon the stress-intensity factor, K, are illustrated by Figures A-4, A-5, and A-6. Apparently, the same values of K result if the specimen is loaded under constant-load or constant-strain conditions as long as the rate of loading is approximately the same. All three plots of stress intensity versus thickness indicate a reduction in the magnitude of K for thicknesses less than 1/4 inch and for thicknesses greater than 1/4 inch. The decrease in K value for thicknesses less than 1/4 inch shown in the figures may be due to buckling in the crack plane. Buckling guides were used as described in the main text.

As discussed previously, four specimens were machined with an offset configuration to determine whether there is any variation in K value due to the location of the reduced section. From Table A-2, the difference in S_1, S_2, K_1, and K_2 for the 1/8-inch sheet and 1/8-inch offset sheet does not appear significant. The maximum gross stress, S_1, is slightly lower for the 1/2-inch offset specimen than for the 1/2-inch sheet specimen. If one focuses on the K_1 values for the 1/2-inch-thick specimens, since these have less scatter than do the K_2 and K_3 values, it appears that there may be a slight effect of specimen location on fracture behavior. This effect might well be expected in the thicker material, since the thicker material is probably less homogeneous in the thickness direction than is the thinner material.

On the basis of these results, it was decided to conduct the main program using 1/16-, 1/4-, 1/2-, and 1-inch-thick panels.

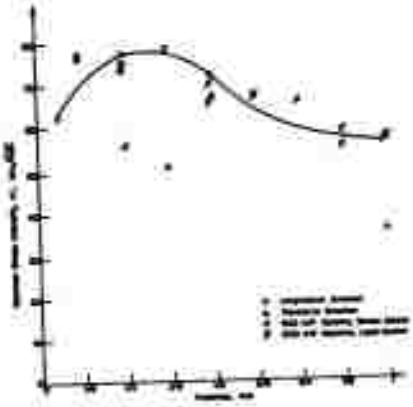

FIGURE A-4. STRESS-INTENSITY FACTOR, BASED ON MAXIMUM STRESS, VERSUS THICKNESS FOR 7075-T7351

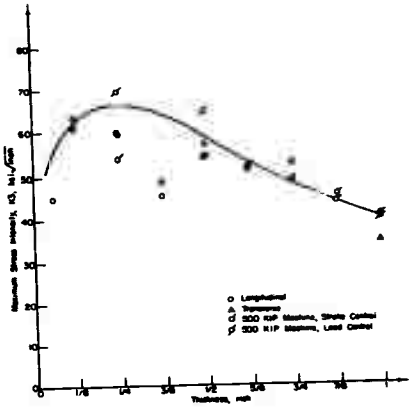

FIGURE A-5. STRESS-INTENSITY FACTOR, BASED ON 5 PERCENT SECANT OFFSET LOAD, VERSUS THICKNESS FOR 7075-T7351

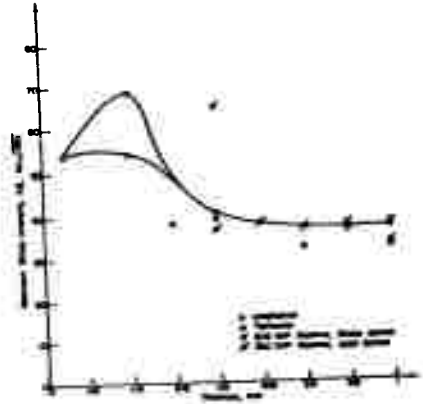

FIGURE A-6. STRESS-INTENSITY FACTOR, BASED ON POP-IN LOAD, VERSUS THICKNESS FOR 7075-T7351

APPENDIX B

TABULATION OF FRACTURE-TOUGHNESS INDICES

APPENDIX B

TABULATION OF FRACTURE-TOUGHNESS INDICES

Tabulations of stress-intensity factors (SIF) and crack-sensitivity indices for the fracture data derived in this program are presented in this appendix. Tables B-1 through B-4 present, respectively, data for 1/16-, 1/4-, 1/2-, and 1-inch-thick 7075-T7351 aluminum-alloy sheet and plate. Each computed column is annotated with the reference expression from which it was derived, the appropriate input data set being indicated below:

$$K_o = f(2c_o, S_3)$$
$$K_1 = f(2c_1, S_1)$$
$$C_m = g(2c_o, S_1)$$

TABLE B-1. FRACTURE-TOUGHNESS INDICES FOR 1/16-INCH-THICK 7075-T73 ALUMINUM ALLOY SHEET

Specimen	Nominal Width, W, in.	5 Percent Secant Offset SIF, K_o, ksi-in.$^{1/2}$	Max Load SIF, K_1, ksi-in.$^{1/2}$	Crack Sensitivity, C_m, in.$^{1/2}$
		Ref. Eq. (4)	Ref. Eq. (4)	Ref. Eq. (14)
57	8	34.5	73.8	0.66
58		40.0	73.9	0.60
59		42.2	97.4	0.57
60		41.0	92.4	0.63
61		49.4	96.2	0.58
62		36.7	88.7	0.69
63		50.0	74.0	0.85
64		35.0	60.7	0.89
65	8	30.0	43.4	1.40
Avg.		39.9	77.8	0.76

TABLE B-2. FRACTURE-TOUGHNESS INDICES FOR 1/4-INCH-THICK 7075-T7351 ALUMINUM ALLOY PLATE

Specimen	Nominal Width, W, in.	5 Percent Secant Offset SIF, K_o, ksi-in.$^{1/2}$	Max Load SIF, K_1, ksi-in.$^{1/2}$	Crack Sensitivity, C_m, in.$^{1/2}$
		Ref. Eq. (4)	Ref. Eq. (4)	Ref. Eq. (14)
28	8	31.2	86.6	0.69
29		40.3	--	0.61
30		53.3	97.3	0.61
31		51.4	91.8	0.63
32		42.7	92.8	0.59
33		45.0	92.3	0.62
34		47.0	99.3	0.63
35		46.7	99.2	0.67
36		53.2	93.8	0.69
37		42.2	85.4	0.73
38		42.1	82.7	0.77
39		41.1	77.6	0.83
41		41.3	71.2	0.81
43		41.0	55.4	0.87
44		39.3	54.0	1.16
45		45.7	57.7	1.14
46		37.0	45.5	1.06
47	8	24.0	59.7	2.47
Avg.		42.5	79.0	0.87
48	16	37.7	92.0	0.54
49		45.9	--	0.59
50		57.3	124.3	0.53
51		83.6	117.8	0.62
52		63.6	114.0	0.68
53		61.7	102.6	0.70
54		58.5	120.0	0.80
55		53.2	--	0.84
56	16	40.1	53.6	1.23
Avg.		55.7	103.5	0.73
89	36	61.1	104.9	0.78
90		64.5	141.5	0.81
91	36	56.6	201.4	0.68
Avg.		60.71	149.26	0.76

TABLE B-3. FRACTURE-TOUGHNESS INDICES FOR 1/2-INCH-THICK 7075-T7351 ALUMINUM ALLOY PLATE

Specimen	Nominal Width, W, in.	5 Percent Secant Offset SIF, K_o, ksi-in.$^{1/2}$	Max Load SIF, K_1, ksi-in.$^{1/2}$	Crack Sensitivity, C_m, in.$^{1/2}$
		Ref. Eq. (4)	Ref. Eq. (4)	Ref. Eq. (14)
1	8	33.8	64.9	0.86
2		35.8	--	0.72
3		34.7	88.8	0.73
4		37.5	82.3	0.74
5		49.1	84.5	0.86
6		35.5	78.8	0.84
7		36.5	61.4	1.11
8		33.3	47.8	1.43
9		34.7	--	1.15
10		34.9	61.8	1.00
11		39.1	66.8	0.87
12		36.8	74.9	0.87
13		34.7	73.6	0.87
14		46.9	--	0.72
15		47.8	--	0.63
16		36.8	47.1	1.19
17		25.0	--	1.40
18		35.6	80.1	0.65
19		41.7	110.0	0.76
20		38.3	67.2	1.01
21		43.1	85.0	0.68
23		41.1	88.5	0.74
24		46.8	81.6	0.70
25		39.1	79.5	0.84
27	8	39.4	75.9	0.87
Avg.		37.3	75.0	0.89
66	16	36.5	142.3	0.75
67		42.6	132.3	0.64
68		--	154.0	0.76
69		54.5	143.6	0.90
70		47.9	115.4	0.68
71		49.5	113.8	0.77
72		46.0	80.1	0.88
73	16	38.4	--	0.98
Avg.		45.0	125.9	0.80
86	36	--	--	1.83
87		46.2	86.7	1.87
88	36	37.5	--	2.29
Avg.		41.83	86.7	2.00

TABLE B-4. FRACTURE-TOUGHNESS INDICES FOR 1-INCH-THICK 7075-T7351 ALUMINUM ALLOY PLATE

Specimen	Nominal Width, W, in.	5 Percent Secant Offset SIF, K_o, ksi-in.$^{1/2}$	Max Load SIF, K_1, ksi-in.$^{1/2}$	Crack Sensitivity, C_m, in.$^{1/2}$
		Ref. Eq. (4)	Ref. Eq. (4)	Ref. Eq. (14)
92	8	33.4	42.5	1.87
93		44.5	52.8	1.45
94	8	39.7	45.4	1.68
Avg.		39.2	46.9	1.67
74	16	32.8	49.5	1.72
75		34.2	60.6	1.59
76		36.8	53.7	1.68
77		38.1	55.8	1.53
78		42.0	66.0	1.35
79		46.2	51.4	1.70
80		38.0	43.9	2.10
81		33.7	46.5	2.05
82	16	25.1	--	3.16
Avg.		36.3	53.4	1.88
83	36	--	69.0	1.55
84		47.6	68.4	1.56
85	36	44.5	64.7	1.89
Avg.		46.0	67.3	1.67

APPENDIX C

MATHEMATICAL ANALYSIS OF CRACK PROPAGATION EQUATION

BLANK PAGE

APPENDIX C

MATHEMATICAL ANALYSIS OF CRACK PROPAGATION EQUATION

A preliminary evaluation of fatigue-crack-propagation data using Equation (28), i.e.,

$$\frac{d\ell}{dN} = \frac{C\,\Delta K^{n}}{(1 - R)K_{c} - \Delta K} \quad ,$$

showed for a given consistent group of data (for example, all 1/4-inch-thick specimens, 8 inches wide) that C and n varied from one specimen to another in a random manner*. In order to provide a single equation for each group of data, it was desired to obtain mean values of C and n for the nine or more specimens of each group. This appendix contains a discussion of a mathematical analysis of the above expression to determine how to characterize the mean values of C and n (arithmetic means, geometric means, etc.), retaining the formal structure of the above equation.

Consider the expression:

$$y_{i} = \frac{C_{i}\,(\Delta K)^{n_i}}{(1 - R)K_{c} - \Delta K} \quad , \; i = 1, \ldots , m, \tag{C-1}$$

where i ranges over the number of specimens in a given group of specimens. Thus, n_i and C_i denote constants fitted to an expression of the above form for each specimen.

If one takes the logarithm of Equation (C-1), adds the equations for each specimen, and divides each term by m, the number of specimens in a group, the following equation results:

$$\frac{1}{m}\sum_{i=1}^{m} \ell n\, y_{i} = \frac{1}{m}\sum_{i=1}^{m} \ell n\, C_{i} + \frac{\ell n(\Delta K)}{m}\sum_{i=1}^{m} n_{i}$$

$$- \frac{1}{m}\sum_{i=1}^{m} \ell n\,[(1 - R)K_{c} - (\Delta K)] \quad . \tag{C-2}$$

*In the analysis, the data pairs for each specimen, $\left(\frac{d\ell}{dN}, \Delta K\right)_{i}$, were analyzed by least-squares regression to provide the best value of C and n for each specimen.

Because the sum of logarithms is equivalent to the logarithm of a product, namely,

$$\sum_{i=1}^{m} \ell n\, y_i = \ell n\, y_1 + \ell n\, y_2 + \ldots + \ell n\, y_m$$

$$= \ell n\,(y_1\, y_2 \cdots y_m) = \ell n \prod_{i=1}^{m} y_i \quad , \tag{C-3}$$

Equation (C-2) can be rewritten as follows:

$$\frac{1}{m}\,\ell n \left(\prod_{i=1}^{m} y_i \right) = \frac{1}{m}\,\ell n \left(\prod_{i=1}^{m} C_i \right) + \ell n\, \Delta K \left[\frac{1}{m} \sum_{i=1}^{m} n_i \right]$$

$$- \frac{1}{m}\,\ell n \left\{ \prod_{i=1}^{m} \left[(1 - R)K_c - (\Delta K) \right] \right\} \tag{C-4}$$

or

$$\ell n \left(\prod_{i=1}^{m} y_i \right)^{\frac{1}{m}} = \ell n \left(\prod_{i=1}^{m} C_i \right)^{\frac{1}{m}}$$

$$+ \left[\frac{1}{m} \sum_{i=1}^{m} n_i \right] \ell n\, \Delta K - \ell n \left[(1 - R)K_c - \Delta K \right] \quad . \tag{C-5}$$

One recognizes in Equation (C-4) that $\frac{1}{m}\,\ell n \left(\prod_{i=1}^{m} y_i \right)$ and $\frac{1}{m}\,\ell n \left(\prod_{i=1}^{m} C_i \right)$ are geometric means and that $\frac{1}{m} \sum_{i=1}^{m} n_i$ is an arithmetic mean, so that one can set

$$\ell n\, y' = \ell n \left(\prod_{i=1}^{m} y_i \right)^{\frac{1}{m}} \quad ,$$

$$\ell n\, C' = \ell n \left(\prod_{i=1}^{m} C_i \right)^{\frac{1}{m}} \quad , \tag{C-6}$$

and

$$n' = \frac{1}{m} \sum_{i=1}^{m} n_i \quad ,$$

where y' and C' are geometric means and n' is an arithmetic mean. These substitutions in Equation (C-5) yield

$$\ell n\, y' = \ell n\, C' + n'\, \ell n(\Delta K) - \ell n\, [\,(1 - R)K_c - \Delta K] \quad . \tag{C-7}$$

By taking antilogarithms, Equation (C-7) becomes

$$y' \frac{C' (\Delta K)^{n'}}{[\,(1 - R)K_c - \Delta K]} \quad , \tag{C-8}$$

or more suggestively,

$$[\text{ Geometric mean of y's}]$$

$$= \frac{[\text{ Geometric mean of C's}]\ \Delta K^{[\text{ Arithmetic mean of n's}]}}{[\,(1 - R)K_c - \Delta K]} \quad . \tag{C-9}$$

This analysis shows that a relation of the same formal structure to Equation (28) in the text is obtained from the averaging process, if the C_i's are replaced by their geometric mean and the n_i's are replaced by their arithmetic mean.

On the basis of this result, the calculations for all groups of test results were based on the arithmetic mean of n and geometric mean of C.

As a numerical test of this decision, the fatigue-crack-propagation data for the fifteen 1/4-inch-thick specimens were analyzed using three different methods of assigning values to C and n in Equation (28). The three methods were as follows:

(1) Arithmetic mean, n; arithmetic mean, C.
(2) Median, n; median, C.
(3) Arithmetic mean, n; geometric mean, C.

In the analysis using one of the above methods, the "average" C and n were computed from the individual C_i and n_i for each specimen. Using the "average" values for each specimen, $d\ell/dN$ values were computed for each ΔK for which data were available. Since the computed values represent average values, one might expect that half of these values should be slightly more than the test values and that half of them should be less than the test values. Accordingly, for each specimen, a Chi-Square test* was made on the positive and negative deviations between the fitted curve and the data. If half of the

---

*Chi-Square test employed $\chi^2 = 2 \cdot \frac{(P - N/2)^2}{N/2} = 4\,(P - N/2)^2/N$, where P denotes the actual number of positive deviations and N/2 denotes the expected number of positive deviations.

deviations were positive, the Chi-Square value would be zero. The larger the value from the Chi-Square test, the greater is the deviation of the average curve from test data.

From the above analysis, using the three methods of "averaging" C and n, the following summary statement can be made:

(1) Method 3, using the arithmetic mean on n and geometric mean on C, gave the best results for 11 out of 15 specimens. *

(2) Method 2, using the median n and C, gave the best results for 4 out of 15 specimens.

(3) Method 1, using the arithmetic n and C, gave uniformly the worst results.

Thus, the computations substantiated the conclusion reached in the mathematical analysis of the crack-propagation equation.

*Best results means that the Chi-Square value for a given specimen obtained with a given method was the lowest value for that specimen obtained with the three methods of "averaging".

UNCLASSIFIED

Security Classification

DOCUMENT CONTROL DATA - R & D

(Security classification of title, body of abstract and indexing annotation must be entered when the overall report is classified)

1. ORIGINATING ACTIVITY (Corporate author)	2a. REPORT SECURITY CLASSIFICATION
Battelle Memorial Institute Columbus Laboratories 505 King Avenue Columbus, Ohio 43201	Unclassified
	2b. GROUP Not applicable

3. REPORT TITLE

Fracture and Fatigue-Crack Propagation Characteristics of 7075-T7351 Aluminum Alloy Sheet and Plate

4. DESCRIPTIVE NOTES (Type of report and inclusive dates)

Final Report

5. AUTHOR(S) (First name, middle initial, last name)

Charles E. Feddersen, Walter S. Hyler

6. REPORT DATE	7a. TOTAL NO. OF PAGES	7b. NO. OF REFS
March 15, 1970	135	30

8a. CONTRACT OR GRANT NO.	9a. ORIGINATOR'S REPORT NUMBER(S)
N00156-68-C-1344	
b. PROJECT NO.	G-8902
c.	9b. OTHER REPORT NO(S) (Any other numbers that may be assigned this report)
d.	

10. DISTRIBUTION STATEMENT

[redacted] ments and foreign [redacted] Commander, Naval Air Development Center, Warminster, Pa. 18974 [redacted] D.C. 20360.

11. SUPPLEMENTARY NOTES	12. SPONSORING MILITARY ACTIVITY
	Department of the Navy Naval Air Development Center Aero Structures Department Warminster, Pa. 18974

13. ABSTRACT: This program was directed to provide information relative to damage tolerance of panels of 7075-T7351 sheet and plate. This implied the generation and analysis of information on flat panels containing centrally located flaws and testing, either under monotonically increasing load or under cyclic loads. The information obtained provided insight into the two major aspects of damage tolerance – residual strength and fatigue-crack propagation – from tests on panels ranging in thickness from 1/16 inch to 1 inch and in width from 8 inches to 36 inches.

The program has shown that there are at least two bench marks in crack growth behavior from the monotonically increasing load test: (1) onset of slow growth at which a flaw initially present begins to grow slowly with increasing load, and (2) critical instability at which unstable and rapid crack growth occurs that results in failure. From the data obtained a generalized residual strength analysis was developed which identifies a fracture toughness property for thin and transition thickness materials as well as presents design data and fracture or residual strength predictions for structural applications. The program has also resulted in the identification of an empirical expression that appears to be quite useful in predicting fatigue-crack propagation and the remaining lifetime of a panel containing a fatigue crack.

DD FORM 1 NOV 65 1473

UNCLASSIFIED

Security Classification

14. KEY WORDS	LINK A		LINK B		LINK C	
	ROLE	WT	ROLE	WT	ROLE	WT
Fatigue						
Fatigue-crack propagation						
Fracture						
Fracture toughness						
Residual strength						
Aluminum alloy						
7075-T7351 plate						